



**Politecnico
di Torino**

Politecnico di Torino

Master of Science in Biomedical Engineering

Master's Degree Thesis

**Design of an Inertial Multi-Sensor Network for the
Monitoring of the Heart Rate During Sleep using
Ballistocardiographic Signals**

Supervisor:

Prof. Gabriella OLMO

Candidate:

Enrico COSENZA

Co-supervisor:

Eng. Giorgio TANTILLO

Academic Year 2020-2021

Abstract

Diseases of the circulatory system are among the chronic degenerative pathologies with the highest morbidity, representing one of the main causes of disability. The general definition of cardiovascular diseases (CVDs) includes all the diseases of the heart and blood vessels. These represent the first cause of access to first aid, as well as death. In order to contain the number of hospitalizations and healthcare costs, innovative prevention and monitoring techniques for patient's health are needed. To date, conventional techniques to monitor the patient's cardiovascular activity are intrusive and invasive. The main goal of this work is to overcome these limitations, by introducing the design of a non-invasive and non-intrusive system for heart rate (HR) detection. This vital sign is obtained starting from the processing of the ballistocardiographic (BCG) signal which is acquired by a network of four IIS2ICLX inclinometers connected to the STM32L4-R9IJ6 microcontroller, produced by STMicroelectronics. The main advantage of this work is to use a multi-sensor network to detect the BCG signal during a sleep cycle, regardless of the subjects positions during the night, suitable for both home and hospital environments. In order to acquire the signal with the highest quality, several tests were performed by placing the sensors in certain regions of the bed, according to the literature. Subsequently, a time-based algorithm was developed in order to compute the heart rate from the ballistocardiographic signal and to manage the most frequent sources of noise, such as motion artifacts. In order to calculate the HR using the signal with the highest SNR among the four acquired, two prediction models were developed: a Multi-Parameter Model (MPM) and a Single-Parameter Model (SPM). The first one identifies, on 10 seconds windows of the ballistocardiogram, the best signal among the four provided by the inertial multi-sensor network, by calculating three statistical parameters (the standard deviation, the kurtosis, and the auto-correlation function). In the same way, the second method identifies, on 30 seconds windows, the best signal by calculating the mean of the cross-correlation coefficients from heart beats found on the ballistocardiogram of the four sensors. To validate the results achieved, the heart rate provided by the proposed system was compared with the HI device, a three-lead certified electrocardiograph designed by STMicroelectronics.

Considering the developed predictive models, the designed inertial multi-sensor network provides the heart rate as follows. The Multi-Parameter Model estimates the HR every 10 and 30 seconds, with an average coverage of 87.95 % (MAE of 4.56 bpm \pm 7.09 bpm) and 93.76 % (MAE of 4.26 bpm \pm 6.55 bpm) of the entire sleep respectively. The Single-Parameter Model estimates the HR every 10 and 30 seconds, with an average coverage of 93.57 % (MAE of 4.25 bpm \pm 6.51 bpm) and 97.66 % (MAE of 3.86 bpm \pm 5.81 bpm) of the entire sleep respectively. Finally, taking full advantage of the characteristics of the network, the Ideal Model provides the heart rate every 10 or 30 seconds, estimating the vital sign for an average coverage of 94.69 % (MAE of 2.30 bpm \pm 4.40 bpm) and 97.68 % (MAE of 1.80 bpm \pm 3.22 bpm) of the entire sleep respectively.

List of acronymus

AAMI American for the Advance Medical Instrumentation

ANSI American Nastional Standards Institute

ACF Auto-Correlation Function

AMI Acute Myocardial Infarction

AR Autoregressive

AV Atrioventricular

BLE Bluetooth Low Energy

BR Breathing Rate

BCG Ballistocardiography

CCF Cross-Correlation Function

CVD Cardiovascular Disease

DB-BCG Direct Body Ballistocardiogram

ECG Electrocardiography

EMFi ElectroMechanical Film

FBGS Fiber Bragg Grating Sensor

FIR Finite Impulsive Response

HF-BCG High Frequency Ballistocardiogram

HR Heart Rate

HRV Heart Rate Variability

IDC Insulation-Displacement Contact

IDE Integrated Development Environment

ICT Information and Communication Technology

IM Ideal Model

IoT Internet of Things

LF-BCG Low Frequency Ballistocardiogram

MEMS Micro Electronic Mechanical System

MISO Master In Slave Out

MA Moving-Average

MCCC Mean Cross-Correlation Coefficient

MOSI Master Out Slave In

MRI Magnetic Resonance Imaging

MPM Multi-Parameter Model

ODR Output Data Rate

PCB Printed Circuit Board

PSD Power Spectral Density

PVDF Polyvinylidene fluoride

SA Sinoatrial

SCLK Serial Clock

SNR Signal to Noise Ratio

SPI Serial Peripheral Interface

SPM Single-Parameter Model

SS Slave Select

STWIN Sensor Tile Wireless Industrial Node

UF-BCG Ultra-low Frequency Ballistocardiogram

WHO World Health Organization

Contents

1	Introduction	9
1.1	Telemedicine and Cardiovascular Monitoring	10
1.1.1	Applications and services of Telemedicine	10
1.2	Physiological Background	13
1.2.1	Cardiovascular Physiology	13
1.2.2	Heart Anatomy	14
1.2.3	The Cardiac Cycle	15
1.2.4	Cardiovascular Diseases (CVDs)	17
1.3	Electrocardiography	18
1.3.1	ECG signal	18
1.4	Ballistocardiography	21
1.4.1	The birth of the ballistocardiography	21
1.4.2	BCG signal	22
1.4.3	Physiological meaning of the BCG signal	23
1.4.4	Mechanical Differences in the first Ballistocardiograph Designs	24
1.4.5	End of the classical Ballistocardiography	26
1.4.6	State of the Art	27
2	Materials and Method	35
2.1	Hardware Design	35
2.1.1	IIS2ICLX inclinometer	36
2.1.2	STeval-STWINK1	38
2.1.3	Communication interface between STWIN and IIS2ICLX	40
2.1.4	Acquisition System	42
2.2	Firmware Design	43
2.2.1	Brief firmware description	43
2.2.2	Firmware Flowchart	44
2.3	Signal Capture	45
2.3.1	Sensors Placement Evaluation	45
2.3.2	Acquisition Protocol	48
2.3.3	Dataset Acquisition Phase	48
2.4	Data Processing	49
2.4.1	Data Processing Flowchart	49

2.4.2	Acquisition Timing Evaluation	50
2.4.3	Signal Pre-processing	51
2.4.4	Motion artifacts management	54
2.4.5	Heart Rate detection	55
2.4.6	Prediction models for selecting the best BCG signal	60
2.5	Evaluation of algorithm performance	64
2.5.1	Hi device	64
2.6	Validation methods	67
3	Results	69
3.1	Heart Rate computation every 10 s	70
3.2	Heart Rate computation every 30 s	72
3.3	Discussion	98
4	Conclusions and future works	99
4.1	Conclusions	100

Chapter 1

Introduction

Cardiovascular diseases (CVDs) are the leading cause of death [1]. According to the World Health Organization (WHO), 17.9 million people die every year from CVDs, a third of global deaths. Because of this high incidence, it is critical that individuals follow a healthy lifestyle and place greater importance on prevention and diagnosis. Although the costs of hospitalization are increasing due to the disproportionate demand from the population, in recent years several devices targeting the remote monitoring of the patient's health have been developed. These systems fall within the scope of *telemedicine* and represent a real revolution for the healthcare. In the case of CVDs, the main parameters to be kept under control are the heart rate and the blood pressure. The portable devices already on the market, that are able to monitor these parameters from home, are usually Holter devices for pressure or for electrocardiography. However, these devices have several drawbacks: they are intrusive because they go into physical contact with the patient and can give hygiene problems, as in the case of the electrodes necessary to perform the electrocardiogram. In addition, these devices often require the presence of a caregiver or nurse capable of housing the sensors on the patient. Finally, the intrusiveness of these devices may be the cause of non-acceptability for the patient.

This work presents a prototype system consisting of four inclinometers able to correlate the heart activities, in a non-invasive and a non-intrusive way, through a mechanical signal: the *ballistocardiogram*.

1.1 Telemedicine and Cardiovascular Monitoring

The term *telemedicine* is composed of two words *tele*, which means "remote", and *medicine*. Although this word was coined in the 1970s, today there is not a unique definition. A study in 2007 found 104 peer-reviewed definitions of the word [2]. According to the definition adopted by the World Health Organization (WHO), telemedicine can be defined as [3]:

"The delivery of health care services, where distance is a critical factor, by all health care professionals using information and communication technologies for the exchange of valid information for diagnosis, treatment and prevention of disease and injuries, research and evaluation, and for the continuing education of health care providers, all in the interests of advancing the health of individuals and their communities."

According to some, the term *telemedicine* refers to services that could only be provided by physicians, while the term *telehealth* indicates services also offered by other professionals, such as nurses and pharmacists [4], but WHO considers the terms interchangeable.

However, telemedicine refers to:

- providing clinical supports;
- overcoming geographical barriers, connecting users who are not in the same physical location;
- involving the use of various types of Information and Communication Technologies (ICT);
- improving health outcomes.

1.1.1 Applications and services of Telemedicine

Telemedicine applications can be classified into two basic types [5]:

- *Store-and-forward (or asynchronous)*: telemedicine involves the exchange of pre-recorded data between two or more individuals at different times, for example the results of a test sent by a clinician to the patient.
- *Real time (or synchronous)*: telemedicine requires the involved individuals to be simultaneously present for immediate exchange of information, as in the case of videoconferencing.

The main media that can be exchanged via synchronous or asynchronous telemedicine are: text, audio, video or images.

More developed societies routinely use telemedicine services as tools for clinical diagnosis and management [3]. For example, monitoring and managing patients with acute and chronic illnesses is made easier with biometric measurement devices, such as the ones that monitor heart rate, blood pressure and blood glucose levels. On the other hand, telemedicine has a great potential to be exploited especially in developing countries. In fact, one of the main advantages of telemedicine is to support traditional medicine by providing effective remote services at low cost. Although telemedicine represents a field which is growing strongly, it doesn't have to be confused with traditional medicine, where the role of the physician cannot be substituted.

The main telemedicine systems are [6]:

- *Teleconsultation*: remote consultation involves both the physician and the patient. An example of teleconsultation is represented by a telephone conversation between two physicians to obtain a second opinion, or the connection between a physician and a patient who wants to receive feedbacks (i.e. consultation) regarding the treatment the subject is undergoing.
- *Tele-education*: this term refers to all types of medical education that an individual can benefit at distance, such as:
 - clinical education from teleconsultation;
 - clinical education via the Internet;
 - academic study via the Internet;
 - public education via the Internet.
- *Telesurgery*: it includes either the presence of the surgeon in the operating room, who drives a robot that does the surgery (*Tele Presence Surgery*) and either the assistance in real time through video or audio connection (*Telementoring*).
- *Telemonitoring*: it consists mainly in the management of vital signs at distance. This stage is characterized by several steps, which are:
 1. *Data acquisition system*, constituted of sensors, generally able to transduce vital signs into a digital signal;
 2. *Data transmission system*, which provides the data transmission from patient to physician;
 3. *Data integration*, integrating and updating the health status of the subject;
 4. *Data examination*, to prevent and to suppress abnormal situation;
 5. *Data storage*, typically cloud or local platform.

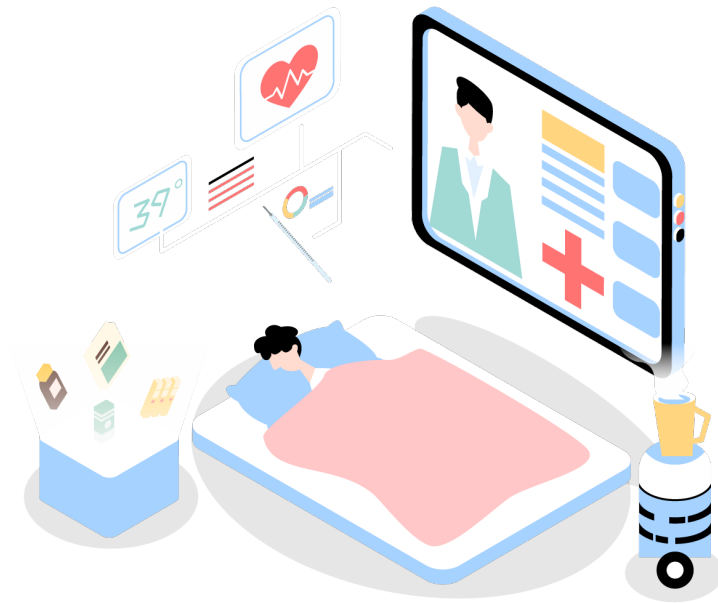


Figure 1.1: Simple representation of the proposed telemedicine system use case.

Referring to telemonitoring, a telemedicine system is a tool capable of recording subject's vital signs using one or more devices, thus providing a collection of information from the patient to the physician. Generally, in the cardiovascular field, the first cardiac activity monitored is the electrical one, performing an electrocardiogram (ECG). As telemonitoring is associated with prevention (long-term) or control activity (as a result of the manifestation of a pathology), it is desirable that this could be implemented taking into account the comfort of the patient. As it will be seen in the dedicated paragraph, the ECG suffers from several disadvantages regarding the long-term monitoring, therefore, the bed-based ballistocardiographic system (BCG) developed in this work is proposed as a future alternative solution to the classic cardiovascular monitoring.

1.2 Physiological Background

1.2.1 Cardiovascular Physiology

The cardiovascular system consists of the heart, blood vessels and blood itself, carrying the blood throughout the body. The cardiovascular system is responsible of the transfer various substances to and from all the regions of the body. Among the substances transported there are two gases: oxygen and carbon dioxide. Oxygen, which is essential for cellular respiration, enters the circulation at the level of the lungs and is transferred to all body cells; carbon dioxide, on the other hand, follows the reverse path.

Blood flows through three types of vessels: *arteries*, *veins* and *capillaries*. The arteries are the channels that carry the blood that comes out of the heart, while the veins are the channels run through by the blood coming back to the heart. Veins and arteries branch up to become very thin capillaries, capable of reaching every single cell of the body [7].

The circulatory system consists of two distinct circuits:

- *pulmonary circulation (or small circulation)*: it connects the heart to the lungs and aims to oxygenate the blood rich in carbon dioxide and make it available to the large circulation;
- *systemic circulation (or large circulation)*: it connects the heart to all the tissues of the body carrying oxygenated blood (arterial blood) that returns to the heart rich in carbon dioxide (venous blood). Finally, the latter is re-introduced into the small circulation to restart a new cycle.

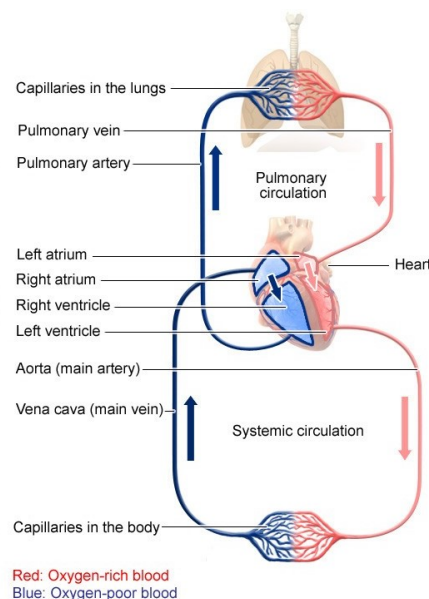


Figure 1.2: Blood circulation.

In the *systemic circulation*, the aorta plays a very important role. It is the greatest arteria which provides the oxygenated blood to the whole body and generally, in the humans, it is 30 to 40 cm long and 2.5 to 3.5 cm in diameter. Two branches originate from the base of the aorta, the right and left coronary arteries, which preside over the arterial supply of the heart [7]. Mechanically, the aorta is a medium in which a large amount of blood is propagated and, together with the heart, is the basic element on which ballistocardiography is based.

1.2.2 Heart Anatomy

The heart is an organ found in the middle mediastinum, a thoracic compartment underneath the sternum, wrapped in a two-layered serous sac called pericardium. The heart shape is like an inverted cone, similar in size to a man's fist, and weighs approximately 230-350 grams. By dividing the heart into two parts it is possible to distinguish the right heart, which pumps blood to the lungs, while the left heart pushes blood to all the other organs and tissues. The heart is made up of four chambers: the superior chambers consist of the right atrium and the left atrium, while the lower ones are constituted of the right ventricle and the left ventricle, which are much larger than the atria. The atria are responsible of reserving the blood flowing from the veins, whilst the ventricle producing sufficient pressure to allow blood circulation [7].

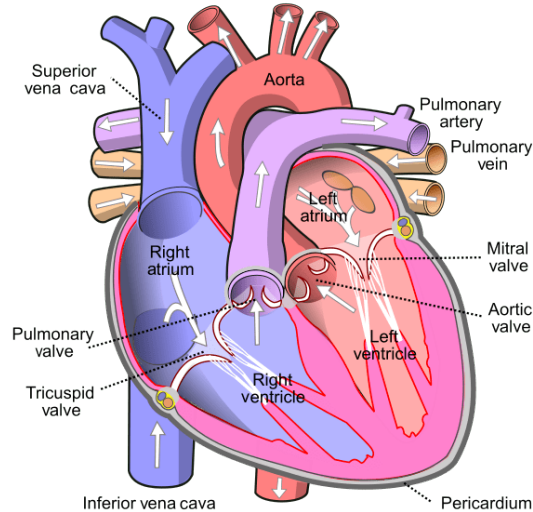


Figure 1.3: The heart.

The heart is equipped with four valves, called heart valves. Their function is to ensure that during the cardiac cycle the flow of blood into the heart proceeds in a single direction, that is established by the pressure gradient.

The heart valves are:

- *two atrioventricular valves*: the mitral valve and the tricuspid valve, placed between the atria and ventricles;

- *two semilunar valves*: the aortic valve and the pulmonary valve, placed between the ventricles and arteries.

1.2.3 The Cardiac Cycle

The cardiac cycle is characterized by two main phases: *systolic phase*, when the heart is contracting, and the *diastolic phase*, when the heart is relaxing. Both the phases are divided into two subphases, which involve the atria and the ventricles. The atrial systole is characterized by the contraction of the atria only and in this phase the blood is transmitted to the ventricles. In the same manner, the ventricular systole is represented by the contraction of the ventricles only, which supply the blood to the vessels. As a consequence of the systolic phase, the heart needs to relax in the diastolic phase characterized by the re-expansion of the atria and ventricles [7].

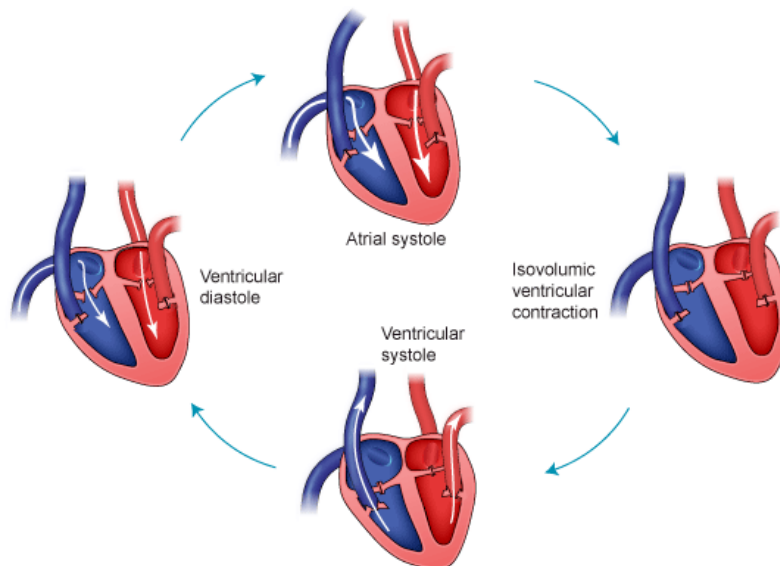


Figure 1.4: The Cardiac Cycle.

In physiology, the Wiggers Diagram (Fig. 1.5) is used to show in a single graph the following parameters:

- aortic pressure;
- ventricular pressure;
- atrial pressure;
- ventricular volume;
- electrocardiogram;
- arterial blood flow;
- cardiac tones.

This graph summarizes all the activities that the heart does in a cardiac cycle. More in detail, systole and diastole are identified also as *cardiac contraction* and *cardiac relaxation*, in which occur the:

- isovolumic contraction;
- slow and fast ventricular ejection;
- isovolumic relaxation;
- rapid inflow;
- diastasis;
- atrial systole.

All these stages allow the heart to pump about 70-80 mL of blood in each cardiac cycle.

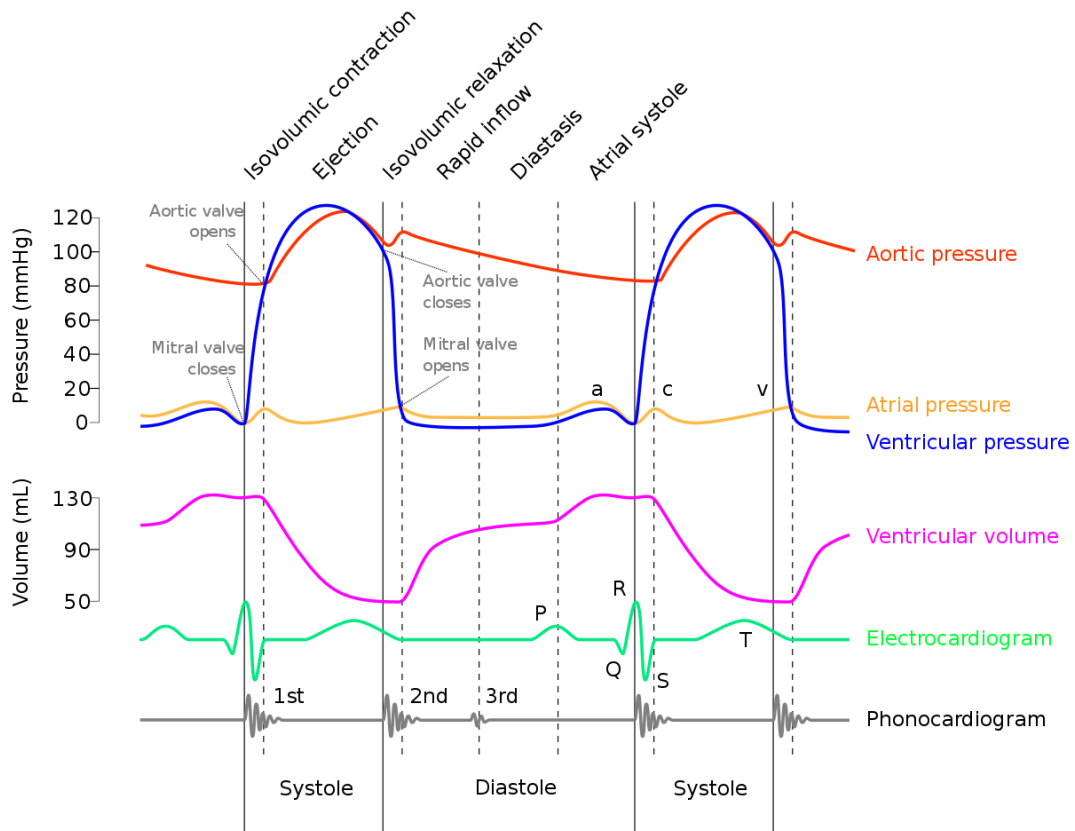


Figure 1.5: The Wiggers Diagram.

1.2.4 Cardiovascular Diseases (CVDs)

Cardiovascular diseases (CVDs) are among the main causes of morbidity, disability and mortality. Ischaemic heart diseases, such as acute myocardial infarction and angina pectoris, and cerebrovascular diseases, such as ischaemic and haemorrhagic stroke, are the most lethal CVDs. However, the most common cardiovascular diseases are [8]:

- *Heart Attack (or myocardial infarction)*: a heart attack occurs when the myocardium is poorly perfused. This is because the blood flow that carries oxygen has been greatly reduced or completely stopped. The main causes of a heart attack are atherosclerotic plaques that accumulate in the coronary arteries. Therefore plaques are an obstacle to the blood flowing through the arteries, which could block or stop blood flow altogether and cause a heart attack.
- *Stroke*: although it manifests itself in the brain areas, stroke belongs to the same cardiovascular disease as related to blood flow. In almost all cases, stroke occurs when a blood vessel that carries blood and oxygen to the brain is occluded. Haemorrhagic stroke can also occur due to malformation of the vessels or abnormal growths of cerebral blood vessels.
- *Heart Failure*: this term refers to the heart not pumping blood as well as it should. The heart is not sufficient to satisfy the metabolic requirements of the body. The difficulty in carrying out some daily actions, such as walking or climbing stairs, could be related to heart failure.
- *Arrhythmia*: this term refers to any alteration of the sinus rhythm. Bradycardia and tachycardia indicate too slow and too fast rhythms, respectively. When any kind of rhythm is completely lost, the heart does not work effectively.
- *Heart Valve Complications*: heart valves can have problems opening and closing. These two conditions are indicated with the terms *stenosis*, when the valves do not open completely, not allowing the blood to run properly and *regurgitation*, when the valves do not close completely, which enables blood to leak through.

Unfortunately, the CVDs have a very strong incidence, but they can be prevented and kept under control, by leading a healthy lifestyle and undergoing periodic visits to a specialist doctor. A complementary solution could be to use devices capable of recording cardiac activities during the day and making them available to a physician, who can remotely monitor the clinical condition of the patient and possibly summon him to his practice for a more thorough control.

1.3 Electrocardiography

Electrocardiography (ECG) is the gold standard to monitor the heart's health [9]. The ECG analysis is performed by using several electrodes placed on the skin. Through this technique it is possible to record the electrical activity of the heart and to display it on a specific trace called electrocardiogram. The electrical activity of the heart is identified by the *depolarization* of the cardiac muscle followed by its *repolarization*.

The ECG exam can be performed mainly in two ways: using twelve electrodes, also called 12-lead ECG, or using few leads. Through the first method it is possible to identify some serious diseases, such as the acute myocardial infarction (AMI) through the ST segment elevation on the electrocardiogram, while the second method is used in some devices to detect suspect activities, for example arrhythmia [10].

1.3.1 ECG signal

The most important vital sign that can be obtained from the ECG is the heart rate, which indicates the number of beats that occur in one minute (bpm). This measure can vary depending on the physical condition of the body. In addition, certain activities such as exercise, sleep, anxiety, stress, illness, and drug use may affect the normal (sinus) rhythm of the heart [11].

From a purely morphological point of view, the electrocardiogram of a healthy subject has some fundamental features that make it the absolute standard of reference. These characteristics include the signal amplitude between 1-10 mV and the signal band between 0.5-125 Hz, as well as its unmistakable appearance which is constituted from (Fig. 1.6):

- *intervals*: which are defined starting from the beginning of a wave to the beginning of the following wave;
- *segments*: which are defined starting from the end of a wave to the beginning of the following wave.

Moreover, the ECG presents:

- **P wave**: the P wave represents the depolarization of the atria (80-100 ms);
- **PR interval**: the PR interval identifies time needed by electrical impulses to travel from the SA sinus node to the AV node (100-120 ms);
- **QRS complex**: the QRS complex represents the rapid depolarization of the ventricles (80-120 ms);
- **QT interval**: the QT interval represents the depolarization and repolarization time of the ventricles (200-400 ms);

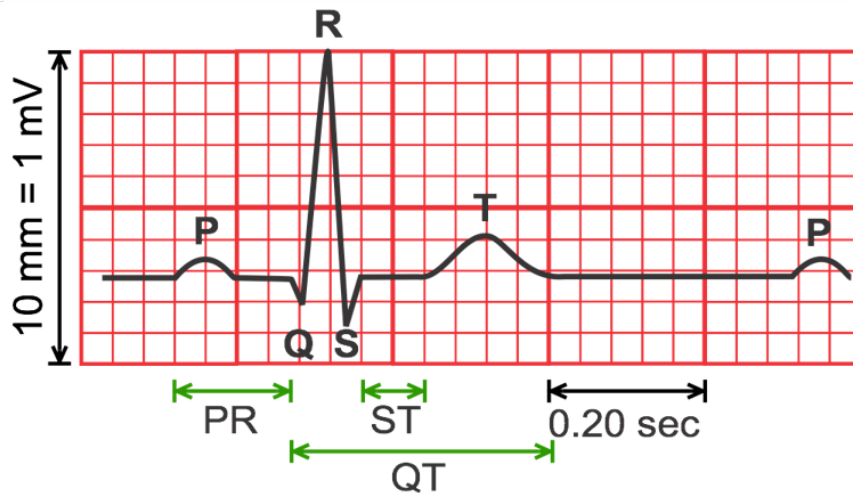


Figure 1.6: Typical ECG signal.

- **ST interval:** it is the period in which the ventricles are completed depolarized;
- **T wave:** the T wave identifies the repolarization of the ventricles (160 ms);
- **U wave:** sometimes this wave is present and probably describes the last repolarization signal of the ventricles.

To obtain the electrocardiogram it is necessary to arrange the electrodes on the patient's skin in two or more places. The placement of the electrodes is not random, but has been defined in such a way as to best record the electrical activity of the heart. The leads that are used to record an electrocardiogram are divided in two groups: *bipolar leads* and *unipolar leads*. The first, second and third main leads belong to the group of bipolar leads, also indicated by the Roman numerals I, II and III. In this case, to obtain a cardiac monitoring it is necessary to use at least two of the three electrodes available, which generally follow the positioning shown in Fig. 1.7. Through unipolar leads it is possible to detect the potential in an anatomical site with respect to a reference. The three increased leads belong to unipolar group, also known as aVR, aVL and aVF, obtained as the combination of the three main leads and the six precordial indicated as V1, V2, V3, V4, V5 and V6 and represented by the placement of the electrodes in the torso area (*precordium*).

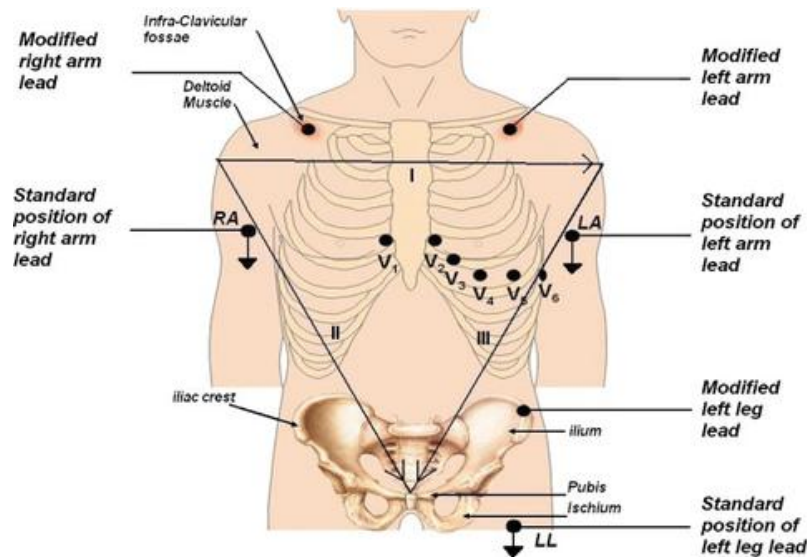


Figure 1.7: Placement of 12-Lead ECG electrodes.

As already mentioned, ECG is to date the main test that is carried out to assess cardiac activity. This type of examination is intrusive, as electrodes must be placed on the patient. Although the simplest monitoring activity requires the use of two electrodes, the problems that the patient faces are as follows:

- for each monitoring session, the electrodes must be positioned carefully so that they do not come off;
- carrying out the activity of the day with the burden of cables;
- possible skin irritation due to electrode placement;
- not negligible cost of the device and replacement electrodes;
- patient acceptability of wearing a device in direct body contact.

The aim of this work is to release the subject from the main disadvantages of the ECG technique, thus making easy to perform the cardiac monitoring in home or hospital bed, in a way completely non-intrusive, non-invasive and especially not expensive.

1.4 Ballistocardiography

Ballistocardiography is a non-invasive technique based on the detection of the human body motion caused by the ballistic forces (recoil and impact) associated to the ejection of blood at each cardiac cycle. Through this method it is possible to identify the cardiac rhythm or some anomalies of the circulating system, recording acceleration, velocity or displacement of the blood flow.

The term ballistocardiography is composed by three words: *ballisto* refers to the Latin *ballista*, which derives from the Greek word *ballein* (to throw), while *cardio* and *graphy*, both derive from Greek words *kardio* and *grafia*, which mean heart and writing, respectively.

1.4.1 The birth of the ballistocardiography

In 1877, Gordon was the first to observe a correlation between the motion of the human body and the heartbeat. He discovered that standing on a spring weighing scale, periodic movements were shown by the readout needle. Gordon noticed that these swinging were synchronous with his heartbeat [12]. Therefore, he began to perform some experiments recording the swinging from a person standing erect. Afterwards, he changed his setup constructing a suspended swinging bed, held by four ropes.

In 1905, Yandell Henderson published a work quite similar to the Gordon's design [13]. He used a 9 kg suspended table supported by four steel wires capable of moving just in one direction. Nevertheless, the system proposed by Henderson encountered some issues, for example the natural frequency of the bed was very low, which was superimposed to the breath signal. Due to this reason, Henderson asked the volunteers to stop breathing during the trial, but then he was able to remove the breathing signal instructing the subjects to make different tasks.

In 1939, Isaac Starr designed a modified suspension bed platform. Thanks to that he achieved significant results [14]. Starr constrained the end of the bed with a still spring. In this way he was capable of increasing the natural frequency of the system, in order to minimize the problems related to the breathing. Starr is considered the pioneer in this field, describing in a detailed manner the signal's morphology and its physiological meaning [14]. Even if he inspired several researchers, they lost the interest for this field. In fact, the number of publications related to ballistocardiography decreased drastically up until the 1980s, almost disappearing at the end of the 1990s. This was probably due to [15]:

- a lack of standard measurement systems;
- a lack of clear physiological meaning;
- low specificity and reliability for the identification of pathological conditions;
- arising of others diagnostic methodologies, such as electrocardiography.

However, in the last two decades, ballistocardiography aroused interest among researchers again. Accomplice of this phenomenon is certainly the meaningful development of technology, in terms of sensors and new sophisticated algorithms. Moreover, the BCG, as a non-invasive method relying on unobtrusive sensors, represents a valid solution to monitor patients' cardiovascular activities directly in their home place.

1.4.2 BCG signal

During the cardiac cycle, the heart impels blood at considerable speed into the aorta. More specifically, during early systole, blood is pushed into the aorta towards the head. Once past the aortic arch, in late systole, blood flows to reach the peripheral vessels. In both cases, a recoil force is developed due to Newton's third law of motion. Ballistocardiographs simply record the action that develops as a result of this phenomenon, in terms of displacement, velocity, or acceleration [16].

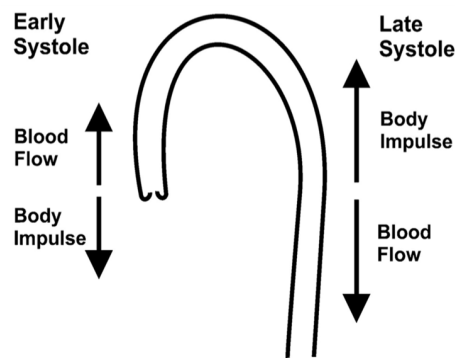


Figure 1.8: Arch aortic and force vectors.

In 1956, the Committee on Ballistocardiographic Terminology decided to use the nomenclature proposed by Starr *et al.* in [14]. Therefore, the BCG signal was labelled with the capital letters from G to O. Before explaining in detail the ballistocardiogram, a bare introduction of the BCG signal (Fig. 1.9) is provided in order to show the signal's morphology:

- **H-I wave:** it represents the blood flow directed to the head (opening of the aortic valve);
- **I-J wave:** it represents the blood flow which is pushed towards the feet, therefore the trend is opposed than the H-I waves;
- **J-K wave:** it represents the blood flow which passes through arteries, therefore the trend changes again (closing of the aortic valve);
- **K-L-M-N-O wave:** this complex represents the dampening of the BCG signal.

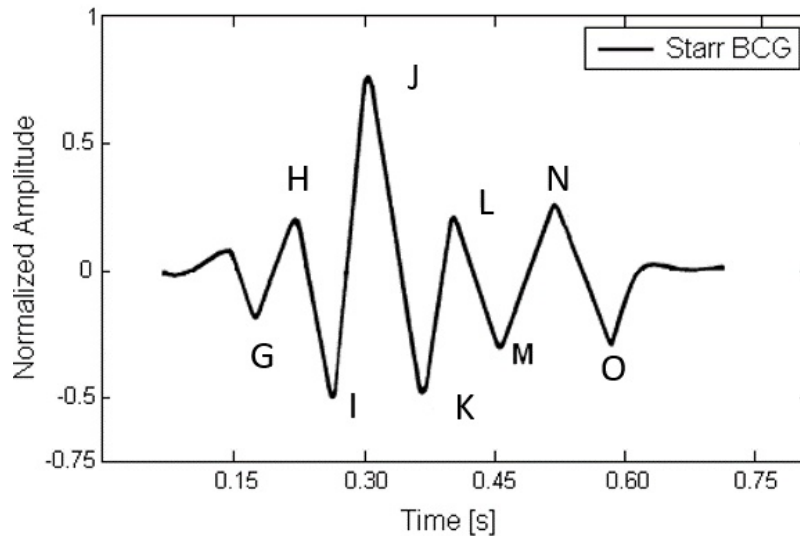


Figure 1.9: BCG signal nomenclature proposed by Starr.

However, the different waves of the BCG signal are classified in three different clusters: *Pre-Systolic Group*, *Systolic Group* and *Diastolic Group* [17]. These groups include the BCG waves named with the capital letters according to the convention aforementioned proposed by the Committee on Ballistocardiographic Terminology.

1.4.3 Physiological meaning of the BCG signal

As anticipated, the BCG is associated to the cardiac phases and it may be divided in the following three groups [17]:

Pre-Systolic Group

The stage which precedes the contraction of the heart is described by the pre-systolic group. The **F wave** is a positive deflection, rarely seen on the ballistocardiogram, originated by atrial contraction. The **G wave** is a small foot-ward wave which is associated to the atrial systole and it comes earlier than the H wave. Compared to the ECG signal, the G wave precedes the QRS complex and follows the P wave.

Systolic Group

During the systole, the heart pumps the blood into the arteries. This activity is seen by the systolic group, characterized mainly by the H, I, J and K waves. The **H wave** is a head-ward deflection which can be seen at the beginning of ejection. The **I wave** is a foot-ward deflection which is associated with ventricular eject. The most dominant wave which can be seen clearly on the ballistocardiogram is the **J wave**. The J wave occurs after the QRS complex, later in systole. The end of systole is identified by the **K wave**, which occurs due to the systemic circulation.

Diastolic Group

In this stage the heart relaxes and fills its chamber with blood. This phase is characterized by the **L, M, N** and **O waves**, which are very dumped. For this reason, these waves may not be shown on the ballistocardiogram.

The BCG signal, being of mechanical origin, can be measured through several sensors, which exploit the swinging of the human body, transducing it into an acceleration, a voltage, a wavelength variation, etc. Moreover, the BCG signal in a healthy subject does not assume always the same shape, but there is a strong difference among different subjects. Therefore, the association between the physiological meaning and the ballistocardiogram is always valid, but not clearly visible in every BCG trace.

1.4.4 Mechanical Differences in the first Ballistocardiograph Designs

In 1956, Scarborough and Talbot made a revisitation and extension of the ballistocardiographic nomenclature and conventions. The first classification of the ballistocardiographs was based on the natural frequency related to the weight and the stiffness of the system [17]. At the time, it was really useful making this classification, because the first approach to the BCG was similar among all the researchers. Therefore, the BCG system were classified in:

- **Ultra low-frequency BCG (UF-BCG):** a platform or hammock supports the body. The system is slightly dumped and the natural frequency is in range 0-0.5 Hz.
- **Low-frequency BCG (LF-BCG):** the LF-BCG design is quite similar to the UF-BCG. The natural frequency of this system is in range 1-2 Hz. Unlike the ULF-BCG system, dumping is critical or more than critical.
- **High-frequency BCG (HF-BCG):** the system does not present external dumping and the fundamental frequency is higher than the UF-BCG and LF-BCG; it is in range 3-9 Hz.
- **Direct Body Ballistocardiographs (DB-BCG):** the body is usually coupled with a rigid flat surface. Therefore, the mechanical characteristic are those of the human body. The frequency are rather similar to those of HF-BCG.

The UF and LF-BCG are affected from one main drawback: their low frequencies superimpose the respiratory component. For this reason, it is required fine control of the subject's respiration. However, these systems had higher bed displacement, which did not require high amplification. On the other hand, HF-BCG system permits a normal breathing, but smaller bed displacement are possible, which required high amplification.

Displacement records from several BCG system are shown in Fig. 1.10. The HF-BCG (I) is really similar to the DB-BCG system (II), but looks quite different to the UF-BCG (IV) systems. Moreover, the signal can be described up to the M wave, because after that the waves became too damped.

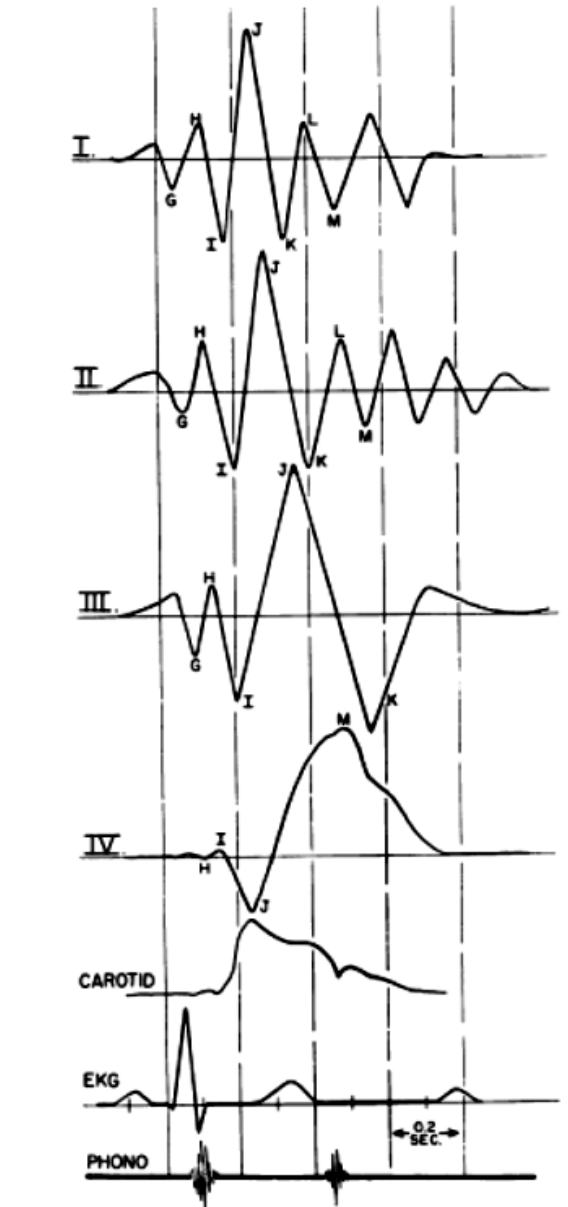


Figure 1.10: Displacement records from BCG systems (I-IV) compared to carotid pulse, EKG and phonocardiogram: I) HF-BCG, II) DB-BCG, III) LF-BCG, IV) UF-BCG.

1.4.5 End of the classical Ballistocardiography

The BCG reached strong interest among the researchers from the 1930s to 1970s. They sought to demonstrate the usefulness and the clinical efficacy of this new methodology. However, the emergence of much more reliable diagnostic techniques, such as ECG, played a fundamental role in the reduction of research and development of ballistocardiographic systems. Interest in BCG also waned due to the small steps that technological development was taking at that time. Therefore, in these years a real first cycle ended which marked the beginning of a real revolution in the field of non-invasive monitoring.

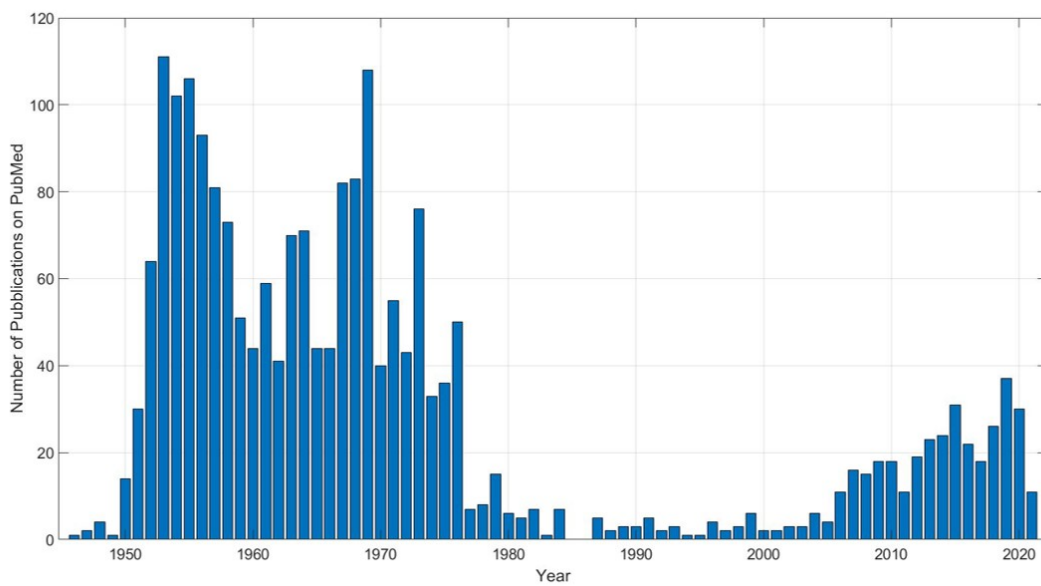


Figure 1.11: Number of Ballistocardiography Publications on PubMed over the years.

1.4.6 State of the Art

The first era of BCG focused on the various methods of signal acquisition, developing systems that were rather difficult to replicate in patients' home environments. At the time, the main purpose was to be able to associate the BCG signal with a physiological meaning. This was the main result achieved at the end of the 50s. Due to the type of technology, it is not possible to identify a real ballistocardiographic device attributable to this period.

In recent years, capturing the BCG signal has become an increasingly appealing challenge that has gained interest among researchers around the world. Several studies attest that the rhythmic activity of the heart was recorded through BCG sensors integrated in mattresses, pillows, beds, chairs, or even weighing scales. Because of these numerous acquisition methods, BCG signal analysis is a challenging process. However, to date the most used sensors for the acquisition of the ballistocardiographic signal are: polyvinylidene fluoride film-based sensors, electromechanical films, strain Gauges, hydraulic sensors, microbend fiber-optic sensors as well as fiber Bragg grating [18]. In the following paragraphs the main characteristics of the newly introduced BCG sensors are reported.

Piezoelectric polyvinylidene fluoride-based sensor

Polyvinylidene fluoride (PVDF) is a high performance partially fluorinated thermoplastic polymer. Due to its piezoelectric properties, this material is exploited in speaker components and sensors. A typical sensor made of PVDF is a fragile film, causing a mechanical bending when subjected to a pressure, thus resulting in a displacement of negative and positive charges in the center of the film. For this reason, the transduction of a pressure in a charge proportional to the applied pressure is obtained. Since PVDF is a very sensitive material, it is possible to detect the small oscillations of the body due to the cardiac activity of the heart [19].

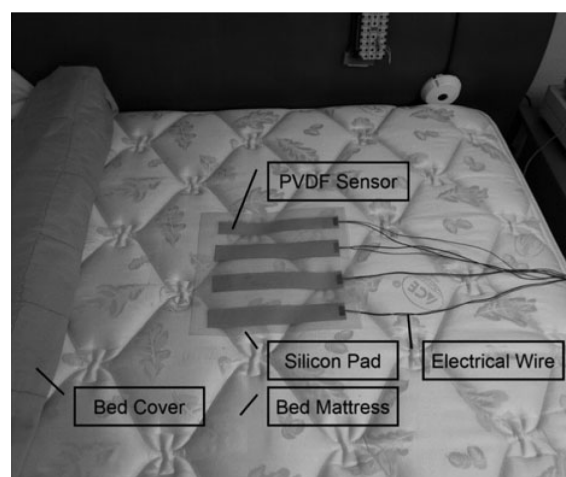


Figure 1.12: Example of PVDF sensor.

Electromechanical film-based sensors

ElectroMechanical Film (EMFi) is a thin, flexible polypropylene film that can function as a sensor or actuator. It is covered with enduringly polarized and electrically conductive layers. EMFi is sensitive to the force that is exerted perpendicular to the surface of the film. When a force is applied to the film, a charge is created on the conductive surface of the sensor, which can be measured as a voltage or a current. EMFi can hold the charge for a long time and therefore this can cause overheating and deterioration of the sensor itself. At the same time, several studies show that is possible to exploit this type of sensor for the detection of the ballistocardiographic signal [20].



Figure 1.13: Example of two EMFi strips.

Pneumatic-based sensors

A pneumatic system is a system that uses compressed air to transmit and control energy. In this case, the ballistocardiogram is related to the rhythmic movement of the air trapped in a cushion placed between two surfaces, i.e. bed and mattress. Several researchers have demonstrated how this system is able to measure heartbeat, respiration, snoring and body movements [21].

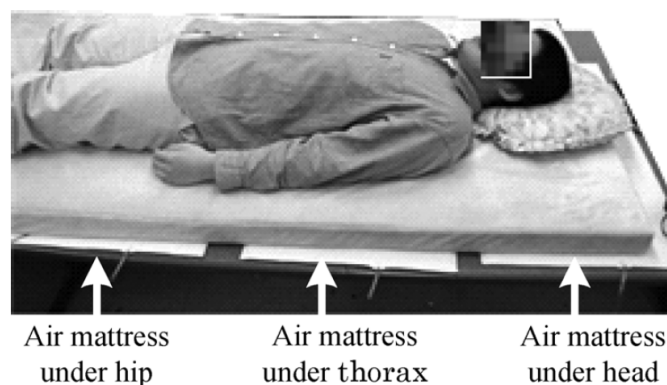


Figure 1.14: Application of Pneumatic-based sensor.

Strain-gauge based sensors

Strain gauge is a measuring instrument used to detect small dimensional deformations of a body subjects to mechanical or thermal stress. Generally, these types of sensors, built into scales or mattresses, are able to detect the cardiac activity of the heart, such as small movements or forces applied by the subject, and to transduce them into a variation of resistance [22].

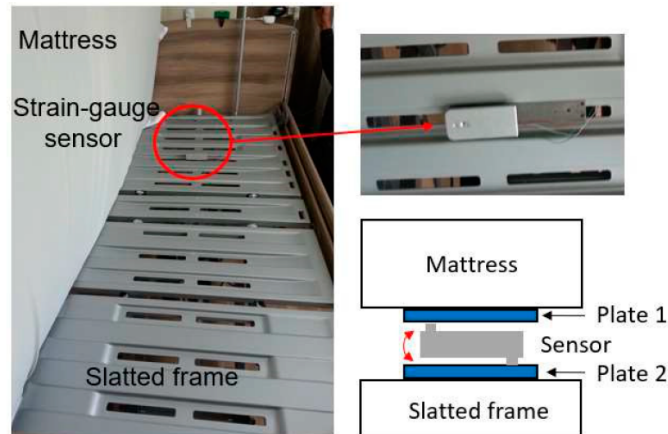


Figure 1.15: Example of measurement setup and Strain-gauge sensor location.

Hydraulic-based sensors

Hydraulic sensors are generally integrated into the beds. These sensors consist of a pressure sensor connected to the end of the transducer, and are suitable for recording the vibration of the discharged hose. The system provides a measurement range that goes from 0 to 10 kPa, perfectly compatible with the pressure that is exerted by a body and transferred to the system consisting of the sensor and the bed. With the proper sensitivity, the hydraulic sensor is thus able to evaluate the low pressure changes due to the heartbeat [23].

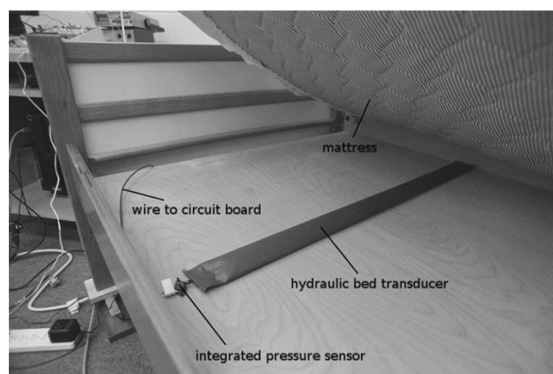


Figure 1.16: Example of Hydraulic-based sensor placed between the bed and the mattress.

Fiber optic-based sensors

Fiber Bragg grating sensors (FBGS) are the most widely used fiber optic-based sensors for ballistocardiographic signal detection [24]. Basically, the FBGS is an optical fiber used as a filter for a specific wavelength. The wavelength shift is due to the change in temperature, voltage or pressure, detected by the FBGS. Because light does not interact with magnetic fields, several authors have shown how these fibers are able to detect the BCG signal in patients lying on MRI beds [25].

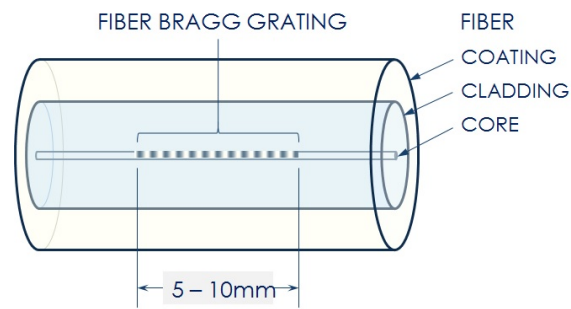


Figure 1.17: Example of a Fiber Bragg grating sensor (FBGS).

Accelerometer-based Sensor

This work addresses a sensor network based on accelerometers, thus an in-depth section describing this kind of transducers follows next.

An accelerometer is a measuring instrument capable of detecting and/or measuring acceleration by performing a calculation of the force affecting the mass of the object (force per unit mass). Typically, an accelerometer is modelled by a mass-spring-damper system shown in Fig. 1.18, where:

- m is the mass;
- k is the spring constant;
- c is the damper coefficient;
- x is the displacement.

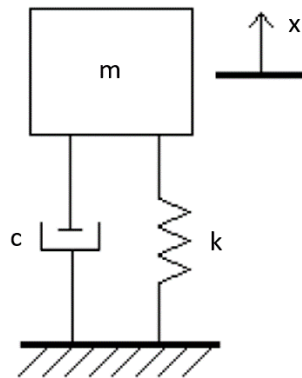


Figure 1.18: Mass-spring-damper model of an accelerometer.

The equation describing the system depicted in Fig. 1.18 is as follows:

$$m\ddot{x}(t) + c\dot{x}(t) + kx(t) = ma(t) \quad (1.1)$$

Eq. 1.1 represents a second-order differential equation. In the time domain, the solution of this equation is a function.

In the frequency domain a second-order system has the following response:

$$H(s) = \frac{1}{s^2 + \zeta\omega_n s + \omega_n^2} \quad (1.2)$$

where:

- ζ is the damping ratio;
- $\omega_n = \sqrt{k/m}$ is the natural frequency of the system.

In general, accelerometers operate in the frequency range of the band represented by a horizontal line in Fig. 1.19, region indicated as *useful frequency range*.

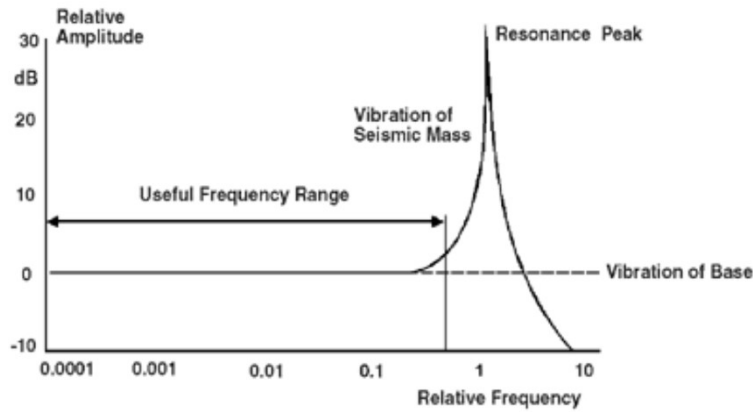


Figure 1.19: Typical frequency response of an accelerometer.

In this area the acceleration is proportional to the displacement measurement:

$$x = \frac{ma}{k} \quad (1.3)$$

The displacement that is measured by the accelerometer is relative to the axis being considered. Devices that are able to derive acceleration along a single axis are called *uni-axial*, while accelerometers that derive acceleration along three axes are called *triaxial*. However, four *biaxial* inclinometers were used in this work. An inclinometer is a linear accelerometer with a reduced measuring range generally used to detect slope, or inclination, due to its high sensitivity to variations of the gravitational acceleration. Since the BCG signal has an amplitude ranging from 0 to 7 mg [26], not all accelerometers could detect this signal. In addition, these types of measurement devices are greatly affected by noise and motion artifacts.

An acceleration measurement can occur if the voltage generated by the sensor has an amplitude greater than the voltage related to noise acceleration, a_{min} given by the following relation [27]:

$$a_{min} = \frac{\text{Noise Voltage}}{\text{Sensitivity}} \quad (1.4)$$

Therefore, high sensitivity values are needed to detect small accelerations.

The noise density is among the descriptive parameters found on the datasheets of various accelerometers. This is one of the characteristics related to the quality of this kind of device. Generally, low values of this parameter are associated with better performances of the device. The noise density can be expressed as:

$$N = \frac{a_{min}}{\sqrt{f}} \quad (1.5)$$

where f is limited by the natural frequency of the sensor $f_0 = \frac{\omega_n}{2\pi}$.

Studies in [28] and [29] use inertial devices for BCG detection. Nevertheless, to date there are several devices on the market that provide some parameters related to cardiac activity from the BCG signal. Among these, none of them relies on an inertial sensor (Tab. 1.1).

	Emfit QS	Beddit	Withings	Sleepace Reston	Beautyrest	Juvo
HR	YES	YES	YES	YES	YES	YES
HRV	YES	NO	NO	NO	NO	NO
Respiration	YES	YES	YES	YES	YES	YES
Breathing disturbances	NO	NO	YES	NO	NO	NO
Sensor Type	EMFi	Piezoelectric force sensor	Piezoelectric force sensor	Piezoelectric force sensor	Piezoelectric force sensor	Microbend fiber optic

Table 1.1: Examples of consumer bed-based sleep monitoring devices.

However, the designed system is based on a multi-sensor inertial network. This choice made it possible to overcome the main limitations affected by other types of transducers, for example:

- compared to FBGS, accelerometers are mechanically more robust;
- the dimensions of the inertial sensors are much smaller than those of pneumatic-based and hydraulic-based sensors;
- compared to EMFi and PVDF sensors, no external pressure (i.e. the weight of the subject lying on the bed) acts on the designed system. The inclinometers are positioned on the mattress and therefore do not suffer from this problem;
- compared to devices on the market, the proposed system consists of multiple transducers.

Ultimately, the designed system is easily transportable in a common bag and the users can easily assemble it by themselves. Therefore, the proposed system is an excellent candidate to perform the heart rate measurement in a non-invasive and non-intrusive way in the home or hospital environment.

Chapter 2

Materials and Method

The aim of this work is to detect the heart rate from the ballistocardiogram, exploiting an inertial multi-sensor network produced by the company STMicroelectronics. The inertial sensors used were four IIS2ICLX inclinometers, embedded in a bed-based recording system and wired-connected to the STEval-STWINKT1 through a SPI interface. The target is to assess if a network of sensors could detect the BCG signal for a sleep cycle and for any position that the subject could assume (i.e. supine, prone, etc.).

The project divides into four main steps:

- **Hardware Design;**
- **Firmware Design;**
- **Signal Capture;**
- **Data Processing.**

2.1 Hardware Design

Of all the sensors that are used for BCG signal acquisition, inertial sensors are certainly the least used. One of the possible reasons could be that a sensor of this type should have a high resolution and a low noise level. Therefore, these two parameters played a key role in the choice of the sensor. In order to choose the most suitable device for this application, it was necessary to evaluate the main inertial sensors produced by STMicroelectronics, simply by visiting the company website and comparing the characteristics of each one described on their datasheet. From this analysis it turns out that the sensors with the best features are the inclinometers IIS3DHHC [30] and the IIS2ICLX [31]. After the most suitable sensors for this application were identified, their main characteristics were compared with the inertial sensors used in the literature.

	STMicroelectronics				
	SCA61T1H1G [32]	ADXL362 [33]	ADXL355 [34]	IIS3DHHC [30]	IIS2ICLX [31]
Supply Voltage [V]	4.75 - 5.25	1.6 - 3.5	2.25 - 3.6	1.71 - 3.6	1.71 - 3.6
Min. Acceleration Range [mg]	± 1	± 2	± 2	± 2.5	± 0.5
Sensitivity [mg/LSB]	1.221	1	3.907	0.076	0.015
Noise Density [$\mu\text{g}/\sqrt{\text{Hz}}$]	8.89	550	22.5	45	15

Table 2.1: Comparison between the inertial sensors used in the literature and the inclinometers produced by STMicroelectronics.

The IIS2ICLX model has been chosen.

2.1.1 IIS2ICLX inclinometer

The IIS2ICLX inclinometer is a high-accuracy (ultra-low noise, high stability and repeatability) and low-power two-axis linear accelerometer with digital output. The IIS2ICLX has a selectable full scale and is capable of providing the measured accelerations to the application over an I²C or SPI digital interface [31].

More in detail, the main features of the IIS2ICLX inclinometer are:

- **Number of axis:** 2 (X-axis and Y-axis);
- **Dimensions:** 5 × 5 × 1.7 mm;
- **Sensitivity:**
 - 0.015 mg/LSB with a full scale of ± 0.5 g;
 - 0.031 mg/LSB with a full scale of ± 1 g;
 - 0.061 mg/LSB with a full scale of ± 2 g;
 - 0.122 mg/LSB with a full scale of ± 3 g;
- **Noise density:** 15 $\mu\text{g}/\sqrt{\text{Hz}}$;
- **Supply voltage:** 1.71 - 3.6 V;
- **Current Consumption:** 420 μA and 3 μA during power-down;
- **Bandwidth:** 0 - 260 Hz;
- **Temperature range:** -40 to 105 C°.

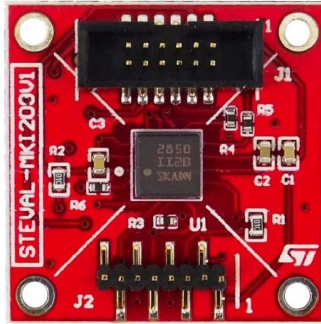


Figure 2.1: STEVAL-MKI209V1K and the IIS2ICLX inclinometer.

In this work, the STEVAL-MKI209V1K evaluation board was used [35]. It has an embedded IIS2ICLX inclinometer sensor, which is connected through a flat cable to a simple adapter board, the STEVAL-MKIGIBV2. As shown in Fig. 2.1 the sensor is soldered precisely in the center of the board. The STEVAL-MKI209V1K allows to communicate with the inclinometer through the use of the STEVAL-MKIGIBV2 adapter board, which makes all of the sensor pins accessible in a fairly simple way, allowing to plug the adapter into a compatible socket.

In general, the sensor IIS2ICLX is used for the following applications :

- precision inclinometers;
- antenna pointing and platform leveling;
- structural health monitoring;
- precise leveling instruments;
- installation and monitoring of equipment;
- robotics and industrial automation.



Figure 2.2: STEVAL-MKIGIBV2 adapter board.

2.1.2 STEval-STWINKT1

The STEval-STWINKT1, common named as STWIN (Sensor Tile Wireless Industrial Node), is a development kit and reference design that simplifies prototyping and testing of advanced industrial IoT applications such as condition monitoring and predictive maintenance [36].

This development board features the STM32-L4R9I6 microcontroller, the thinking unit of the system. The STM32L4R9ZI devices is an ultra-low-power microcontroller (STM32L4+ Series MCU) based on the highperformance Arm Cortex-M4 32-bit RISC core, which operates at a frequency up to 120 MHz. In fact, this microcontroller is recommended for those applications that require low power consumption, but at the same time high performance. Considering that this work is designed for a long time monitoring application, the chosen microcontroller fully meets the desired requirements.

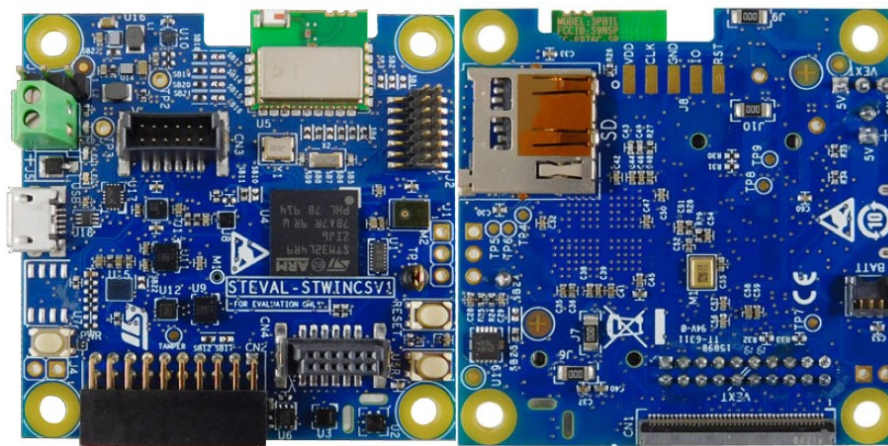


Figure 2.3: STWIN Core System board top and bottom.

In addition, the STWIN board includes the following sensors:

- HTS221 relative humidity and temperature sensor;
- LPS22HH digital absolute pressure sensor;
- STTS751 low-voltage digital local temperature sensor;
- TS922 rail-to-rail, high output current, dual operational amplifier;
- IIS3DWB ultra-wide bandwidth (up to 6 kHz), low-noise, 3-axis digital vibration sensor;
- IIS2DH ultra-low-power high performance MEMS motion sensor;
- IIS2MDC ultra-low-power 3-axis magnetometer;
- MP23ABS1 analog MEMS microphone;
- IMP34DT05 industrial grade digital MEMS microphone.

Regarding connectivity, the STWIN can communicate with other devices through the Bluetooth® Smart v4.2 protocol or via WiFi by connecting the STWIN to the appropriate connector STEval-STWINWV1 Wi-Fi expansion board, not included in the STEval-STWINKT1 kit.

The STWIN components that have been exploited in this project are as follows:

- 480mAh 3.7V Li-Po Battery: to avoid plugging the device into an electrical outlet;
- STMOD+ connector: in order to connect the four IIS2ICLX inclinometers using the SPI interface easily accessible from this connector;
- microSD card socket: necessary for saving data during the acquisition phase of the BCG signal;
- green and orange leds: in order to give a visual feedback to the user about the recording session;
- buttons: to turn the device on and off (PWR button), to start (RESET button) and to stop data acquisition (USR button).

The STMOD+ connector plays a fundamental role for the system that provides the connection between the microcontroller and the four accelerometers. In fact, through this connector it is possible to power the inclinometers and to exploit the SPI interface to make the communication happen. The power supply voltage on this connector, indicated in the datasheet as V_{ext} and selectable by the jumper J3 of the STWIN, can be at minimum 3.7 V (if the board is powered by the supplied battery) and at maximum 5 V (if the board is connected to the mains or to a PC). As reported in the previous paragraph 2.1.1., the inclinometers can be powered at a maximum voltage of 3.6 V, therefore, in order to use the power supply lines of this connector, the following board modification has been necessary: the central pin V_{ext} of the voltage selector has been soldered on the test point TP3, which provides a continuous voltage of 3.3 V and thus inhibiting the use of jumper J3.

2.1.3 Communication interface between STWIN and IIS2ICLX

To allow communication between the STWIN and the four IIS2ICLX inclinometers, the SPI protocol accessible from the STMOD+ connector of the development board was exploited.

The Serial Peripheral Interface (SPI) is a communication bus developed by Motorola. The master controls the bus, emits the clock signal and decides when to start and to stop the communication [37].

Typically, the SPI protocol is based on four signals which are:

- **MOSI (Master Out Slave In):** through this line the information travels from the Master to the Slave;
- **MISO (Master In Slave Out):** through this line the information travels from the Slave to the Master;
- **SCLK (Serial Clock):** the clock signal, that provides the time base for communication, is shared on this line;
- **SS (Slave Select):** whenever the master decides to communicate with the slave this line changes state, generally the switching is from logic high state to logic low state.

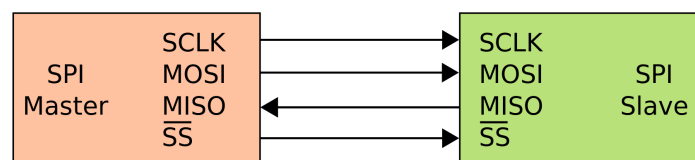


Figure 2.4: SPI bus: example of connections between a single-master and a single-slave.

Fig. 2.4 shows an example of connection between a single-master and a single-slave. Whatever the case, it is possible to interface more slaves to the master by sharing the same SS or increasing the number of SS, one for each peripheral. The first method, also known as the *Daisy Chain*, involves communication between a master and multiple slaves by sharing the same SS. This type of connection allows the number of lines to the SS to be minimized, but if this line was to be damaged the communication between the master and slaves would be completely gone. The second method requires the connection between the master and the slaves to be made via dedicated SSs, one for each peripheral. Regarding this, if the connection between a peripheral and the master were interrupted, the other slaves involved could continue to communicate with the master. The main drawback of this method is that for each slave a physical line for the SS is required .

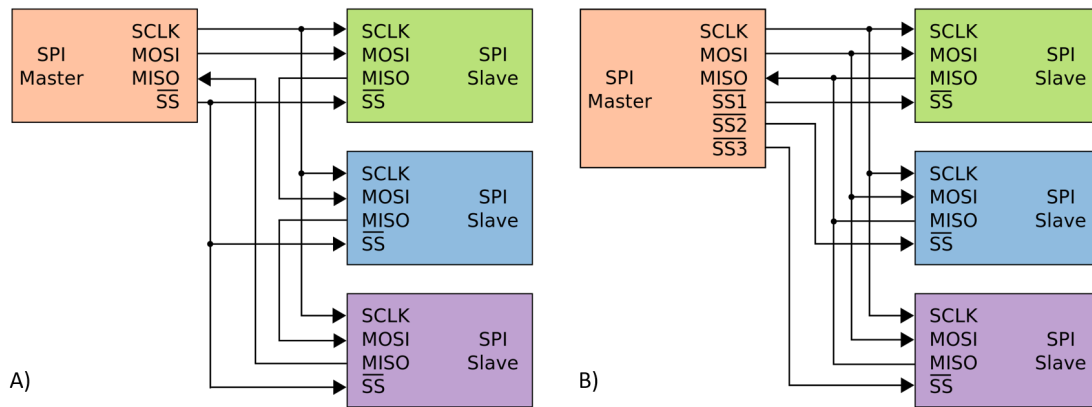


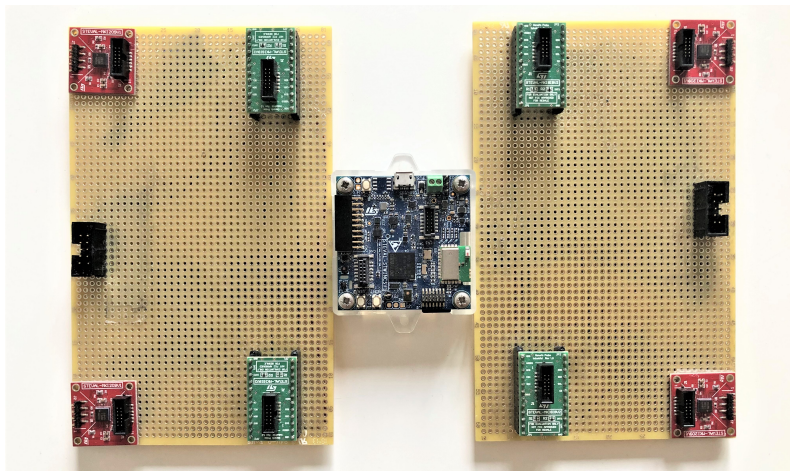
Figure 2.5: Example of connection between master and three slaves: A) SS shared between slaves (i.e. *Daisy Chain* configuration); B) SS independent for each slave.

Since this work involves the connection between four sensors, a configuration with four separate SSs lines has been chosen for the SPI interface, in order to guarantee communication between the STWIN (master) and each IIS2ICLX inclinometer (slaves).

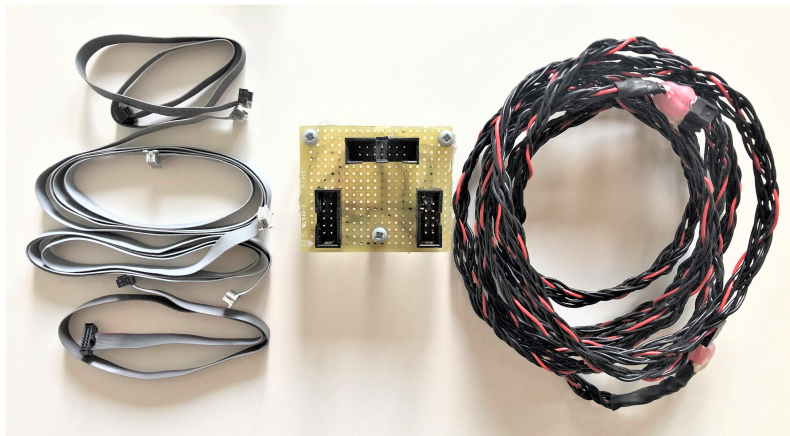
2.1.4 Acquisition System

The prototype system was built in the STMicroelectronics laboratory, exploiting the components presented in the previous paragraphs. Two stripboards were used to connect the four inclinometers, one for each pair of sensors. On each of these two sockets have been soldered, in order to plug the STEval-MKIGIBV2 adapter boards, fundamental for the communication of the four sensors through the appropriate flatcables. The common lines (i.e. power supply, ground, MISO, MOSI, CLK) and the SSs lines, were soldered to a male IDC connector. This configuration allows the signals from each stripboard to be collected into a bridge-board designed to connect the STWIN.

The setup just described is shown in Fig. 2.6.



(a) The STWIN and the two stripboards with the four IIS2ICLX inclinometers and the STEval-MKIGIBV2 adapter boards.



(b) The four flat cables (on the left); the bridge-board (at the center) and the cable used (on the right).

Figure 2.6: The prototype system.

2.2 Firmware Design

The microcontroller has been programmed using the C programming language and exploiting the KEIL integrated development environment (IDE). The implemented firmware allows the microcontroller to perform the following tasks:

- capturing data from each sensor;
- saving the acquired data on a microSD;
- providing feedback to the user by blinking LEDs;
- battery management.

2.2.1 Brief firmware description

Once the device is turned on it is possible to capture data from each sensor. This occurs exclusively in the presence of the micro SD card. The start of the recording is confirmed by the blinking of two leds: the orange led confirms that the micro SD card is correctly inserted and the green led confirms that the data saving is taking place successfully. The USR and RESET buttons are used to stop and to start recording respectively. Data acquisition is performed according to the "polling mode", i.e. the data is read from the single register of each sensor and, in this case, they are saved in a CSV file stored in the micro SD card. The recording times are managed by a timer, which enables the request of the data to the four sensors every 0.025 s, allowing the microcontroller to sample data at a frequency of 40 Hz. Moreover, in order to verify that the timing of acquisitions complies with the specifications, the program records the timestamp, the time instant in which the data is acquired. A typical example of the data returned by the microcontroller is shown in Tab. 2.2.

X1	X2	X3	X4	Y1	Y2	Y3	Y4	Timestamp
[mg]	[10 ⁻⁶ s]							
-2.90	7.19	-9.62	4.10	19.99	-2.20	6.19	-8.81	91067201158

Table 2.2: Examples of acquired data from the BCG system.

2.2.2 Firmware Flowchart

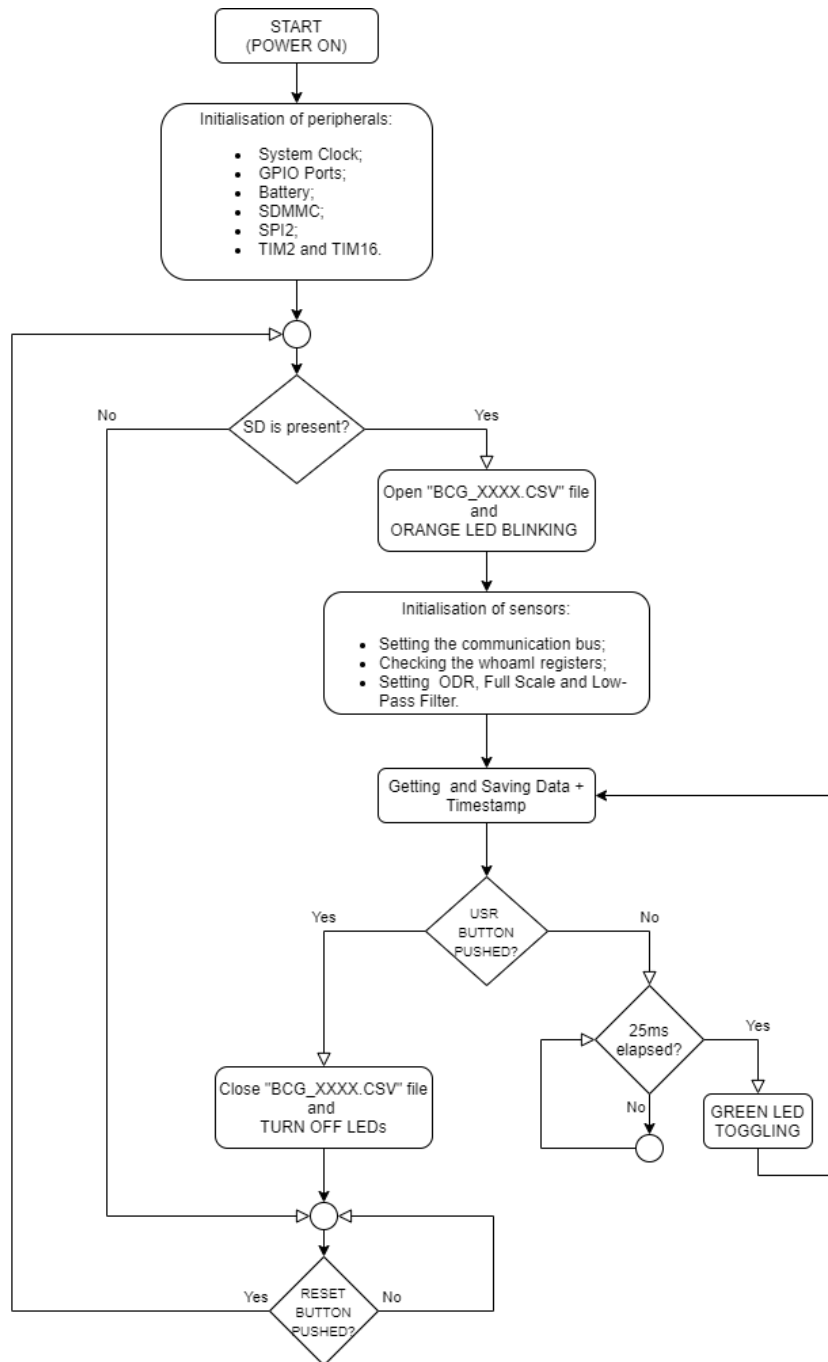


Figure 2.7: Firmware flowchart.

2.3 Signal Capture

2.3.1 Sensors Placement Evaluation

The system described in the previous paragraphs is the one used to record the ballistocardiographic signals of several subjects lying on the bed. The identification of the best areas where to place the four sensors has been a relevant part of this study. Initially, the coupling between the sensors and the mattress has been decided, by paying attention to the sources that could introduce noise. The first tests were carried out by positioning the sensors directly between the mattress and the mattress cover. The next step was to identify the best signal by performing a qualitative analysis, i.e. evaluating the morphology of the BCG signal for each sensor position. To do this, four regions have been identified: head, shoulders, hip and legs. Each region was subdivided into other sub-areas, and in each of these the sensors were placed in order to record, and subsequently to evaluate, the quality of the signal.

Fig. 2.8 shows the protocol just described for evaluating the best positions.

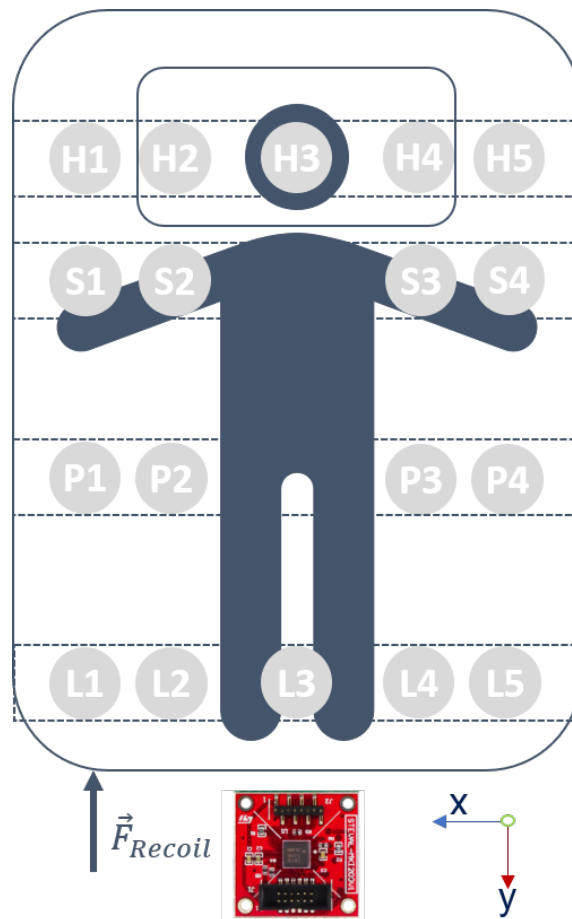


Figure 2.8: Evaluation of the sensor placement in the four identified positions: head (H*), shoulders (S*), hip (P*), and legs (L*), where "*" indicates the i -th sub-areas. The recoil force vector related to the BCG and the sensor orientation are shown at the bottom of the figure.

From this analysis it was possible to identify the best four sensors positions and the best inclinometer axis. In accordance with the direction of the recoil force, the Y axis represents the axis that gives more information, being parallel to the recoil force axis. This consideration reflects the study performed by Gubner *et al.* [38]. In addition, it was noted that the BCG is also visible on the X-axis. On the other hand, the X-axis is very sensitive to respiratory activity, which, however, was not addressed in this study. Ultimately, the head and the legs were the chosen regions, because the BCG signal has a better peak-to-peak amplitude and morphology than the other regions. The sub-areas chosen are those indicated in Fig. 2.8 with H1, H5, L1, and L5, i.e. the areas that are closest to the corners of the mattress. This choice allows to obtain two fundamental benefits: the first concerns the quality of the signal and the second concerns the minimum encumbrance of the sensors on the mattress, and consequently less discomfort for the subject.

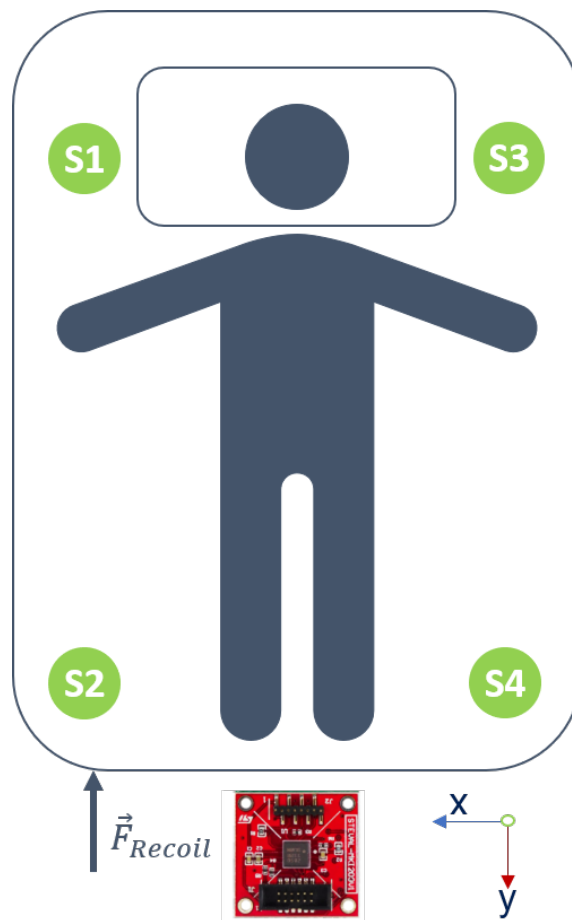


Figure 2.9: Representation of the four IIS2ICLX inclinometers in the four chosen positions.

Note that the nomenclature of Fig. 2.9 changes from Fig. 2.8 solely to make it easier to read. From this moment on, the Y1 and Y3 axes refer to the sensors positioned, respectively, on the right and left sides of the subject in supine position at head level. Following the same logic, the Y2 and Y4 axes refer to the sensors positioned at leg level.

A real example of the designed system configuration is shown in Fig. 2.10.



Figure 2.10: Real configuration of the four IIS2ICLX inclinometers.

2.3.2 Acquisition Protocol

The acquisition protocol requires sensors to be placed in the four identified zones of the mattress. After this, the subjects can lie down on the mattress and sleep in their preferred position. Regarding the duration of the acquisitions, this turned out to be dependent from subject to subject. However, the signal processing phase, which will be explained later, will not take into account the first 30 minutes and the last 30 minutes of the signal.

2.3.3 Dataset Acquisition Phase

The performance of the algorithm described later has been evaluated using a data set of 9 recordings from healthy volunteers, including 7 men and 2 women. The main subjects characteristics are summarized in Tab. 2.3.

Subject	Gender	Age	Height [cm]	Weight [kg]	BMI [kg/m ²]
1	Male	25	180	80	24.69
2	Female	23	155	46	19.15
3	Male	25	165	60	20.57
4	Female	27	164	54	20.08
5	Male	22	183	63	18.81
6	Male	31	179	73	22.78
7	Male	26	173	67	21.05
8	Male	24	169	67	23.46
9	Male	25	178	73	23.04

Table 2.3: Subjects characteristics.

2.4 Data Processing

Data processing was performed by using the MATLAB 2021 development environment, using the Signal Processing Toolbox™ package.

2.4.1 Data Processing Flowchart

Below there is the flowchart that summarizes all the main phases of data processing.

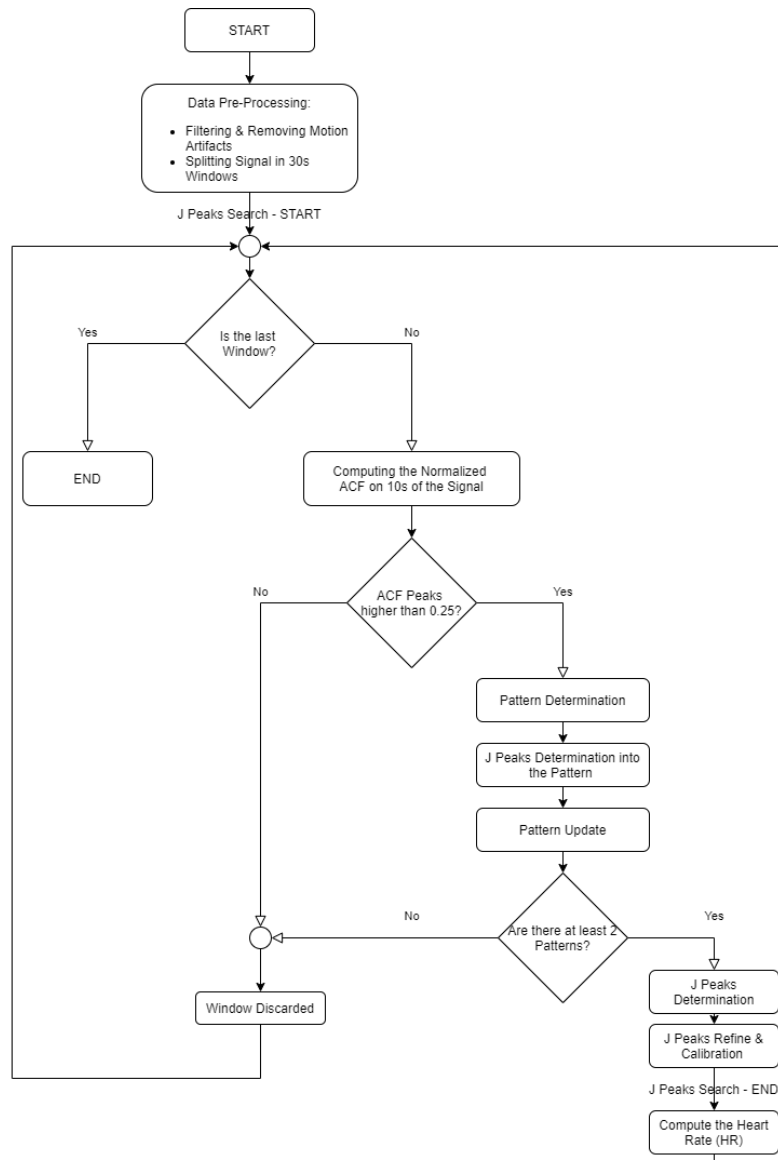


Figure 2.11: Data Processing Flowchart.

2.4.2 Acquisition Timing Evaluation

The issue related to timing is among the most important specifications that must be met during the signal acquisition. In this project, the two pairs of inertial sensors are placed at a distance of 180-200 cm, depending on the size of the mattress. This distance introduces a delay for signal acquisition. However, by checking the timing of data acquisition from each individual sensor, it is found that the time interval between data acquired from each pair of sensors is much smaller than the desired sampling interval, therefore this delay has been neglected. The timing for data acquisition is managed by two timers. The first enables the signal capturing, allowing a sampling rate of 40 Hz, while the latter saves the instant of time when the data is taken, i.e. the timestamp. Due to its high precision, the timer peripheral allows a very accurate time base for the signals acquisition. However, a preliminary analysis has been performed to verify that the timings, and consequently the number of samples in a determinate time interval, corresponded to what was expected. The result of this analysis is shown in Fig. 2.12, in which the timestamp (oblique line) and the sampling rate (horizontal line) are plotted.

The results obtained through this analysis completely met the specifications. Therefore, the next step related to data pre-processing has been carried out.

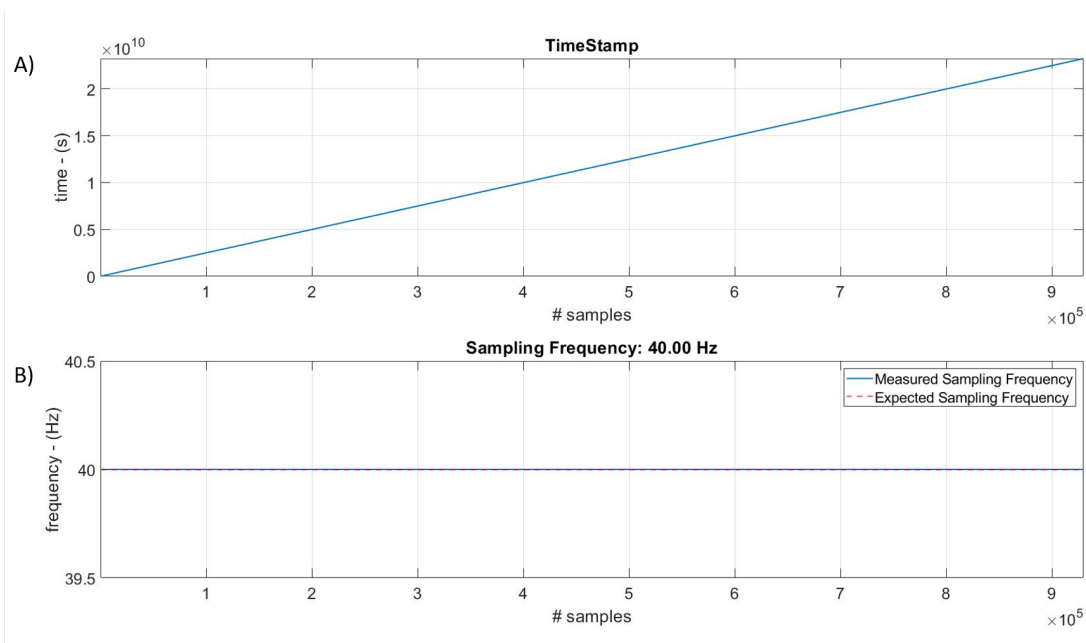


Figure 2.12: Timing Analysis: A) Timestamp and B) Sampling Frequency.

2.4.3 Signal Pre-processing

The raw data acquired include both the BCG signal and the components related to breathing, background noise and subject movements. Therefore, the signal pre-processing step is necessary to manage only those components belonging to the band of interest, by reducing the effect of noise sources. The bandwidth of the BCG signal is 1-10 Hz, thus, in order to exclude all the components with a frequency not belonging to this range, the data of each sensor were filtered through a digital filter.

Before proceeding with filtering, a frequency analysis was performed, calculating the power spectral density (PSD) of the signal in order to assess that the BCG bandwidth was in the desired range (Fig. 2.13).

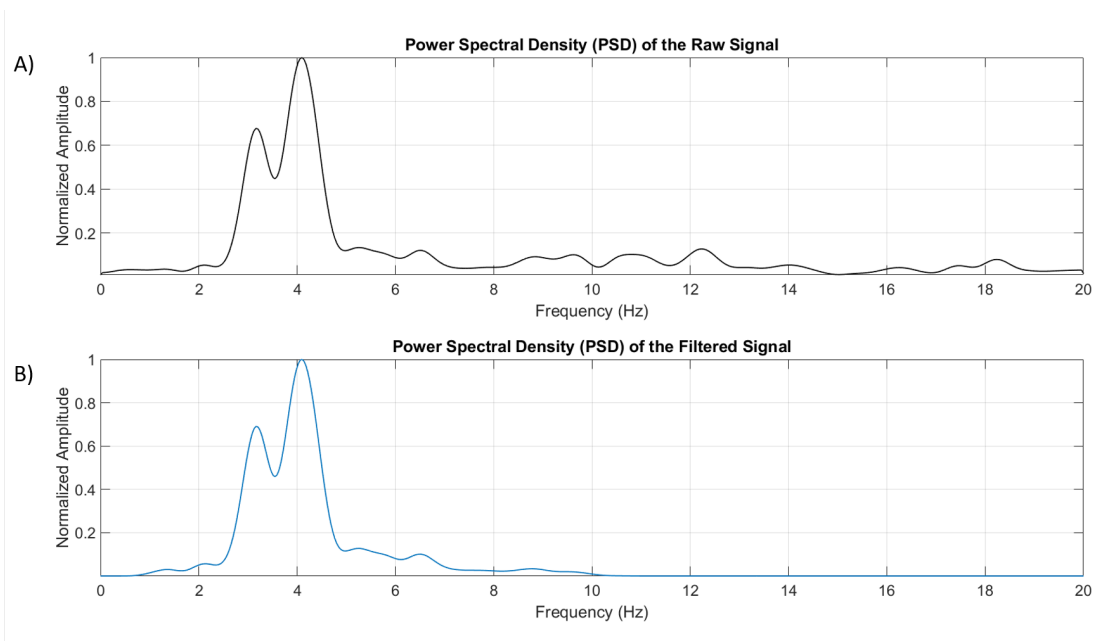


Figure 2.13: Example of the PSD : A) Raw Signal and B) Filtered Signal.

The signal components belonging to the unwanted bandwidth were attenuated by digital filtering.

The theory of digital filtering involves the use of two types of filters: the FIR (Finite Impulsive Response) filters and the IIR (Infinite Impulsive Response) filters [39]. The FIR filters are realized from a moving average (MA) representation and their representation in the time domain is usually defined by a finite number of samples of the input signal. On the other hand, the IIR filters are realized from an autoregressive representation (AR) and their time domain representation requires an infinite number of samples of the input signal. For this work, a FIR filter has been chosen for three main reasons: the first is that FIR filters are the most widely used filters in the microcontrolled devices, the second is that FIR filters can have a linear phase and the third is that FIR filters make it possible to perform the filtering operation based only on the "input" samples. This last reason allows to perform digital filtering of a signal in real-time.

Data were filtered using MATLAB's *fir1* function, which takes the filter order and the bandpass as input (Fig. 2.14).

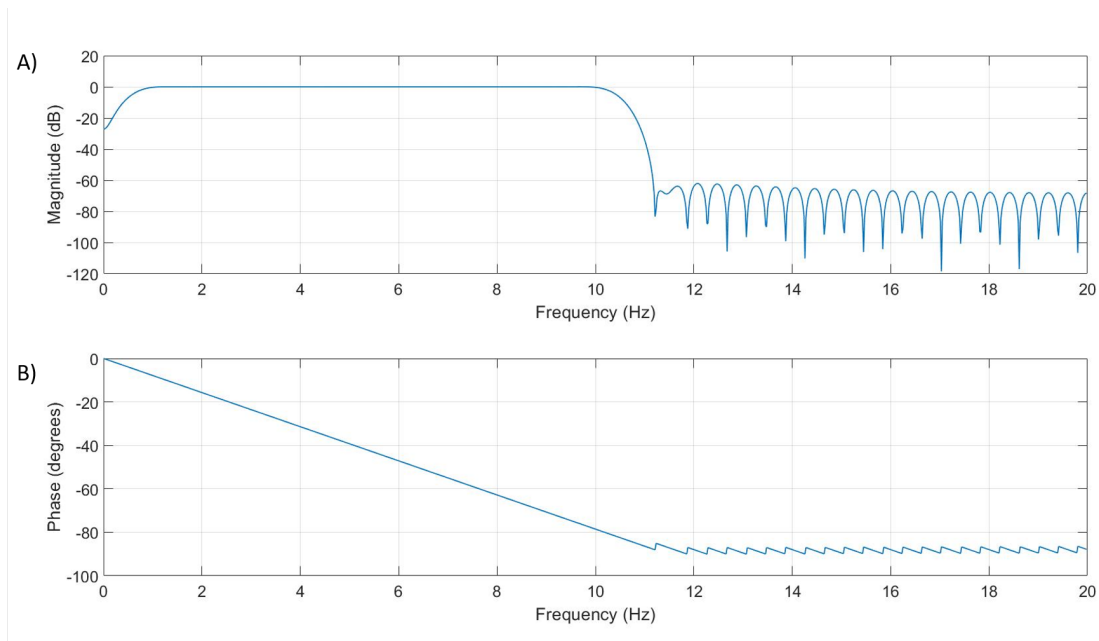


Figure 2.14: The FIR filter designed: A) Magnitude Response (dB) and B) Phase Response.

A downside of this type of filters is that they introduce a transient equal to half the order of the filter itself. This aspect was treated by performing a realignment of the signal. Finally, in order to obtain a smoother signal, the Savitzky-Golay filter was implemented in cascade with the FIR filter, using the MATLAB's *sgolayfilt* function. This filter allows to increase the precision of the data without distorting the signal tendency [40].

The filters chain providing the final data starting from the raw ones is composed of the two filter stages previously described and the low-pass filter integrated on each inclinometer (Fig. 2.15).

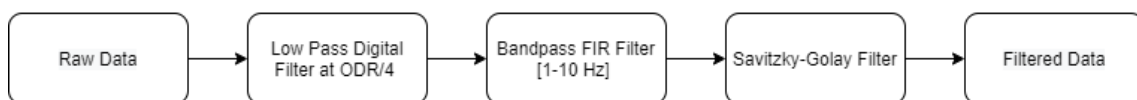


Figure 2.15: Block diagram of the filtering stage.

The function of each filtering step is presented below:

- *Low-Pass Digital Filter at ODR/4*: this filter represents the first stage of filtering that is carried out on each inclinometer. The cut-off frequency of the digital low-pass filter is one quarter of the ODR (Output Data Rate) of the sensor. The ODR has been set to 208 Hz, in order to ensure the correct sampling of the data from each sensor, thus obtaining a cut-off frequency equal to 52 Hz;
- *Bandpass FIR Filter*: this step was necessary because the sensors do not integrate a bandpass filter with the desired cutting frequencies [1,10 Hz];

- *Savitzky-Golay Filter*: this filter allows the implemented algorithm to improve the detection of the J wave, which is fundamental for the calculation of the heart rate. This is because the filter smooths the signal, thus preventing the occurrence of unwanted peaks.

The effectiveness of filtering can be appreciated in Fig. 2.16, which shows the difference between the raw and filtered data for the BCG signal.

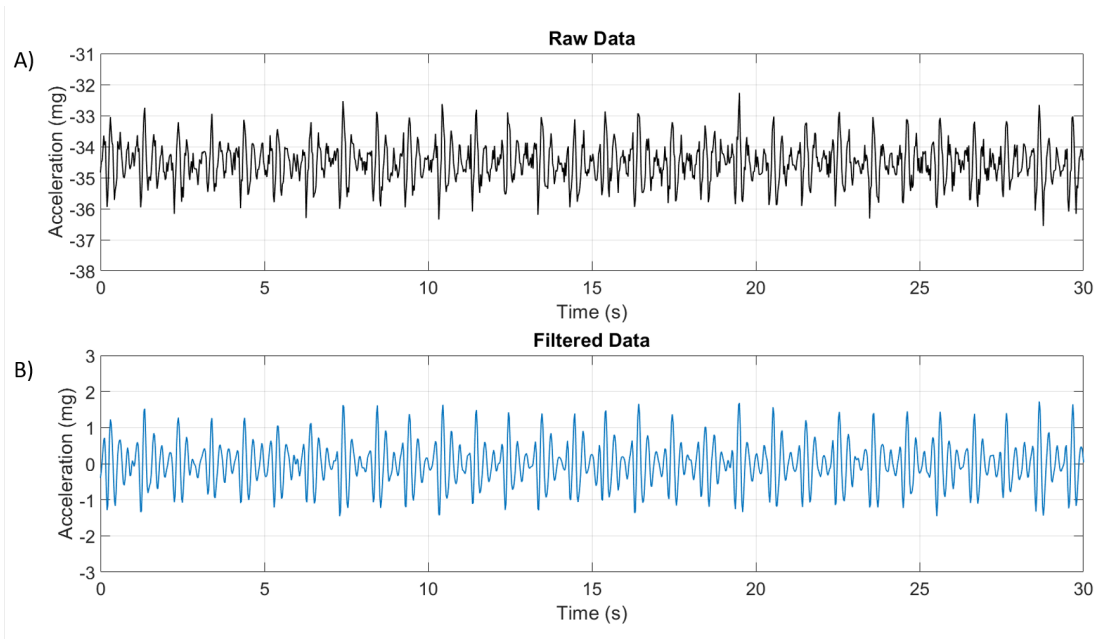


Figure 2.16: Comparison between: A) the raw signal and B) the filtered signal.

2.4.4 Motion artifacts management

Generally, during the acquisition phase of biomedical signals, such as ECG or X-ray imaging, subject motion may affect the quality of the data. In most cases, for short acquisitions, the subject involved is asked to maintain a fixed position. For this application, it is unthinkable to imagine that a subject could maintain the same posture for several hours. In fact, during sleep it happens that the patient may move, changing position several times. Apart from the subject movement, the effect of the sheets must be considered too. These just described represent the sources of disturbance that can occur most frequently in this particular application. Therefore, the management of motion artifacts is of paramount importance.

In this work, motion artifacts were handled as follows. For every 2 s of signal the standard deviation is calculated. If this value is greater than at least 3 times the standard deviation value calculated over a 10 s of the adjacent signal window, most likely a motion artifact occurred and therefore this region of the signal is set to zero.

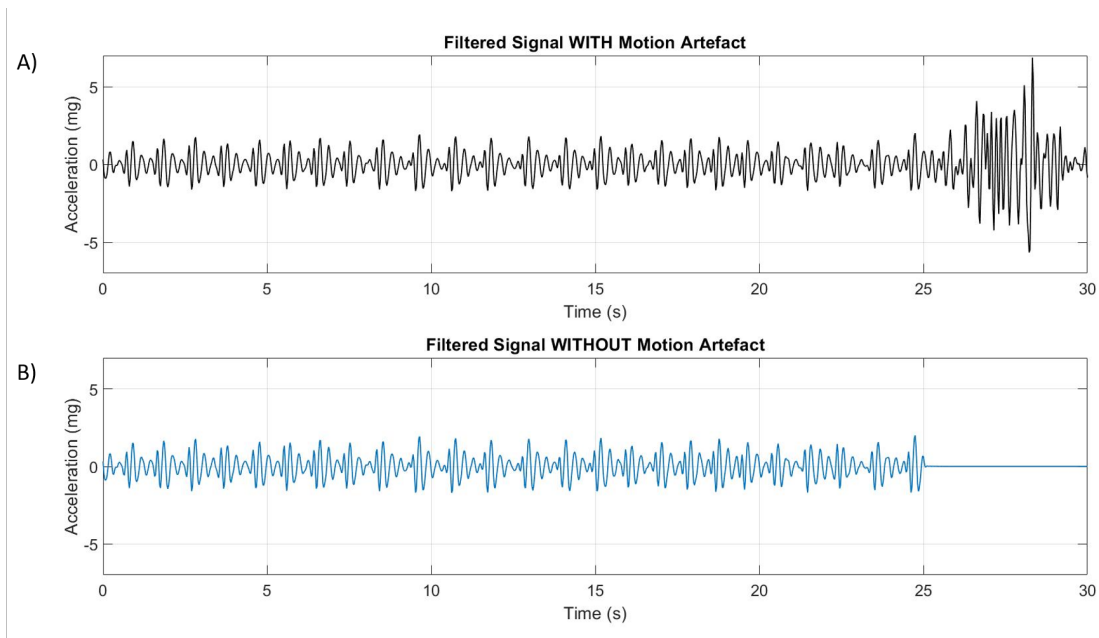


Figure 2.17: Example of BCG signal: A) BCG signal WITH motion artifact and B) BCG signal WITHOUT motion artifact.

2.4.5 Heart Rate detection

Among the waves characterizing the ballistocardiogram, the J wave is typically the most prominent. In parallel, because of the inter-subjects variability in BCG signal morphology, the search for the J wave represents one of the toughest challenges to be faced. There are several approaches used in the literature that employ alternative methods to search for the J peak. For example, algorithms working in the frequency domain return the heart rate based on the PSD peak of the signal, but with low accuracy and high computational costs. For this reason, in order to detect the heart rate in the time domain, a method based on the search of the J peak of the ballistocardiogram was implemented. The method that will be discussed below involves a correlation based approach, inspired by the studies performed by Xin Wen et al [41].

The BCG signal acquired during a complete sleep cycle, is divided into 30 s portions, before being processed by the algorithm as follows:

- **Pattern Determination;**
- **Heartbeat Detection;**
- **Interval Calibration and Refinement;**
- **Heart Rate Calculation.**

Pattern Determination

The main assumption on which this phase of the algorithm is based is that in a time span of 10 s the BCG signal is highly correlated with itself. Therefore, considering the portion of the signal that the algorithm takes as input (i.e. 30 s), a section equal to 10 s is selected. Subsequently, the normalized auto-correlation function (ACF) is calculated. This function allows to evaluate how much a signal at the time t is correlated with the same signal translated by an amount equal to τ . The maximum value of this function is assumed when the delay τ is 0, i.e. when the signal is superimposed with itself. In the case of the BCG signal, it can be assumed that the signal morphology does not change much in a short time span. Therefore, by calculating the auto-correlation function, it can be seen that in some temporal instants there are prominent peaks that occur synchronously with the heartbeat. The region of the BCG signal identified by the temporal position of these peaks identifies the pattern, i.e. portions of the signal that will be correlated with the remaining region of interest of the ballistocardiogram.

Fig. 2.18A shows an example of the normalized ACF. Peaks that are useful for pattern determination are those that have an amplitude greater than 0.25 and they must be at least three times larger than adjacent peaks, as described in [41].

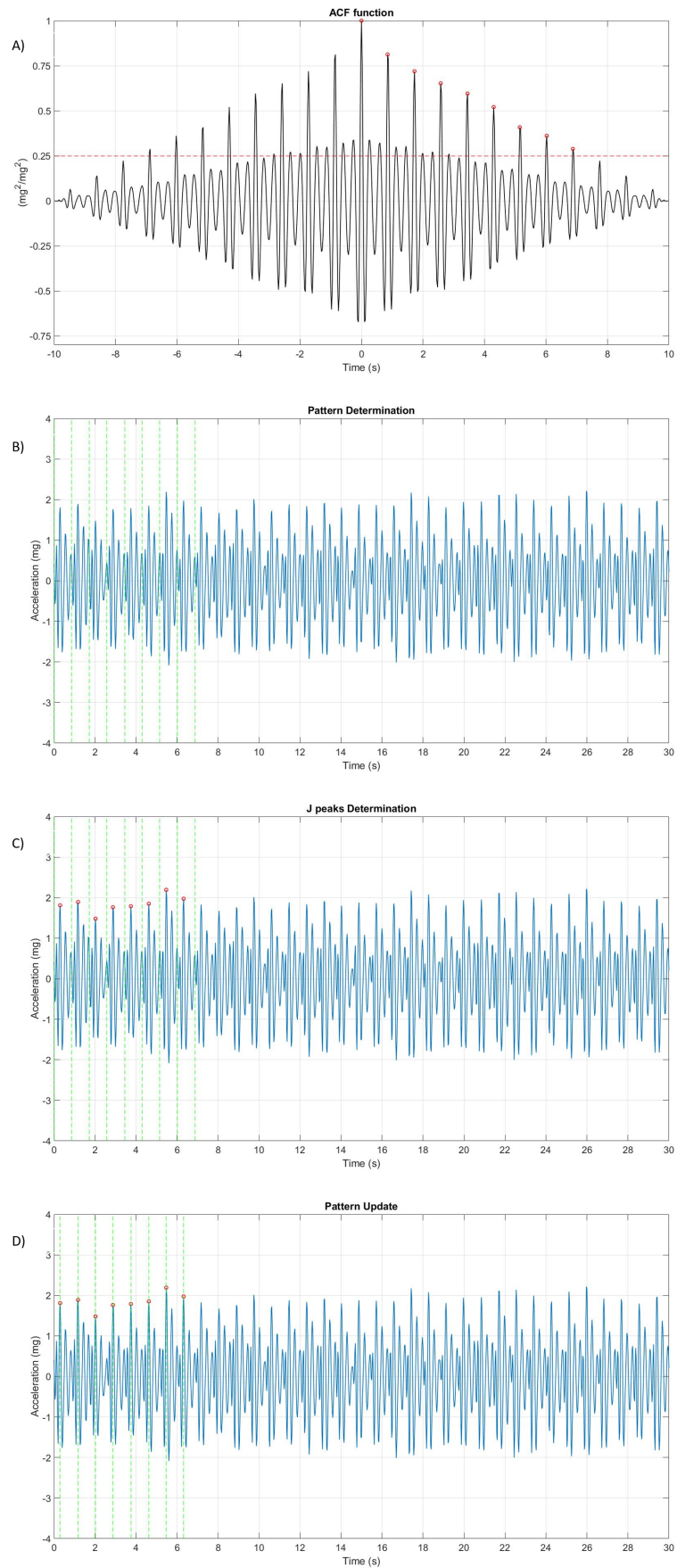


Figure 2.18: The process of the Pattern Determination: A) The ACF function; B) Patterns identified by the vertical green lines; C) The J peaks detected in the Pattern intervals by the red circles; D) Pattern Update associated with the J peaks detected.

Once the time instant at which these peaks of the ACF occur is detected (Fig. 2.18A), the pattern can be determined by considering the BCG signal (Fig. 2.18B). It can be seen in Fig. 2.18B that the auto-correlation function allows only the temporal instant in which a beat is present to be detected. Pattern accuracy was improved by identifying the contours of these intervals as the time instant in which the J peak occurs. This wave belongs to the IJK complex associated with a ventricular cardiac ejection phase [42]. Generally, the most prominent wave in this complex is the J-wave, which is identified in this algorithm as the local maximum with the largest rise and fall. The J peaks just detected represent the contours of the adjusted patterns.

Heartbeat Detection

The heart rate that can be calculated by the algorithm is in a range between 40-120 bpm. Although the upper limit would seem to be a fairly low value, it must be remembered that the aim of this work is to assess the heart activity of a resting subject lying on a bed.

Starting from the last pattern identified in Fig. 2.18D, a portion of signal of variable length is considered. This portion represents the candidate beat and, considering an initial signal length of 20 samples (i.e. 0.5 s), the cross-correlation function (CCF) between it and each identified pattern is calculated. Subsequently, the portion of the BCG signal will be increased with each iteration of one sample. This procedure is repeated until the length of the signal becomes of 60 samples (i.e. 1.5 s). A matrix will be constituted of the cross-correlation coefficients calculated in this phase of the algorithm. This matrix is composed of 40 rows, equal to the number of times the cross-correlation function is calculated between the candidate beat of variable size and a single pattern, and N columns, where N indicates the number of patterns that have been identified in the previous section. Averaging each row, the size of the cross-correlation coefficients matrix $40 \times N$, becomes a matrix of size 40×1 , consisting of the mean of the cross-correlation coefficients. The index L of this column, where the maximum value R of the cross-correlation function occurs, represents the instant in which the portion of the signal of variable length is maximally correlated with the patterns (Eq. 2.1).

$$L = \operatorname{argmax}(R) \quad (2.1)$$

Consequently, this instant represents the time interval in which the J peak is most likely to occur, if the R cross-correlation value is greater than 0.4. This threshold was chosen because the value proposed in [41], equal to 0.5, does not allow the processing of a large number of beats. On the other hand, this value leads to less accuracy in the detection of beats, accuracy that is preserved by the later stages of the algorithm and by using the inertial multi-sensor network designed.

Interval Calibration and Refinement

The accuracy of the heartbeat detection is based on the average value of the cross-correlation coefficients: the higher this value, the higher the probability that the candidate beat is similar to the reference beats. Fig. 2.19A shows that the time of each beat may not perfectly match the time of the J peak. Therefore, a refinement phase and a calibration phase were implemented to improve the accuracy of the heartbeat search. In the refinement phase, the region adjacent to the candidate beat is explored and the J peak is selected as the maximum signal value. In the calibration phase, any errors made in the refinement phase are handled by checking that the time distance between two consecutive beats is within the 40-120 bpm range and that the amplitudes of the J peaks are within a specified range.

Fig. 2.19B shows the benefit obtained by implementing the procedure described.

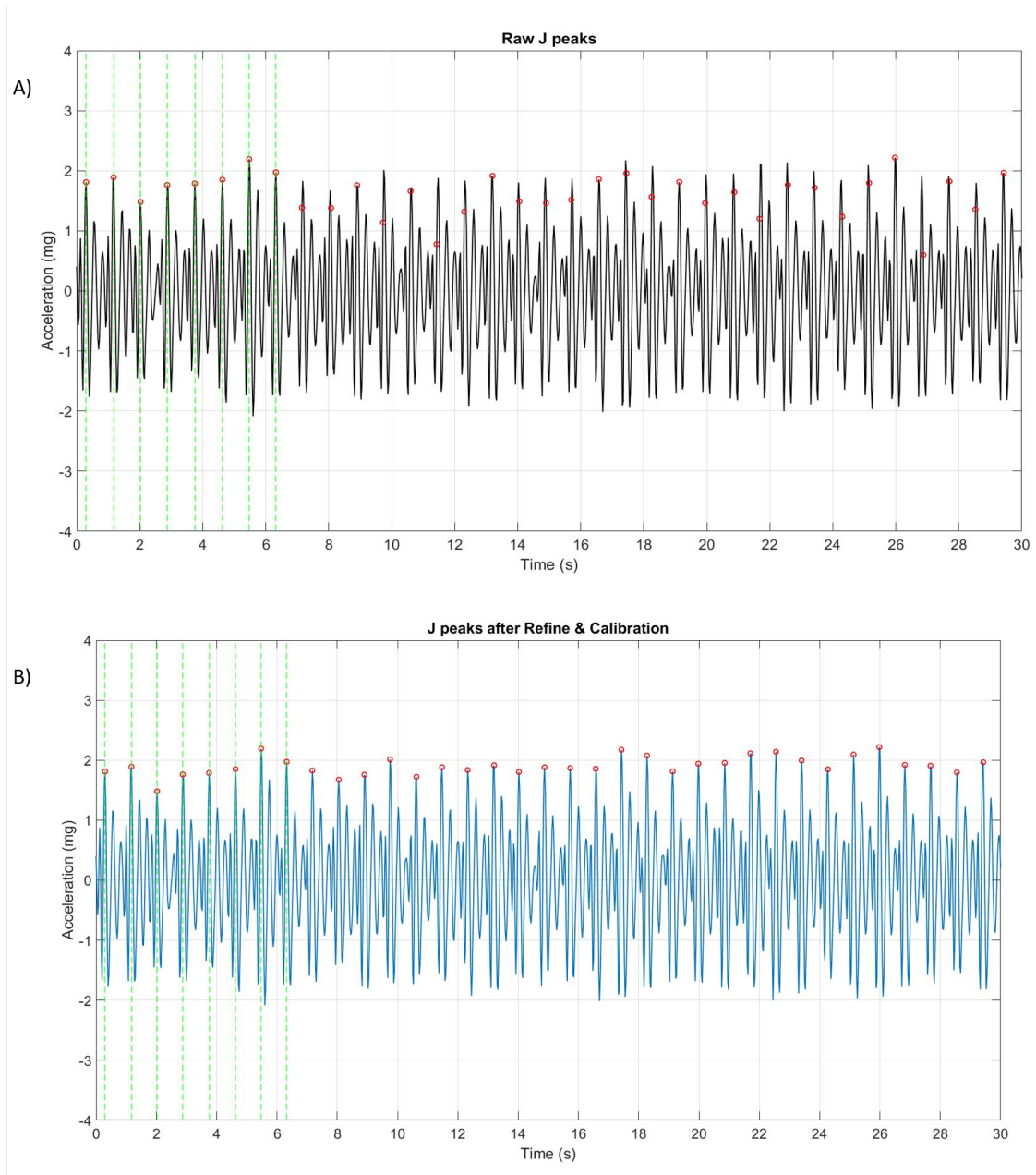


Figure 2.19: J peaks detection : A) J peaks determined by performing CCF and B) J peaks detection after refinement and calibration.

Heart Rate Calculation

The heart rate is computed according to the following formula:

$$HR = \frac{60}{J_{i+1} - J_i} \quad [bpm] \quad (2.2)$$

i.e. considering the time difference as the instants at which two consecutive J peaks occur.

This algorithm provides the option of returning the heart rate every 10 s or every 30 s by averaging the HR values calculated in these intervals.

2.4.6 Prediction models for selecting the best BCG signal

The proposed algorithm calculates the heart rate on the basis of a single trace of the ballistocardiogram. It should be noted that the system consists of four sensors, potentially all suitable to acquire the BCG signal, but surely only one of them is capable of providing the ballistocardiogram with the highest SNR (Signal to Noise Ratio). Therefore, it was necessary to establish a criterion to identify which of the four signals would be processed by the algorithm. To do this, two main approaches were performed: the *Multi-Parameter Model (MPM)* and the *Single-Parameter Model (SPM)*.

Multi-Parameter Model

The implemented *Multi-Parameter Model* is predictive, i.e. it is possible to choose *a priori* the BCG signal with the highest SNR from the four sensors. This method is based on the calculation of the following statistical parameters on a 10 s window of the signal: *standard deviation*, *kurtosis* and *auto-correlation function*.

The *standard deviation* σ_X is a statistical index that is used to indicate how much the data x_i deviates from the mean value \bar{x} (Eq. 2.3).

After analyzing several traces of the BCG signal, it was noted that, within certain limits, the higher this value, the greater the probability of having a high SNR.

The standard deviation is defined as follows:

$$\sigma_X = \sqrt{\frac{\sum_{i=1}^N (x_i - \bar{x})^2}{N}} \quad (2.3)$$

where:

- x_i is the i -th sample of signal;
- \bar{x} is the mean;
- N is the number of data points.

The *kurtosis* is a statistical parameter indicating the degree of flattening of a distribution. Experience has shown that regarding the BCG signal, the distribution curve has a greater number of elements in the central part, thus having very flat tails. Comparing to the standard deviation, within certain limits, a low value of this parameter is probably related to a high SNR of the BCG signal.

The kurtosis is defined as follows:

$$K_X = \frac{1}{N} \frac{\sum_{i=1}^N (x_i - \bar{x})^4}{\sigma_X^4} \quad (2.4)$$

where:

- σ_X is the standard deviation;
- \bar{x} is the mean;
- N is the number of data points.

The *auto-correlation function* allows to evaluate the similarity between a signal $x[n]$ and the delayed signal itself $x[n - m]$. As already explained, the maximum value of this function is obtained when $[m]$ is zero, i.e. when the two signals are perfectly superimposed. Moreover, if there is a strong similarity between the different segments of the BCG signal, the auto-correlation function will present several prominent peaks. Consequently, the higher the sum of the positive peaks in this function, the higher the probability that the BCG signal will have better quality.

The ACF is defined as follows:

$$R_{xx}[n] = \sum_{m=-\infty}^{+\infty} x[m]x[n + m] \quad (2.5)$$

where:

- $x[m]$ is the main sequence;
- $x[n + m]$ is the delayed sequence.

Based on these observations, it is possible to create a predictive model, capable of predicting which of the four sensors would provide the best signal. Each of the described parameters is calculated for all four sensors, thus, computing this parameter four times. Hence, the maximum value for standard deviation and auto-correlation, and the minimum value for kurtosis, calculated, are replaced by fixed scores. The other values are set to zero and a sum is computed between the scores assigned for each sensor. The highest value of this sum will correspond to the sensor with the best BCG signal quality.

However, this method has several disadvantages. For example, the choice of the best sensor is based on several parameters, and it is necessary to make several calculations for each signal provided by the inclinometers. In addition, the combination of different parameters may sometimes lead to choose a signal trace that is not what is expected. For example, this could occur when in a time window of the BCG signal acquired by one of the four sensors, a motion artifact is not correctly identified. In this particular case, the scores assigned to the standard deviation and the kurtosis may be higher for this sensor than the others. Therefore, this favoring the choice of the unexpected sensor. On the

other hand, a fundamental advantage of using this approach is that the search for the J peaks is carried out only once, i.e. the calculation is performed on the basis of the i -th sensor chosen.

Single-Parameter Model

The *Single-Parameter Model* allows to choose the BCG signal with the highest SNR by evaluating, on 30 s windows of the signal, a single parameter: the mean of the cross-correlation coefficients (MCCC). This parameter indicates how well the detected heartbeats on the ballistocardiogram correlate on average with the patterns. This model exploits the main operation performed by the proposed algorithm. The SPM stores the cross-correlation coefficients calculated for each identified heartbeat. After that, for each 30 s window of the four acquired signals, the mean of the cross-correlation coefficients is computed. This value represents the MCCC and it is related to the accuracy in the heartbeats detection. The higher the MCCC, the higher, most likely, the reliability of the calculated heart rate.

The two main differences between the MPM and the SPM basically concerns the number of parameters that need to be calculated and the computational cost. The tests carried out show that the MPM requires less computing time than the SPM, although the latter is based on the calculation of one parameter only. This occurs most likely because of the different implementation of the two methods. As already discussed, the MPM chooses the best signal (10 s windows) based on the calculation of the described parameters, which are closely related to the signal's morphology. This was the first method implemented. However, due to some of its critical issues, such as the one presented in the dedicated paragraph, an additional model that would be able to overcome these limits was implemented. Therefore, the SPM is proposed as an alternative to the MPM. It identifies the best signal (30 s windows) based on the reliability of the detected beats. Both methods are promising and for this reason the results obtained from these will be shown in Chapter 3.

Fig. 2.20 compares the two different approaches described.

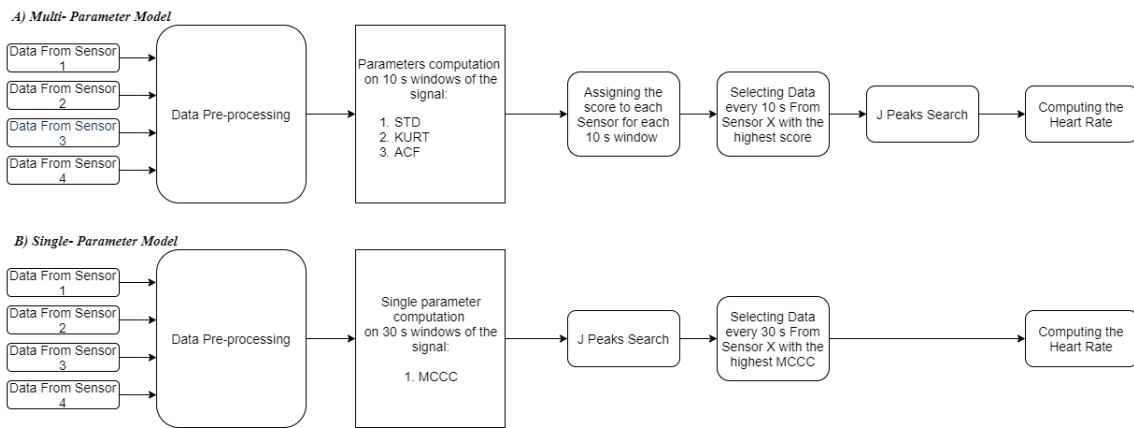


Figure 2.20: Block diagram of: A) the *Multi-Parameter Model* and B) the *Single-Parameter Model*.

2.5 Evaluation of algorithm performance

The performance of the proposed algorithm was evaluated by comparing the heart rate calculated from the ballistocardiogram against a reference device: the Hi electrocardiograph.

2.5.1 Hi device

The Hi is a non-invasive and wearable medical device of Class IIa, designed by STMicroelectronics and addressed for telemedicine purposes. Hi is a battery-powered electronic device intended to be worn on the chest in order to acquire, store and transmit the ECG and other physiological parameters to an external device for analysis and storage.

The main features of Hi are listed below:

- 1 or 3-lead ECG signal acquisition acquired at 128 Hz;
- automatic monitoring of events according to thresholds, possibility of manual reporting of events;
- heart rate calculation;
- physical activity level estimation and body position detection via built-in acceleration sensor;
- use of standard ECG electrodes (patches);
- flexible structure to adapt to the shape of the body, for greater comfort of use;
- IP67 waterproof rating; the device is fully protected against dust, sand and any small solid body in general; it is also submersible to a depth of 1 m for up to 30 minutes, so it can also be used in the shower or during a bath;
- uses CR2450 (non-rechargeable) or LIR2450H (rechargeable) button batteries, lasting up to 3 days (depending on the mode of use);
- communication with external devices via Bluetooth BLE 4.1.

In order to retrieve the measurements made by the Hi, it is necessary to have an external device that can connect to Hi via Bluetooth; this device can be a smartphone, a tablet or a suitably configured PC, and it is not supplied with Hi.



Figure 2.21: The Hi device.

The Hi device has only one button and three LEDs to interact with the user for basic operations (on/off, event signalling) and to display the status of the device.

Specifically:

- One Central button:
 - turns the device on/off;
 - during the monitoring session, a press allows to record an event, which will then be sent together with the recorded ECG data.
- The LED on the left (yellow):
 - remains off during normal operation;
 - blinks slowly when the battery charge level is low and needs to be replaced or recharged (depending on the type of battery used).
- The LED on the right (yellow):
 - blinks if the device has notifications waiting to be sent to the external device via Bluetooth, or if one or more of the contacts is not properly connected.
- The central LED (green):

- it is on when the device is turned on and waiting to receive commands via Bluetooth;
- fast blinking when the device is sending the captured data to the connected external device (Streaming mode);
- flashes slowly when the device is saving data in the internal memory (Monitoring mode).

The correct positioning of the Hi's electrodes are shown in Fig. 2.22.

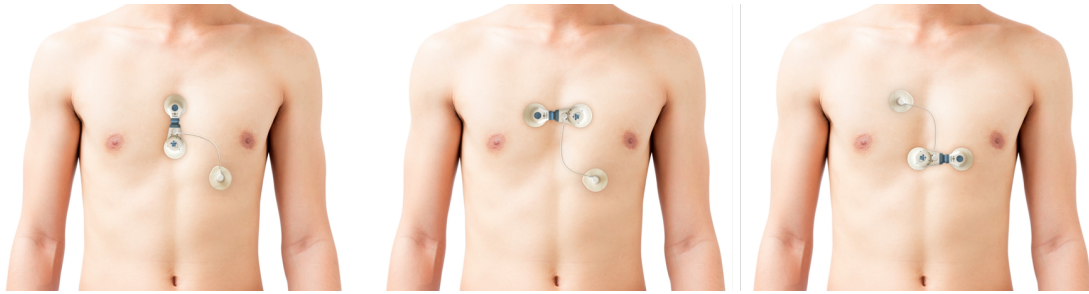


Figure 2.22: Preferred electrode position on the left, alternative electrode position on the center and on the right.

In order to compare the performance of the proposed system, the following parameters were provided from Hi:

- Heart rate: every 10 and 30 seconds;
- Activity level and body posture: through the embedded accelerometer.

2.6 Validation methods

The validation process of the designed system is based on the calculation of the following statistical parameters:

- **Mean Absolute Error (MAE):** it indicates the mean deviation of a predicted value x_i deviates from the reference value y_i .

MAE is expressed by the formula:

$$MAE = \frac{1}{N} \sum_{i=1}^N |y_i - x_i| \quad (2.6)$$

where:

- y_i is the actual value;
 - x_i is the predicted value;
 - N is the number of the measurement performed.
- **Mean Absolute Percentage Error (MAPE):** it expresses how much a predicted value x_i deviates from the actual value y_i . This difference is divided by the actual value y_i to obtain a relative measure that can be expressed as a percentage. Each absolute value of this calculation is added up and finally divided by the number of items N to obtain an averaged value of this measure.

MAPE is expressed by the formula:

$$MAPE = \frac{100}{N} \sum_{i=1}^N \left| \frac{y_i - x_i}{y_i} \right| \quad (2.7)$$

where:

- y_i is the actual value;
- x_i is the predicted value;
- N is the number of the measurement performed.

These parameters are calculated considering the following indicator:

$$Coverage[\%] = \frac{Covered\ Sleep\ Time}{Total\ Sleep\ Time} \cdot 100 \quad (2.8)$$

where:

- *Covered Sleep Time*: it represents the duration of the subject's sleep in which the HR from the BCG signal could be calculated;
- *Total Sleep Time*: it is the duration of the total recording.

In Chapter 3, the curves showing the time-varying heart rate trend provided by the ballistocardiographic system compared to the reference and the Bland-Altman Plot will be shown.

The scenarios that will be compared are basically two, when the heart rate is calculated every 10 s and when it is calculated every 30 s. The heart rate computed by Hi electrocardiograph will be compared with the heart rate calculated from the:

- *Each single-sensor*;
- *Multi-Parameter Model (MPM)*;
- *Single-Parameter Model (SPM)*;
- *Ideal Model (IM)*.

The heart rate calculated from the ballistocardiogram of each sensor will be compared with the proposed models, in order to demonstrate the usefulness and benefits that could come from an inertial multi-sensor network. The *Ideal Model* is built a posteriori, choosing the sensor (for each data window) minimizing the difference between the computed heart rate and the reference one. This last analysis shows the potentialities of the proposed system and the aspects that can be improved in the future.

Chapter 3

Results

This section shows the results obtained by the designed inertial multi-sensor network with respect to the data provided by the Hi electrocardiograph. In addition, in order to show the behavior of the system during data acquisition, graphs of the results obtained from two limit cases, best case and worst case, related to Subject 3 and Subject 7 respectively, will be shown.

In order to ease the reading, the following nomenclature will be used:

- S1, S2, S3 and S4: results provided by the inclinometer according to Fig. 2.9;
- MPM: results provided by the Multi-Parameter Model;
- SPM: results provided by the Single-Parameter Model;
- IM: results provided by the Ideal Model.

3.1 Heart Rate computation every 10 s

The following tables summarize the results obtained from the calculation of the heart rate every 10 s.

Subject	Mean Absolute Error (MAE)						
	S1 [bpm]	S2 [bpm]	S3 [bpm]	S4 [bpm]	MPM [bpm]	SPM [bpm]	IM [bpm]
1	5.48 ± 7.60	5.24 ± 7.13	4.42 ± 7.12	4.28 ± 6.01	4.46 ± 6.59	5.27 ± 7.21	3.05 ± 5.39
2	3.61 ± 5.93	3.61 ± 5.79	3.73 ± 6.00	4.48 ± 6.92	3.36 ± 5.64	3.00 ± 4.89	1.97 ± 3.78
3	2.58 ± 4.57	2.71 ± 4.66	2.86 ± 5.20	2.91 ± 5.19	3.04 ± 5.61	2.39 ± 4.54	1.57 ± 3.33
4	3.37 ± 5.74	-	3.59 ± 6.21	2.92 ± 5.21	3.16 ± 5.28	2.37 ± 4.25	1.52 ± 3.09
5	5.24 ± 7.78	-	5.08 ± 7.60	7.10 ± 10.10	5.12 ± 7.76	4.28 ± 6.86	2.72 ± 4.95
6	4.49 ± 7.64	7.48 ± 9.56	4.79 ± 7.89	-	4.21 ± 7.58	4.08 ± 7.28	2.61 ± 5.35
7	6.96 ± 9.37	7.71 ± 10.25	9.48 ± 11.35	7.82 ± 10.86	8.55 ± 10.67	8.51 ± 10.10	3.31 ± 5.58
8	3.59 ± 6.18	5.51 ± 8.60	5.01 ± 8.22	5.46 ± 8.83	4.14 ± 7.28	4.20 ± 7.05	1.86 ± 4.00
9	6.33 ± 8.79	6.24 ± 8.21	5.20 ± 7.59	6.07 ± 8.10	4.97 ± 7.41	4.14 ± 6.37	2.17 ± 4.11
<i>Total averages</i>	4.63 ± 7.07	5.50 ± 7.74	4.91 ± 7.46	5.13 ± 7.65	4.56 ± 7.09	4.25 ± 6.51	2.31 ± 4.40

Table 3.1: MAE of the HR calculated every 10 s.

Subject	Mean Absolute Percentage Error (MAPE)						
	S1 [%]	S2 [%]	S3 [%]	S4 [%]	MPM [%]	SPM [%]	IM [%]
1	11.11 ± 13.13	10.67 ± 12.47	8.85 ± 11.88	8.46 ± 10.49	9.04 ± 11.50	10.69 ± 12.78	6.12 ± 9.29
2	5.62 ± 6.94	5.68 ± 6.80	5.87 ± 7.21	7.00 ± 7.98	5.25 ± 6.59	4.73 ± 5.70	3.05 ± 4.55
3	3.78 ± 5.15	3.98 ± 5.14	4.17 ± 5.76	4.28 ± 5.88	4.47 ± 6.56	3.47 ± 4.92	2.27 ± 3.73
4	5.14 ± 7.09	-	5.39 ± 7.37	4.35 ± 6.19	4.79 ± 6.22	3.56 ± 4.98	2.23 ± 3.54
5	7.63 ± 8.47	-	7.33 ± 8.46	10.41 ± 10.90	7.44 ± 8.41	6.29 ± 7.44	4.42 ± 5.91
6	9.39 ± 14.20	15.87 ± 17.44	10.19 ± 15.04	-	8.86 ± 14.37	8.67 ± 14.00	5.45 ± 10.12
7	13.69 ± 14.14	13.65 ± 14.72	18.68 ± 17.53	15.17 ± 15.82	16.83 ± 16.46	17.01 ± 16.67	6.40 ± 8.07
8	7.15 ± 10.50	11.36 ± 16.13	10.13 ± 14.43	11.13 ± 15.82	8.39 ± 13.30	8.49 ± 10.47	3.60 ± 6.66
9	9.19 ± 9.23	9.02 ± 8.26	7.53 ± 8.39	8.82 ± 8.15	7.23 ± 7.96	5.94 ± 6.68	3.02 ± 4.45
<i>Total averages</i>	8.08 ± 9.87	10.03 ± 11.57	8.68 ± 10.67	8.70 ± 10.15	8.03 ± 10.15	7.65 ± 9.29	4.06 ± 6.26

Table 3.2: MAPE of the HR calculated every 10 s.

Subject	Coverage						
	S1 [%]	S2 [%]	S3 [%]	S4 [%]	MPM [%]	SPM [%]	IM [%]
1	72.14	60.02	63.50	69.86	75.01	91.07	91.07
2	85.59	85.85	93.38	65.36	92.08	97.14	97.14
3	96.82	98.49	97.73	96.97	96.37	99.39	99.39
4	96.82	-	96.52	97.48	97.30	98.26	98.26
5	81.68	-	82.83	74.64	87.09	93.66	93.66
6	79.89	51.08	78.49	-	81.89	88.34	91.05
7	78.45	79.10	81.32	79.15	83.04	88.54	89.60
8	77.28	81.32	79.05	74.36	82.23	93.74	93.74
9	93.34	73.85	94.84	91.67	96.50	97.83	98.33
<i>Total averages</i>	84.67	75.67	85.30	81.19	87.95	94.22	94.69

Table 3.3: Coverage of the HR calculated every 10 s.

3.2 Heart Rate computation every 30 s

The following tables summarize the results obtained from the calculation of the heart rate every 30 s.

Subject	Mean Absolute Error (MAE)						
	S1 [bpm]	S2 [bpm]	S3 [bpm]	S4 [bpm]	MPM [bpm]	SPM [bpm]	IM [bpm]
1	5.08 ± 7.00	5.03 ± 6.78	4.17 ± 6.64	4.14 ± 5.54	4.37 ± 6.40	4.96 ± 6.70	2.28 ± 4.04
2	3.21 ± 5.23	3.11 ± 5.00	3.36 ± 5.43	3.96 ± 6.22	2.86 ± 4.84	2.46 ± 4.01	1.35 ± 2.36
3	2.16 ± 3.99	2.30 ± 4.02	2.47 ± 4.56	2.49 ± 4.52	2.65 ± 5.07	1.87 ± 3.72	1.11 ± 2.37
4	3.25 ± 5.39	-	3.36 ± 5.79	2.75 ± 4.66	2.98 ± 4.77	2.10 ± 3.58	1.29 ± 2.31
5	4.68 ± 6.86	-	4.48 ± 6.65	6.45 ± 9.15	4.65 ± 6.90	3.72 ± 5.81	2.26 ± 3.68
6	4.10 ± 7.68	6.96 ± 9.00	4.54 ± 7.44	-	4.03 ± 7.34	3.75 ± 6.67	1.83 ± 3.41
7	6.46 ± 8.31	7.07 ± 9.16	9.10 ± 10.47	7.38 ± 9.87	8.03 ± 9.68	7.91 ± 9.16	2.56 ± 4.03
8	3.32 ± 5.75	5.43 ± 8.36	4.81 ± 7.82	5.43 ± 8.82	3.88 ± 6.87	4.01 ± 6.79	1.51 ± 3.27
9	6.23 ± 8.46	6.11 ± 7.82	5.08 ± 7.34	5.89 ± 7.64	4.87 ± 7.10	3.93 ± 5.86	1.97 ± 3.49
<i>Total averages</i>	4.28 ± 6.52	5.14 ± 7.16	4.60 ± 6.90	4.81 ± 7.05	4.26 ± 6.55	3.86 ± 5.81	1.80 ± 3.22

Table 3.4: MAE of the HR calculated every 30 s.

Subject	Mean Absolute Percentage Error (MAPE)						
	S1 [%]	S2 [%]	S3 [%]	S4 [%]	MPM [%]	SPM [%]	IM [%]
1	10.32 ± 12.40	10.22 ± 11.95	8.42 ± 11.51	8.39 ± 10.08	8.86 ± 11.37	10.09 ± 12.41	4.61 ± 7.26
2	5.05 ± 6.34	4.94 ± 6.16	5.32 ± 6.78	6.27 ± 7.50	4.52 ± 5.96	3.92 ± 4.93	2.12 ± 2.84
3	3.16 ± 4.76	3.38 ± 4.66	3.61 ± 5.37	3.69 ± 5.34	3.89 ± 6.16	2.71 ± 4.30	1.60 ± 2.76
4	4.99 ± 6.86	-	5.07 ± 7.04	4.12 ± 5.67	4.56 ± 5.85	3.18 ± 4.42	1.91 ± 2.78
5	6.93 ± 7.71	-	6.53 ± 7.75	9.55 ± 10.08	6.86 ± 7.70	5.54 ± 6.58	3.30 ± 4.15
6	8.55 ± 13.07	14.74 ± 16.67	9.61 ± 13.95	-	8.42 ± 13.80	7.93 ± 12.79	3.82 ± 6.15
7	12.80 ± 13.01	13.65 ± 13.38	17.91 ± 16.28	14.35 ± 14.43	15.81 ± 15.28	15.75 ± 15.37	4.95 ± 5.52
8	6.59 ± 9.85	11.22 ± 15.74	9.76 ± 13.79	11.08 ± 16.00	7.91 ± 12.79	8.11 ± 12.40	2.97 ± 5.95
9	9.06 ± 8.93	8.85 ± 8.05	7.37 ± 8.27	8.59 ± 7.78	7.10 ± 7.74	5.67 ± 5.86	2.78 ± 3.87
<i>Total averages</i>	7.49 ± 9.21	9.57 ± 10.94	8.18 ± 10.08	8.26 ± 9.61	7.55 ± 9.63	6.99 ± 8.78	3.12 ± 4.59

Table 3.5: MAPE of the HR calculated every 30 s.

Subject	Coverage						
	S1 [%]	S2 [%]	S3 [%]	S4 [%]	MPM [%]	SPM [%]	IM [%]
1	85.63	69.59	74.43	81.54	86.08	98.49	97.28
2	93.51	94.03	99.09	72.24	97.02	99.61	99.48
3	98.64	99.55	98.79	98.03	98.18	99.55	99.55
4	98.34	-	98.00	98.56	98.22	98.56	98.56
5	92.51	-	92.65	84.47	94.87	98.75	98.61
6	88.57	61.54	90.02	-	90.64	95.84	97.51
7	86.23	87.29	88.50	87.90	89.71	91.53	91.68
8	86.08	90.32	86.99	84.42	90.62	97.43	97.28
9	96.84	78.04	96.67	95.34	98.50	99.17	99.17
<i>Total averages</i>	91.82	82.91	91.68	87.81	93.76	97.66	97.68

Table 3.6: Coverage of the HR calculated every 30 s.

The following graphs report the HR value calculated every 10 s from the S1, S2, S3 and S4 sensors for the entire acquisition of Subject 3.

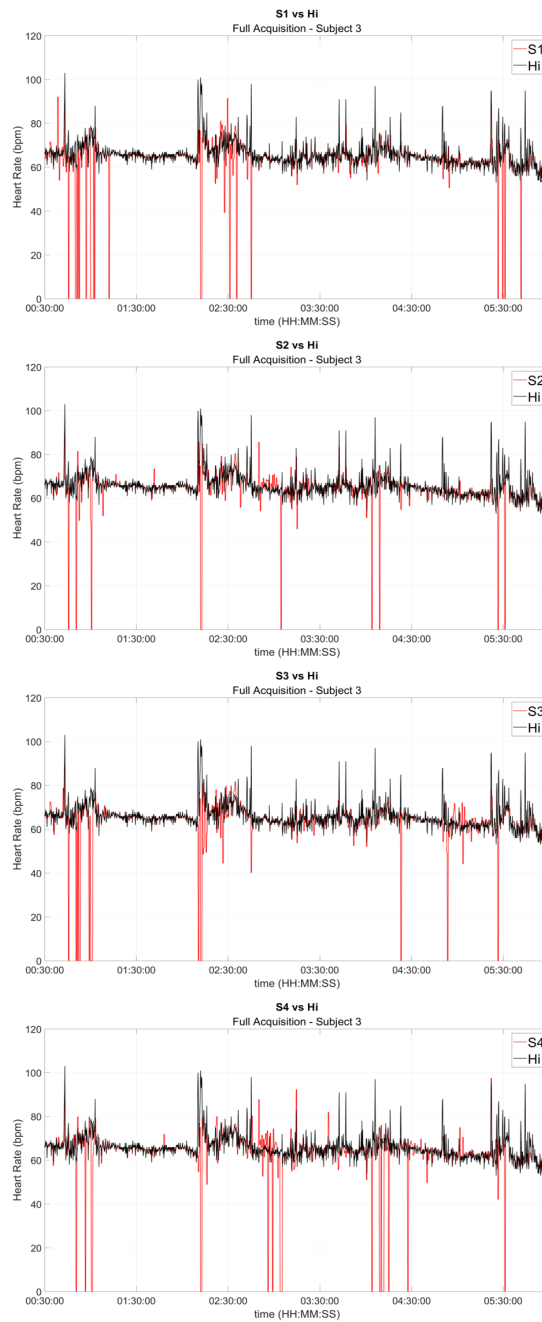


Figure 3.1: Full acquisition of Subject 3: HR provided every 10 s by each sensor (S1, S2, S3 and S4) vs Hi.

The following graphs report the HR value calculated every 10 s from the three models MPM, SPM and IM for the entire acquisition of Subject 3.

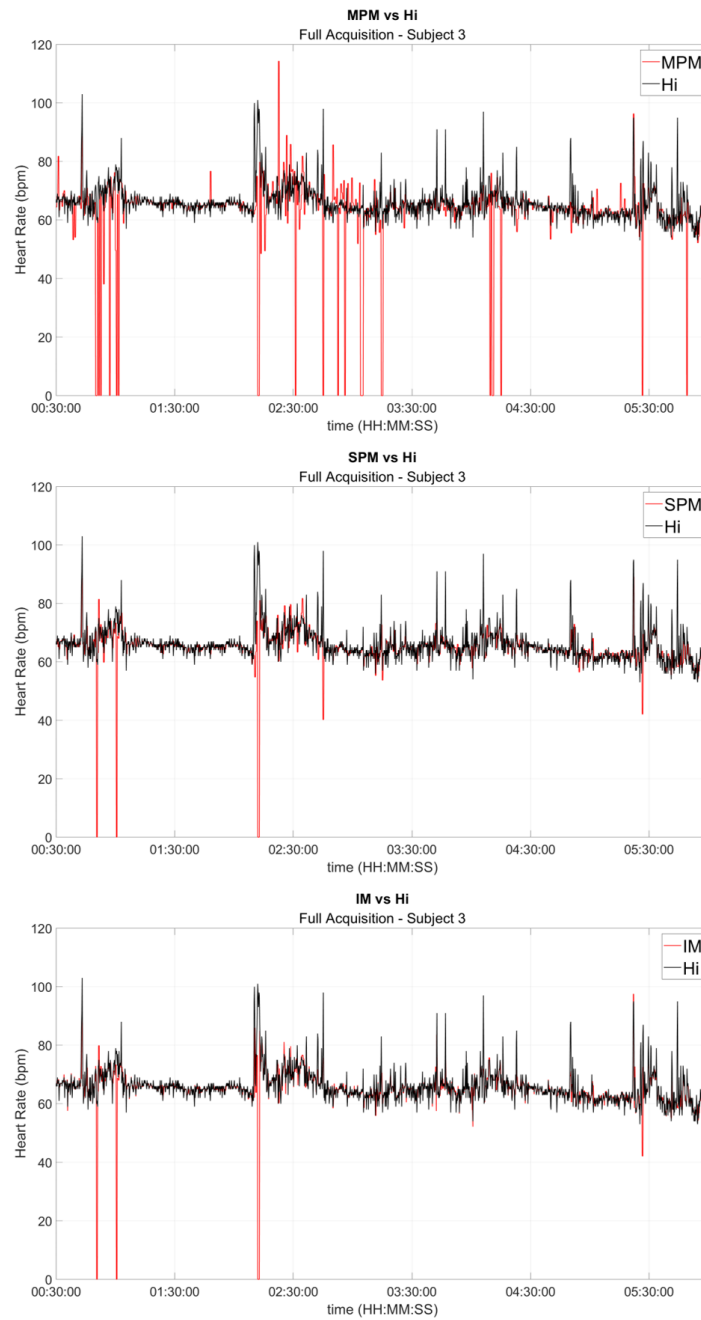


Figure 3.2: Full acquisition of Subject 3: HR provided every 10 s by each designed model (MPM, SPM and IM) vs Hi.

The following graphs report the comparable HR value calculated every 10 s from the S1, S2, S3 and S4 sensors of Subject 3.

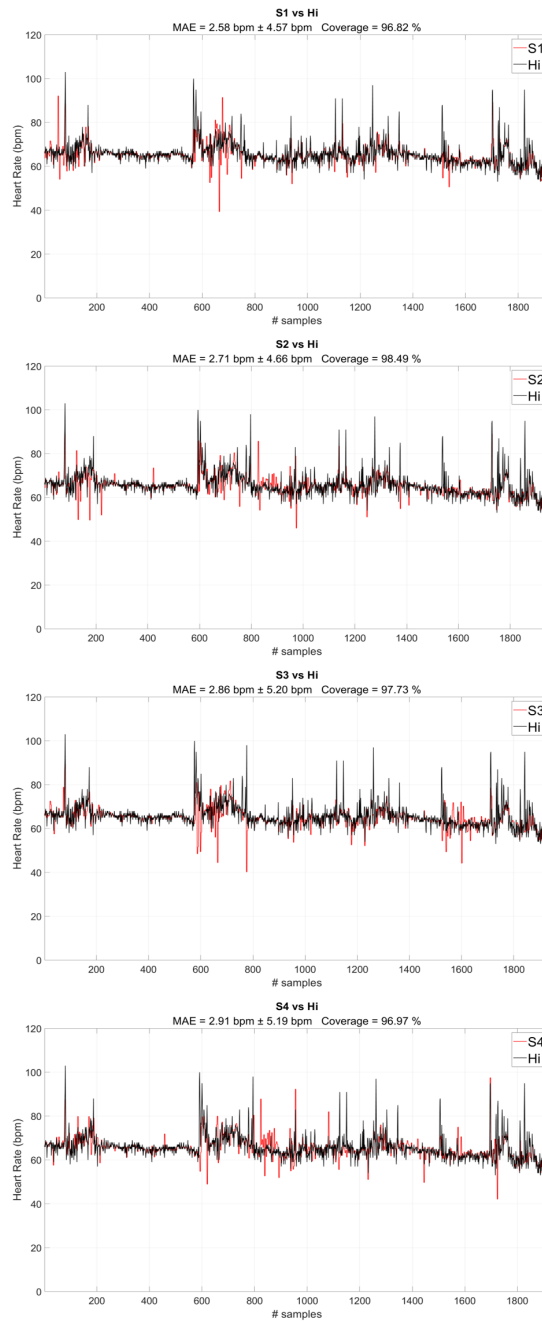


Figure 3.3: Covered acquisition of Subject 3: HR provided every 10 s by each sensor (S1, S2, S3 and S4) vs Hi.

The following graphs report the comparable HR value, calculated every 10 s from the three models MPM, SPM and IM of Subject 3.

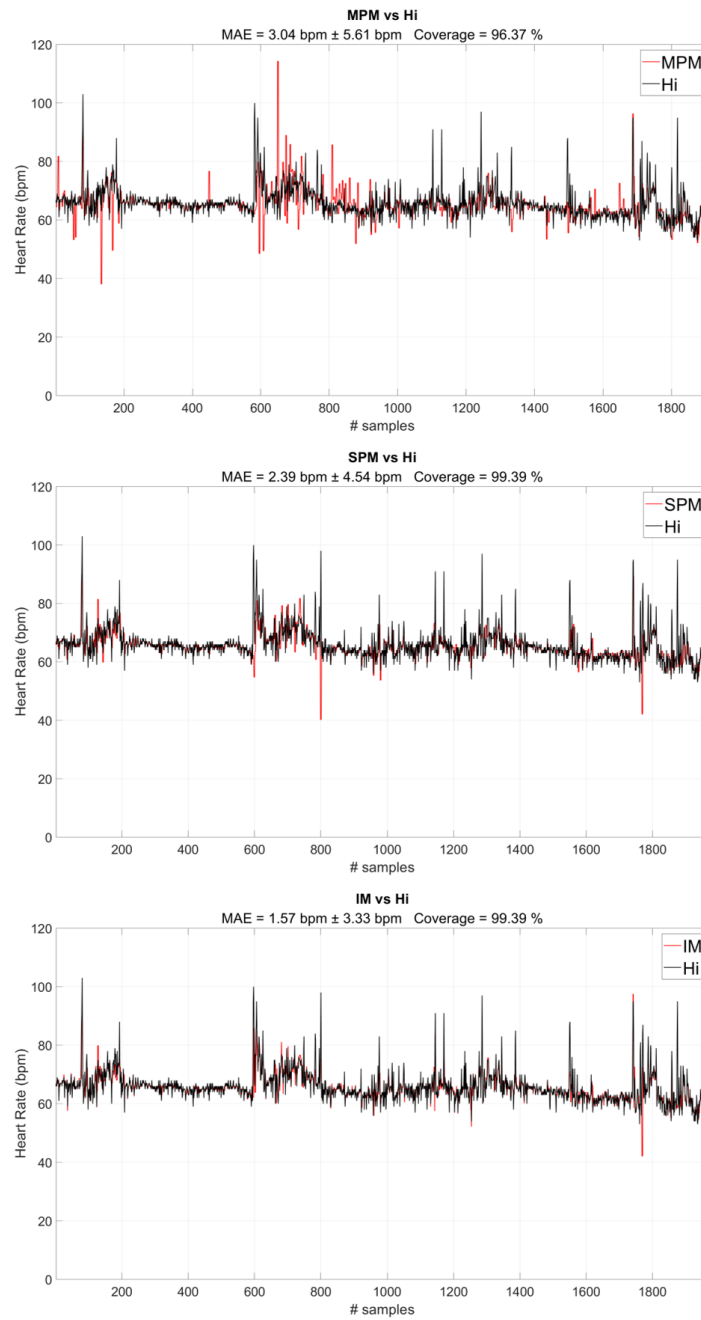


Figure 3.4: Covered acquisition of Subject 3: HR provided every 10 s by each designed model (MPM, SPM and IM) vs Hi.

The following graphs report the Bland-Altman Plot of the comparable HR value calculated every 10 s from the S1, S2, S3 and S4 sensors of Subject 3.

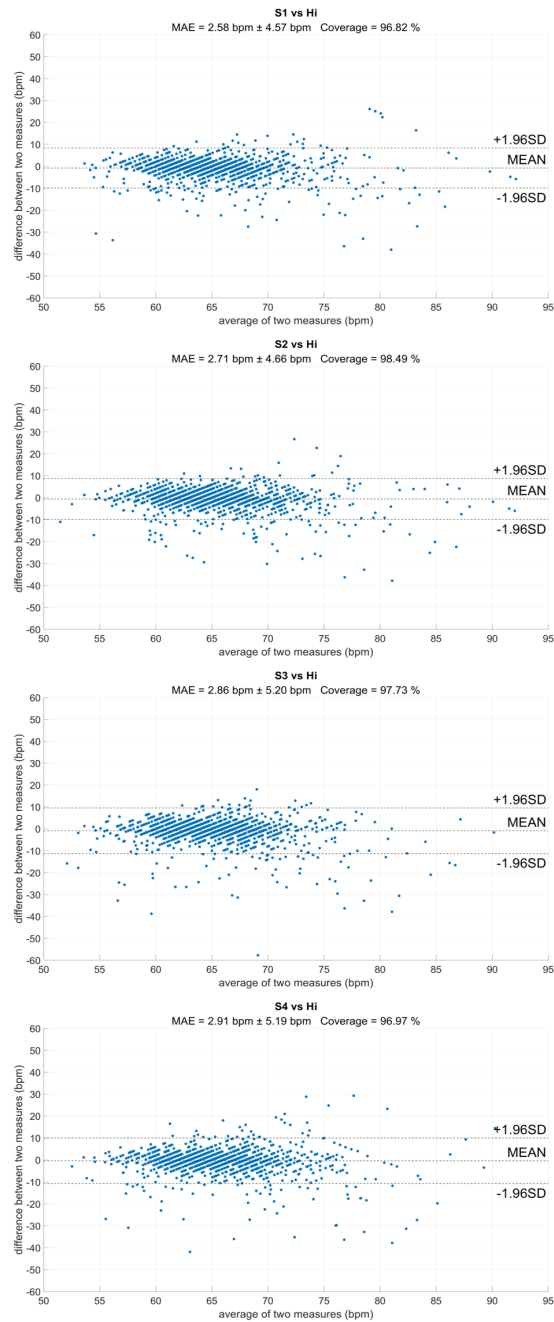


Figure 3.5: Bland Altman - Plot of the covered acquisition of Subject 3: HR provided every 10 s by each sensor (S1, S2, S3 and S4) vs Hi.

The following graphs report the Bland-Altman Plot of the comparable HR value calculated every 10 s from the three models MPM, SPM and IM of Subject 3.

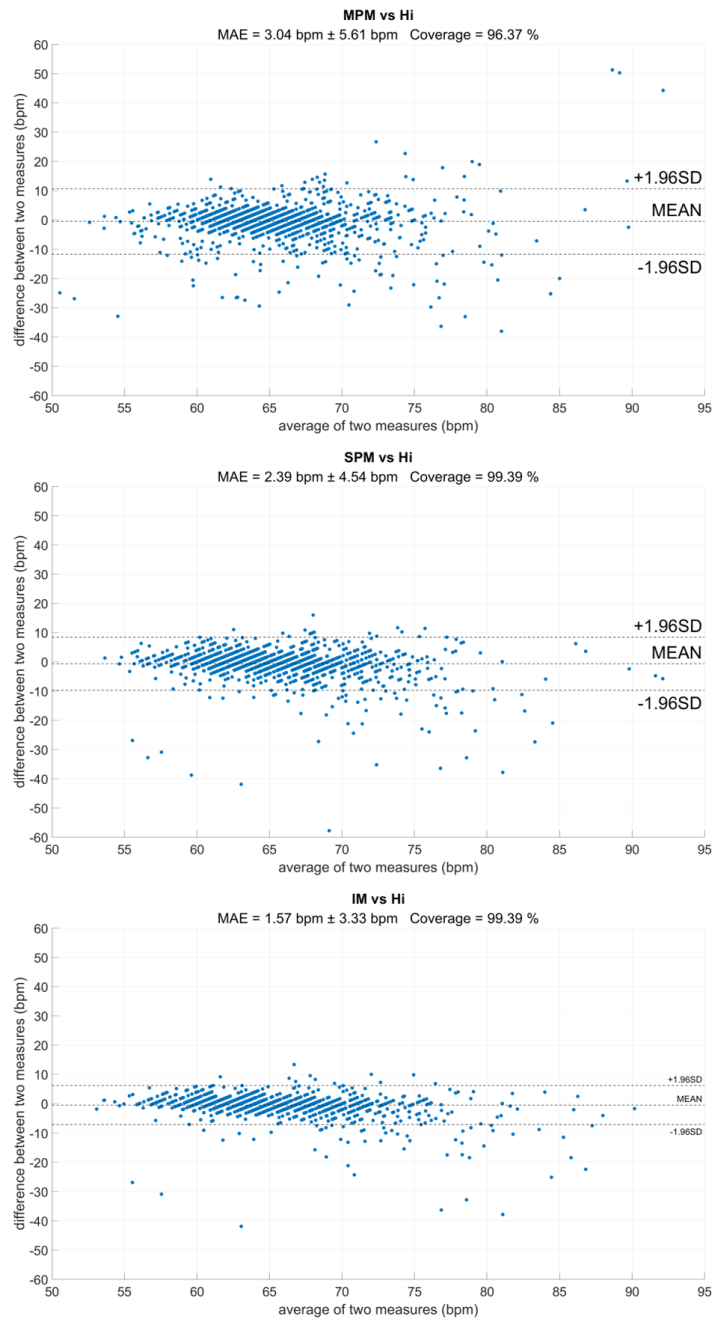


Figure 3.6: Bland Altman - Plot of the covered acquisition of Subject 3: HR provided every 10 s by each designed model (MPM, SPM and IM) vs Hi.

The following graphs report the HR value calculated every 30 s from the S1, S2, S3 and S4 sensors for the entire acquisition of Subject 3.

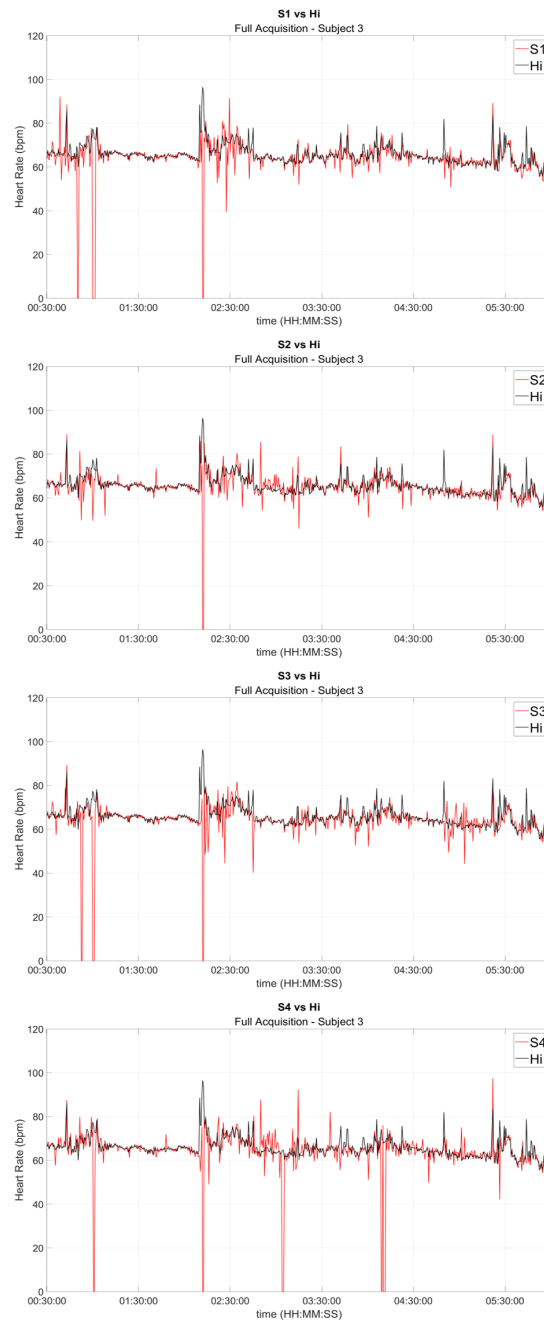


Figure 3.7: Full acquisition of Subject 3: HR provided every 30 s by each sensor (S1, S2, S3 and S4) vs Hi.

The following graphs report the HR value calculated every 30 s from the three models MPM, SPM and IM for the entire acquisition of Subject 3.

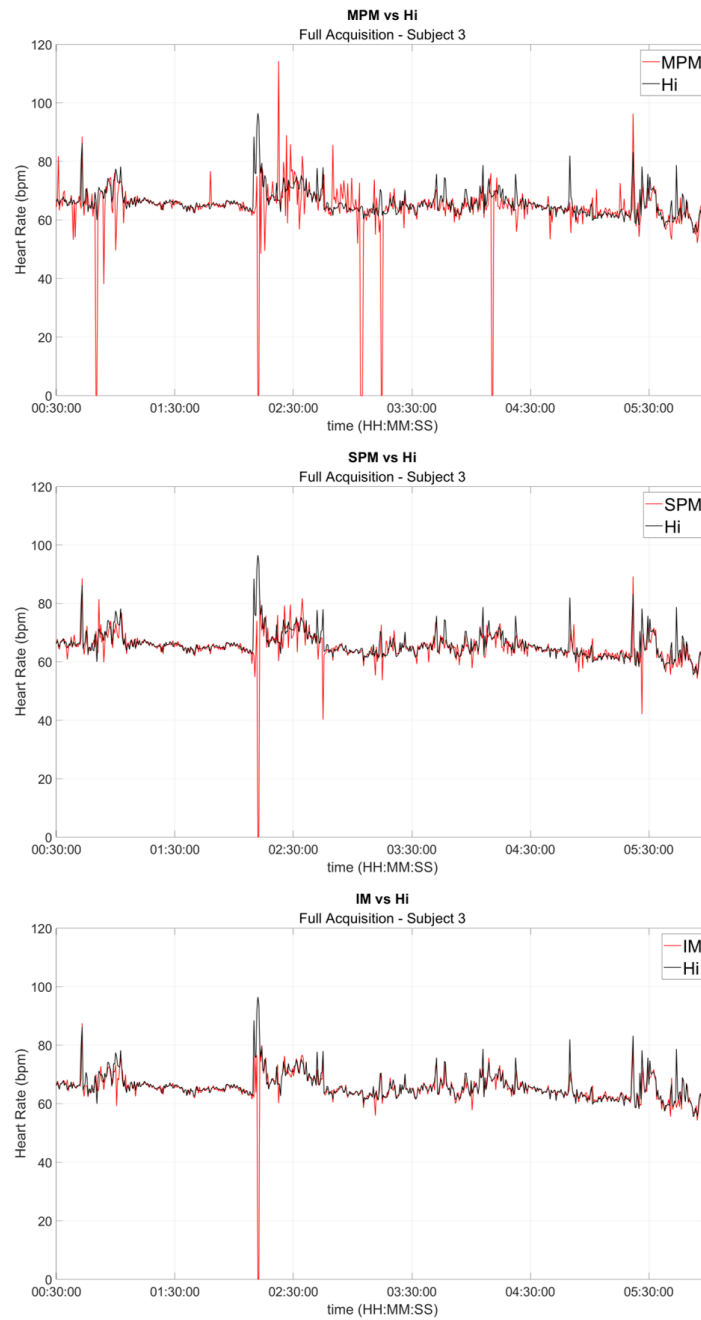


Figure 3.8: Full acquisition of Subject 3: HR provided every 30 s by each designed model (MPM, SPM and IM) vs Hi.

The following graphs report the comparable HR value calculated every 30 s from the S1, S2, S3 and S4 sensors of Subject 3.

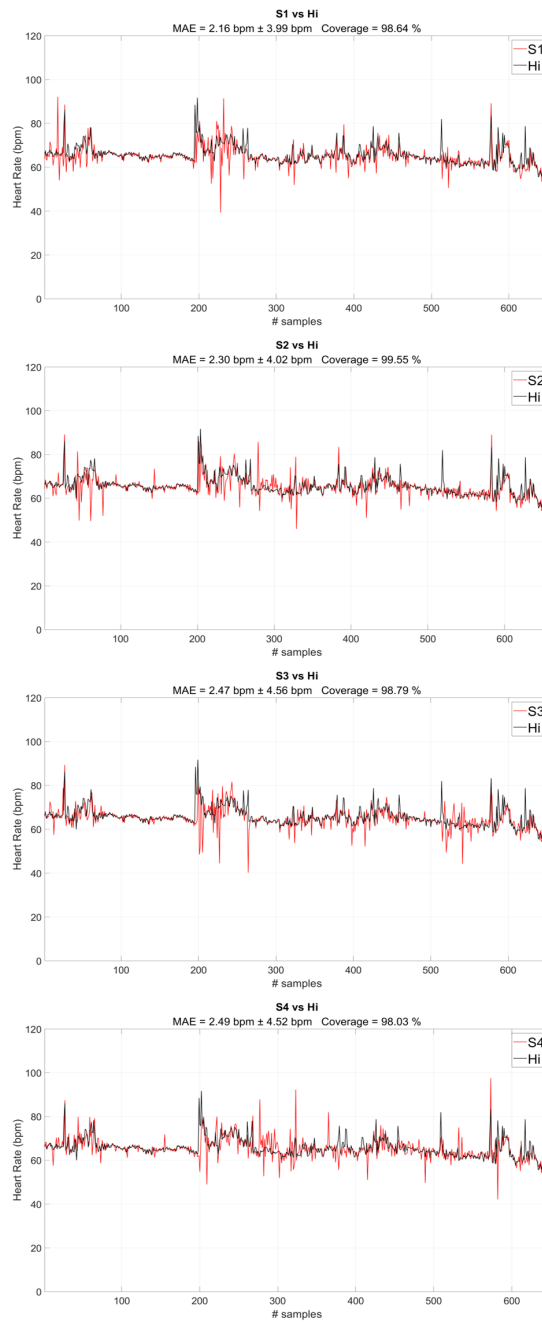


Figure 3.9: Covered acquisition of Subject 3: HR provided every 30 s by each sensor (S1, S2, S3 and S4) vs Hi.

The following graphs report the comparable HR value, calculated every 30 s from the three models MPM, SPM and IM of Subject 3.

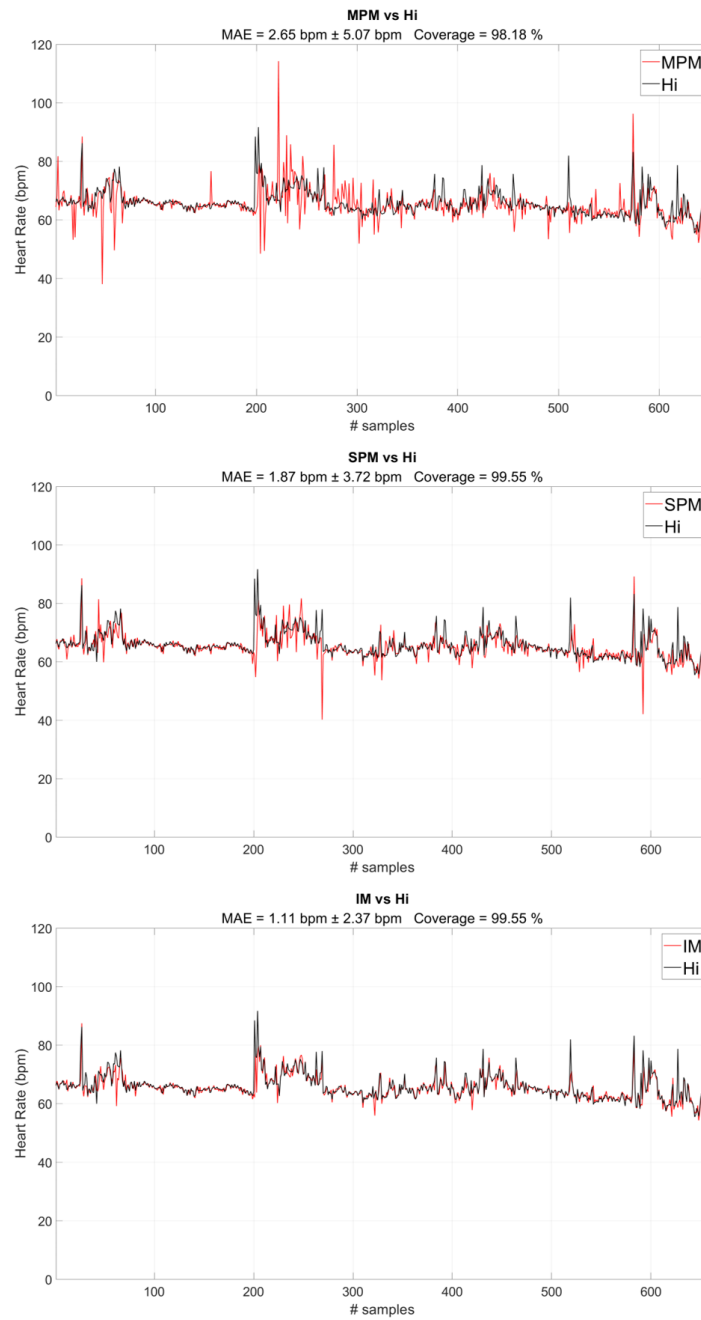


Figure 3.10: Covered acquisition of Subject 3: HR provided every 30 s by each designed model (MPM, SPM and IM) vs Hi.

The following graphs report the Bland-Altman Plot of the comparable HR value calculated every 30 s from the S1, S2, S3 and S4 sensors of Subject 3.

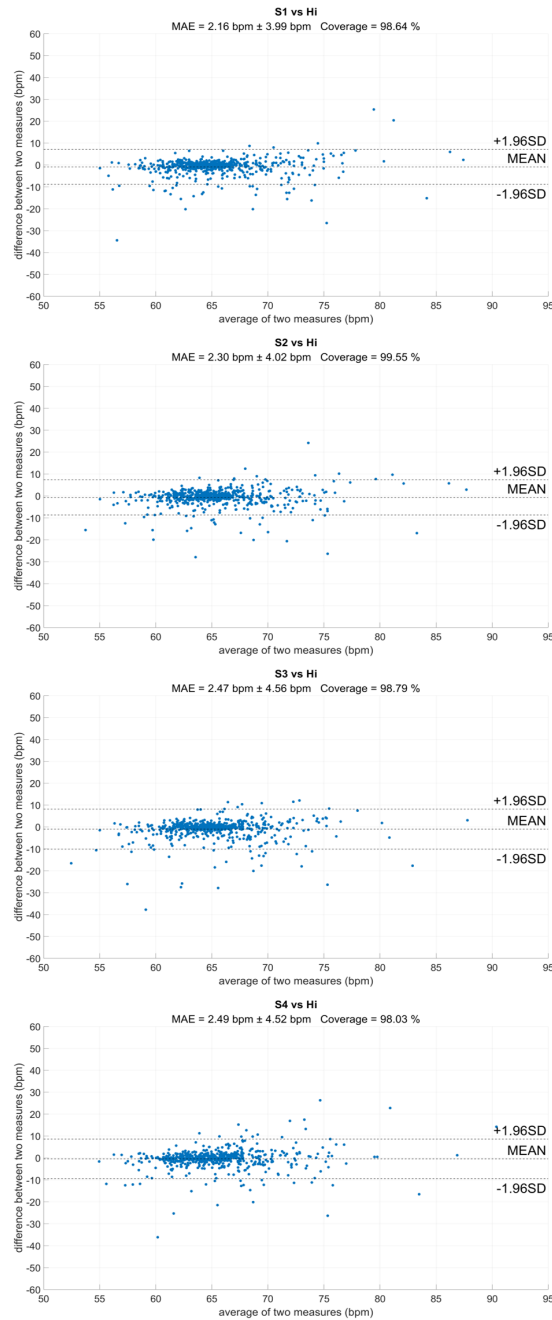


Figure 3.11: Bland Altman - Plot of the covered acquisition of Subject 3: HR provided every 30 s by each sensor (S1, S2, S3 and S4) vs Hi.

The following graphs report the Bland-Altman Plot of the comparable HR value calculated every 30 s from the three models MPM, SPM and IM of Subject 3.

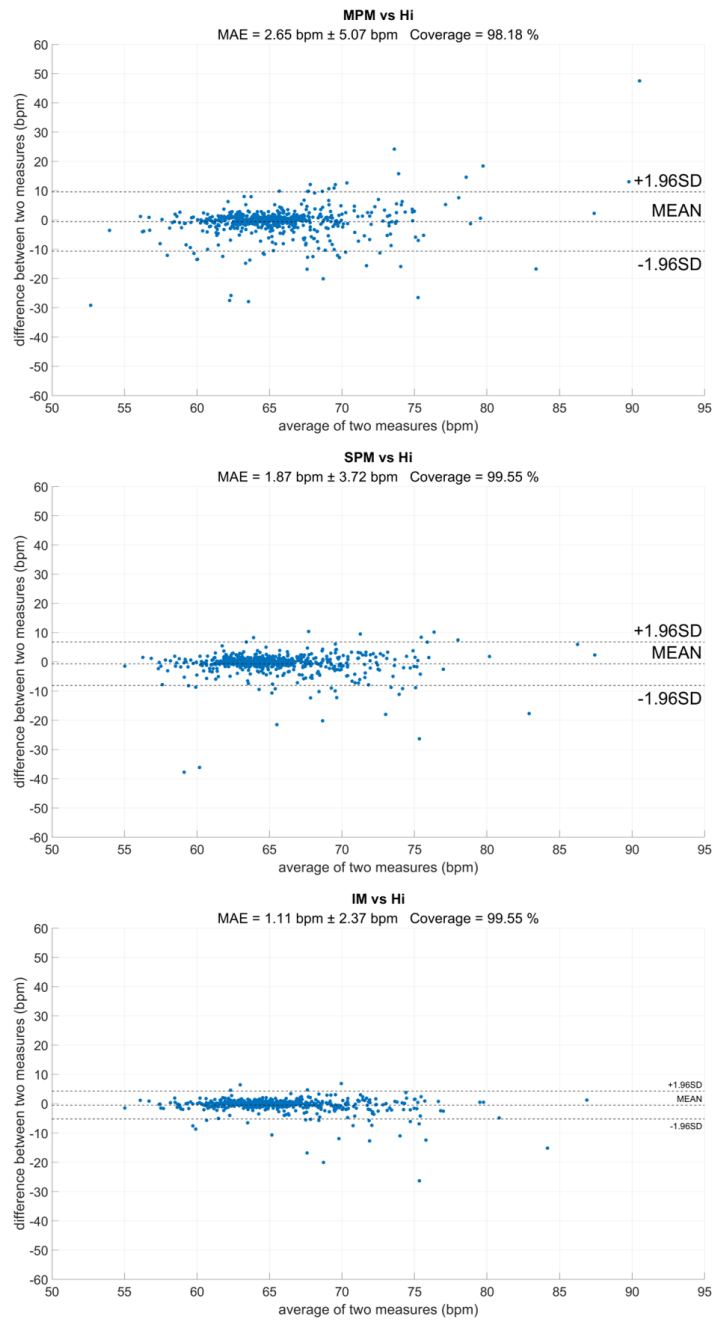


Figure 3.12: Bland Altman - Plot of the covered acquisition of Subject 3: HR provided every 30 s by each designed model (MPM, SPM and IM) vs Hi.

The following graphs report the HR value calculated every 10 s from the S1, S2, S3 and S4 sensors for the entire acquisition of Subject 7.

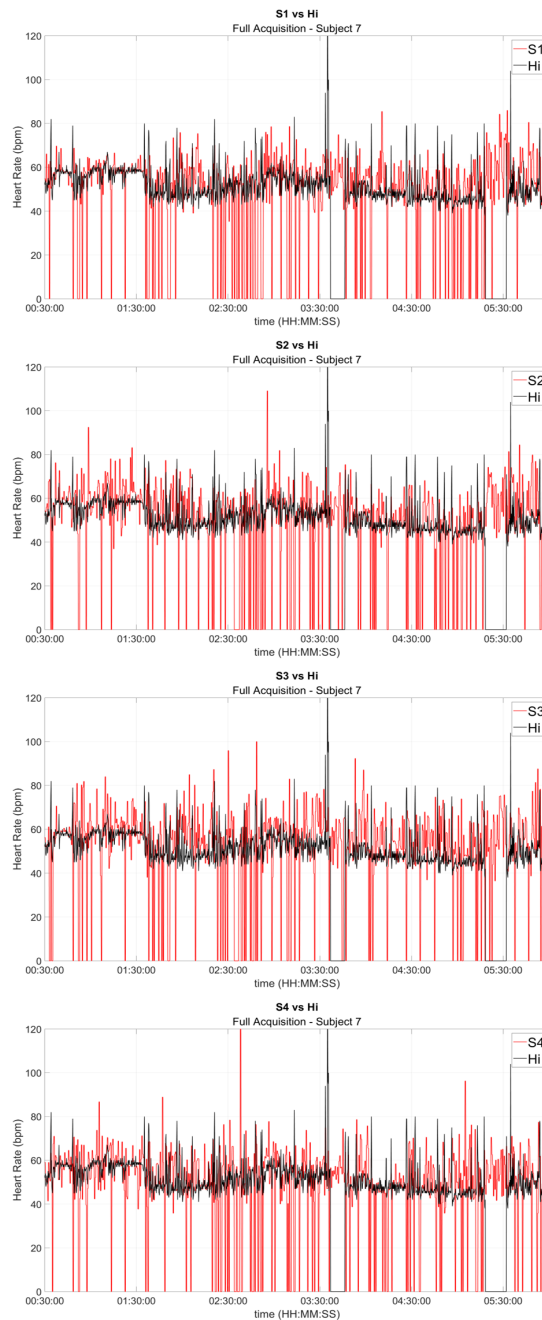


Figure 3.13: Full acquisition of Subject 7: HR provided every 10 s by each sensor (S1, S2, S3 and S4) vs Hi.

The following graphs report the HR value calculated every 10 s from the three models MPM, SPM and IM for the entire acquisition of Subject 7.

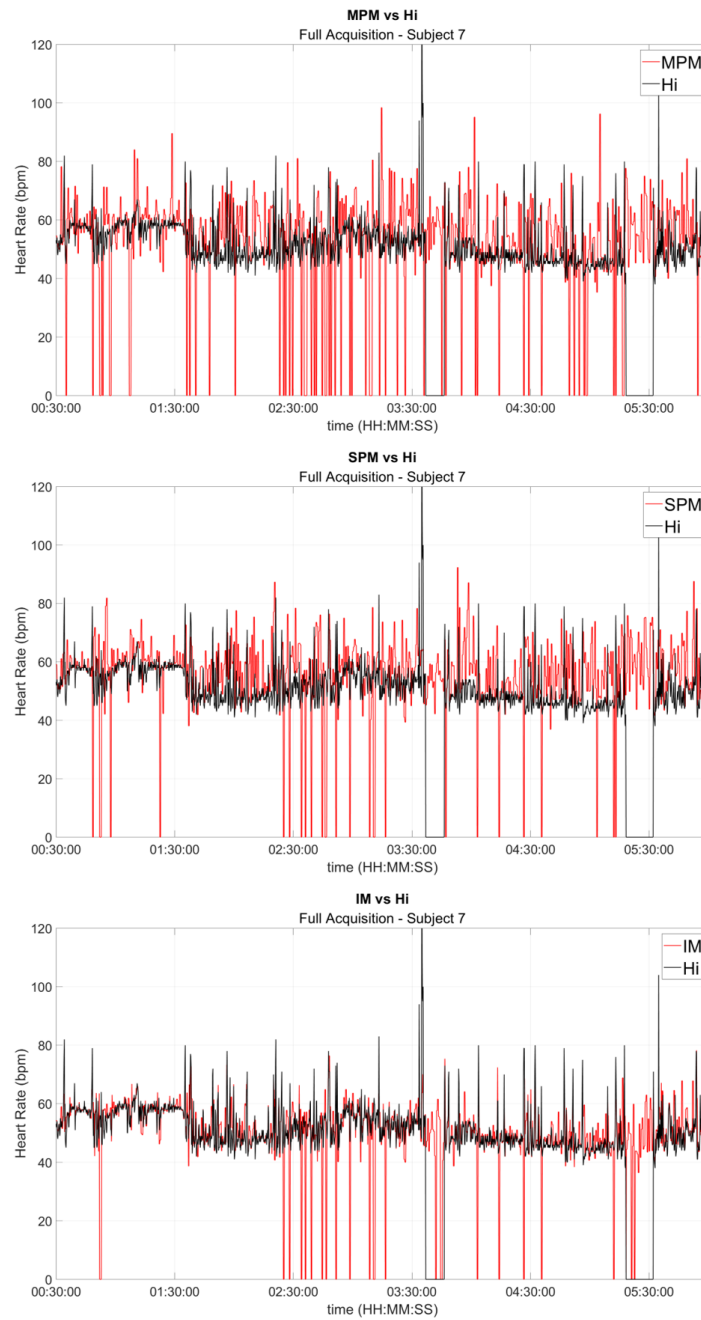


Figure 3.14: Full acquisition of Subject 7: HR provided every 10 s by each designed model (MPM, SPM and IM) vs Hi.

The following graphs report the comparable HR value calculated every 10 s from the S1, S2, S3 and S4 sensors of Subject 7.

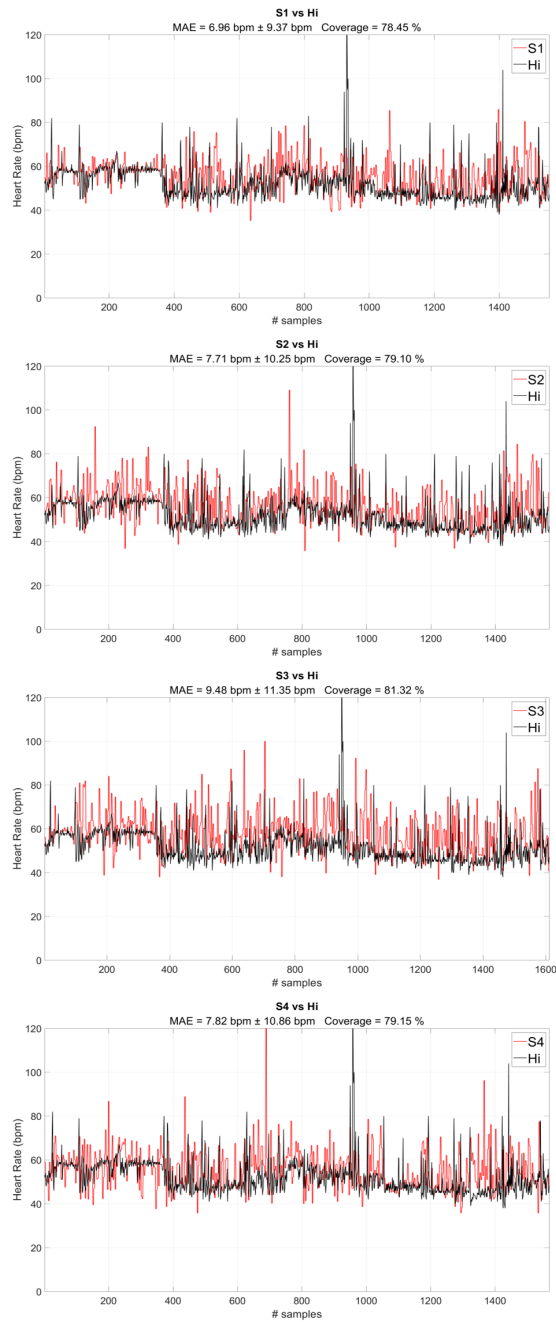


Figure 3.15: Covered acquisition of Subject 7: HR provided every 10 s by each sensor (S1, S2, S3 and S4) vs Hi.

The following graphs report the comparable HR value, calculated every 10 s from the three models MPM, SPM and IM of Subject 7.

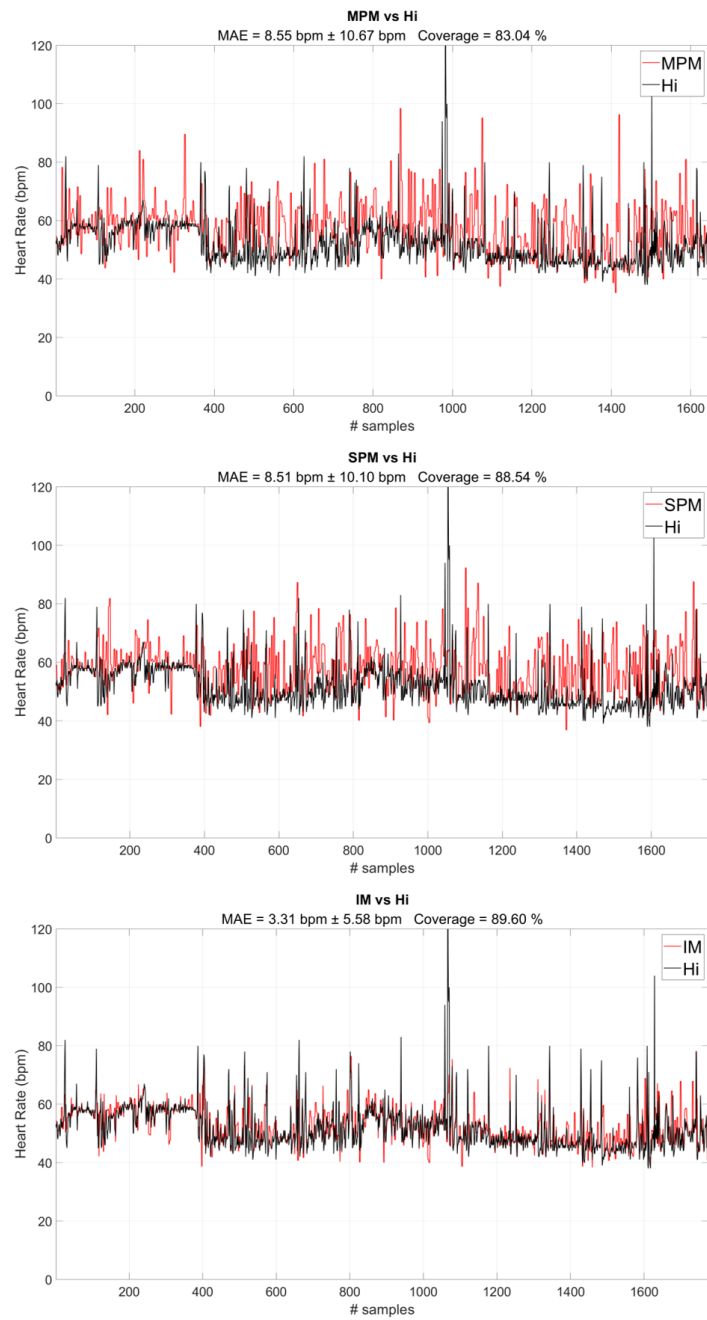


Figure 3.16: Covered acquisition of Subject 7: HR provided every 10 s by each designed model (MPM, SPM and IM) vs Hi.

The following graphs report the Bland-Altman Plot of the comparable HR value calculated every 10 s from the S1, S2, S3 and S4 sensors of Subject 7.

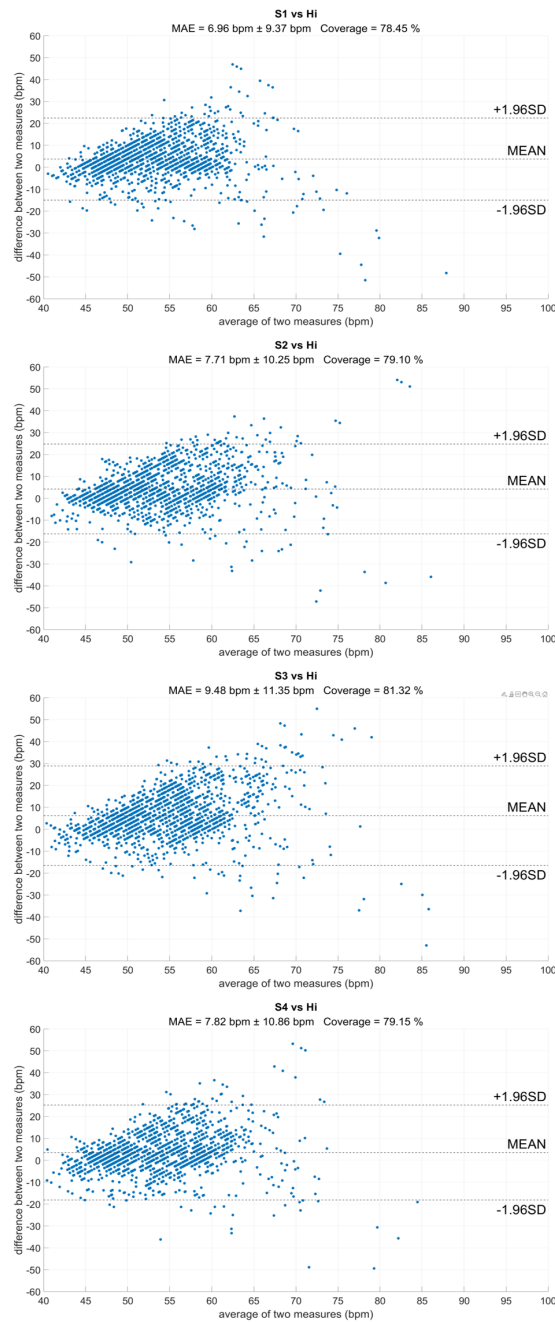


Figure 3.17: Bland Altman - Plot of the covered acquisition of Subject 7: HR provided every 10 s by each sensor (S1, S2, S3 and S4) vs Hi.

The following graphs report the Bland-Altman Plot of the comparable HR value calculated every 10 s from the three models MPM, SPM and IM of Subject 7.

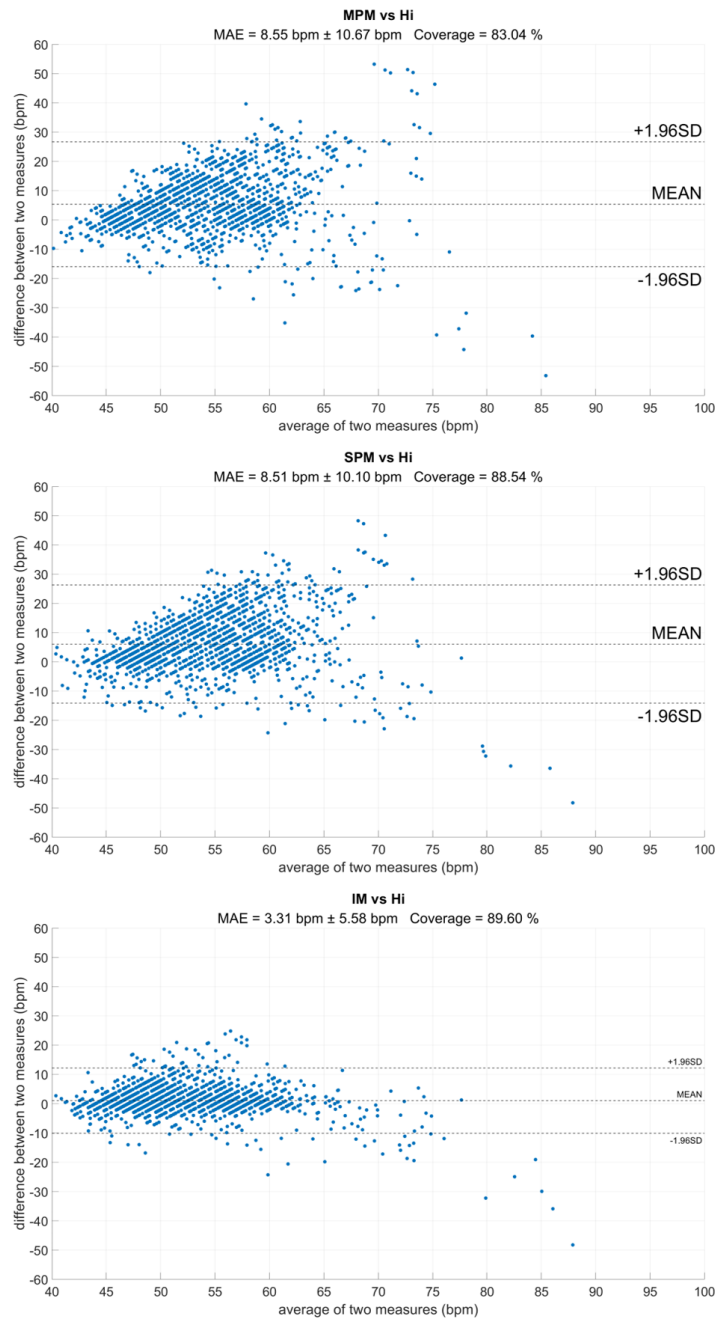


Figure 3.18: Bland Altman - Plot of the covered acquisition of Subject 7: HR provided every 10 s by each designed model (MPM, SPM and IM) vs Hi.

The following graphs report the HR value calculated every 30 s from the S1, S2, S3 and S4 sensors for the entire acquisition of Subject 7.

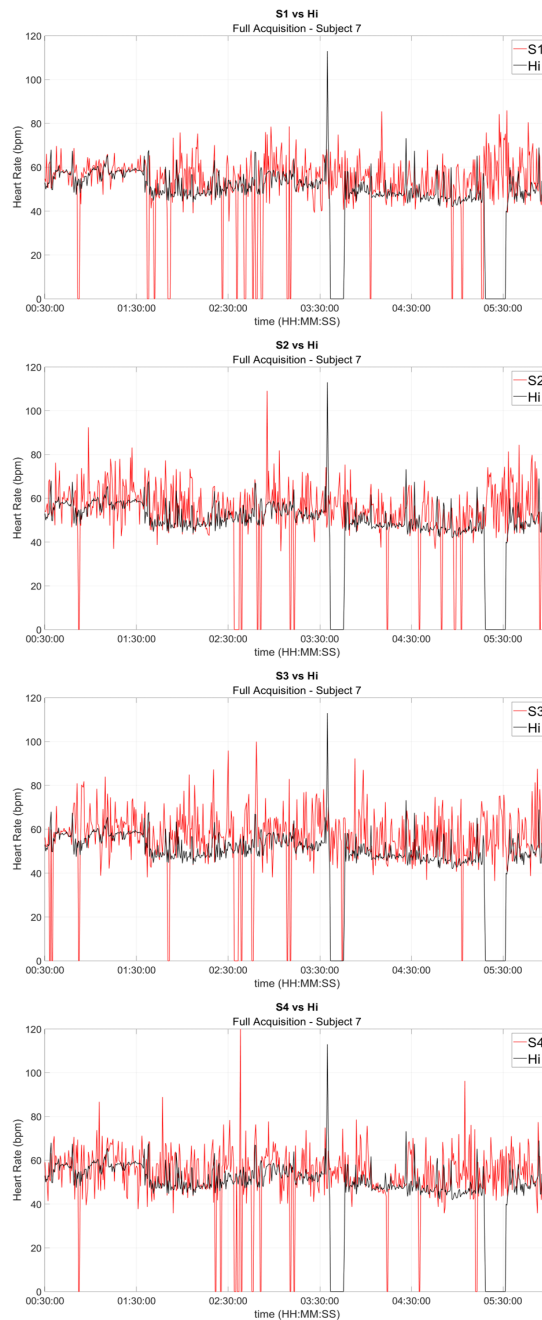


Figure 3.19: Full acquisition of Subject 7: HR provided every 30 s by each sensor (S1, S2, S3 and S4) vs Hi.

The following graphs report the HR value calculated every 30 s from the three models MPM, SPM and IM for the entire acquisition of Subject 7.

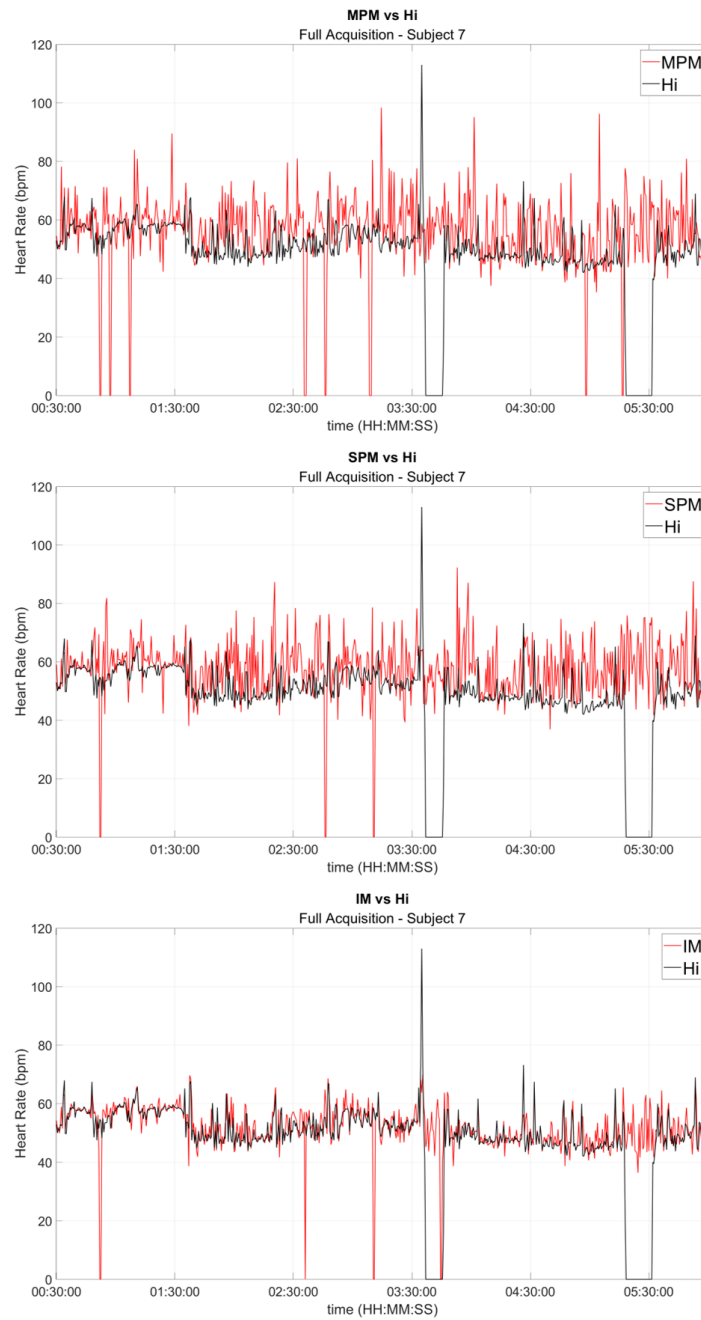


Figure 3.20: Full acquisition of Subject 7: HR provided every 30 s by each designed model (MPM, SPM and IM) vs Hi.

The following graphs report the comparable HR value calculated every 30 s from the S1, S2, S3 and S4 sensors of Subject 7.

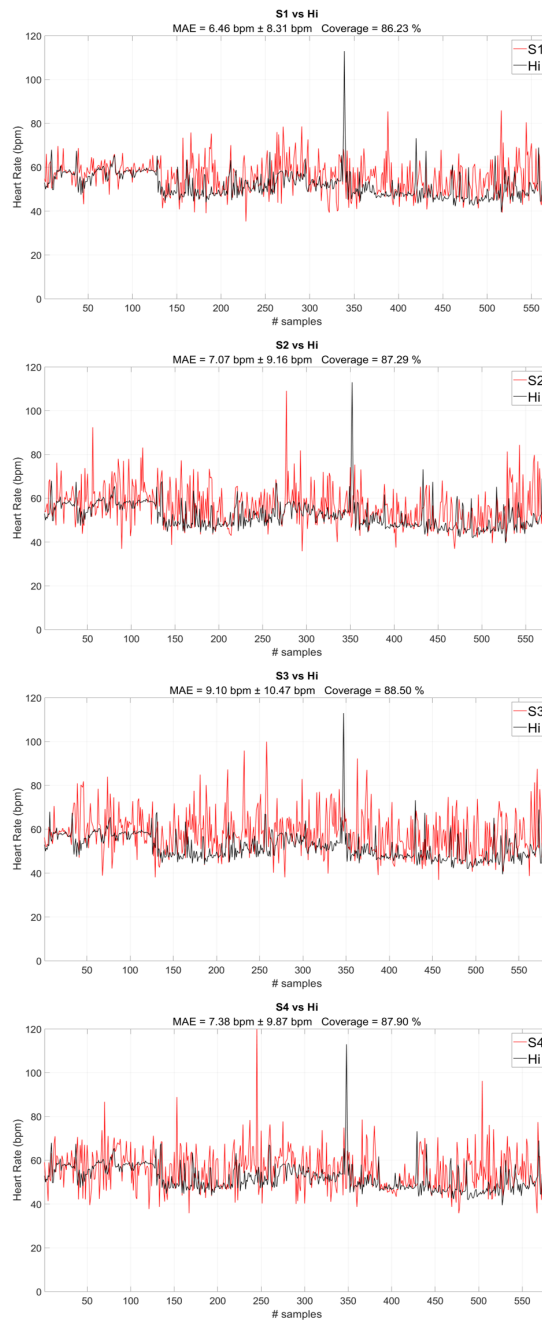


Figure 3.21: Covered acquisition of Subject 7: HR provided every 30 s by each sensor (S1, S2, S3 and S4) vs Hi.

The following graphs report the HR value calculated every 30 s from the three models MPM, SPM and IM for the entire acquisition of Subject 7.

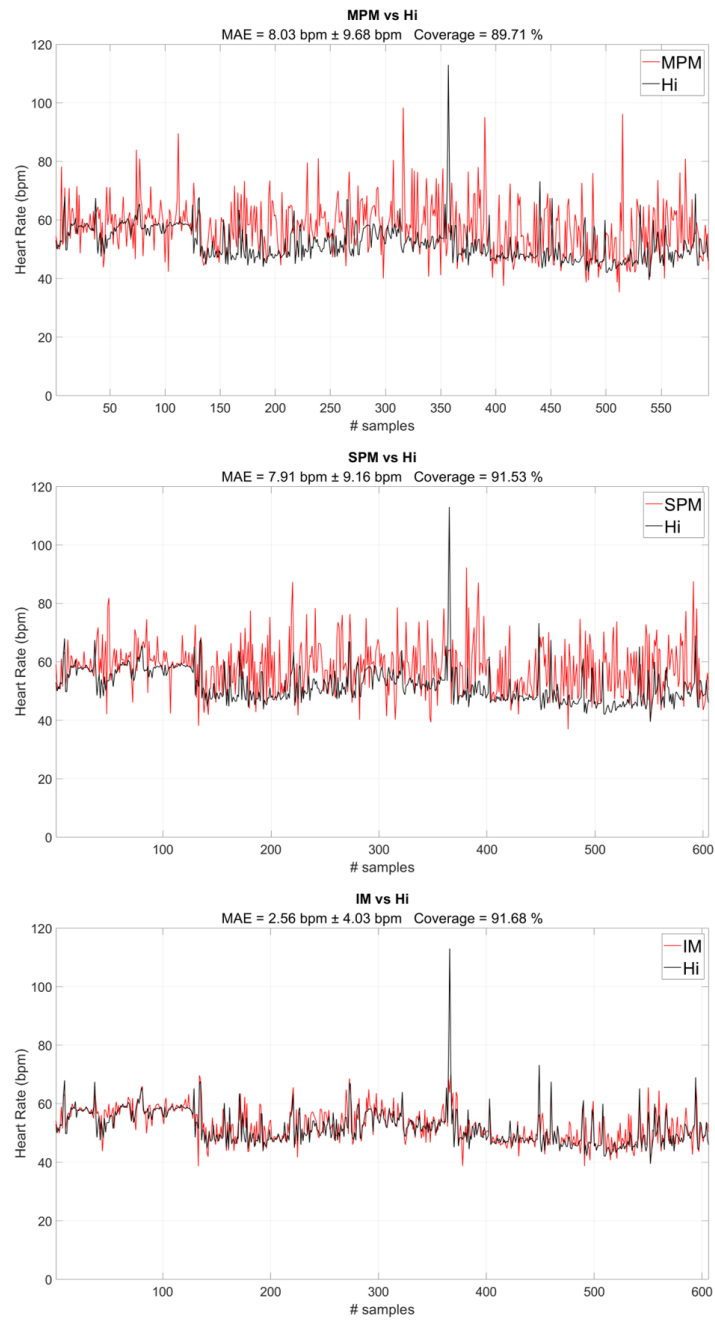


Figure 3.22: Covered acquisition of Subject 7: HR provided every 30 s by each designed model (MPM, SPM and IM) vs Hi.

The following graphs report the Bland-Altman Plot of the comparable HR value calculated every 30 s from the S1, S2, S3 and S4 sensors of Subject 7.

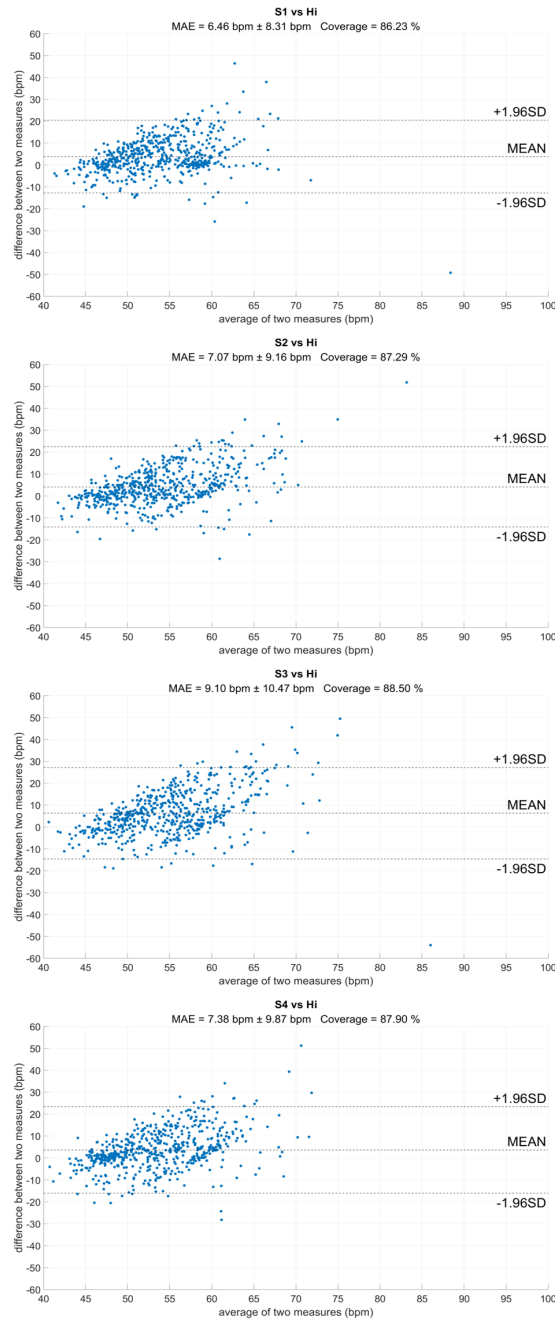


Figure 3.23: Bland Altman - Plot of the covered acquisition of Subject 7: HR provided every 30 s by each sensor (S1, S2, S3 and S4) vs Hi.

The following graphs report the Bland-Altman Plot of the comparable HR value calculated every 30 s from the three models MPM, SPM and IM of Subject 7.

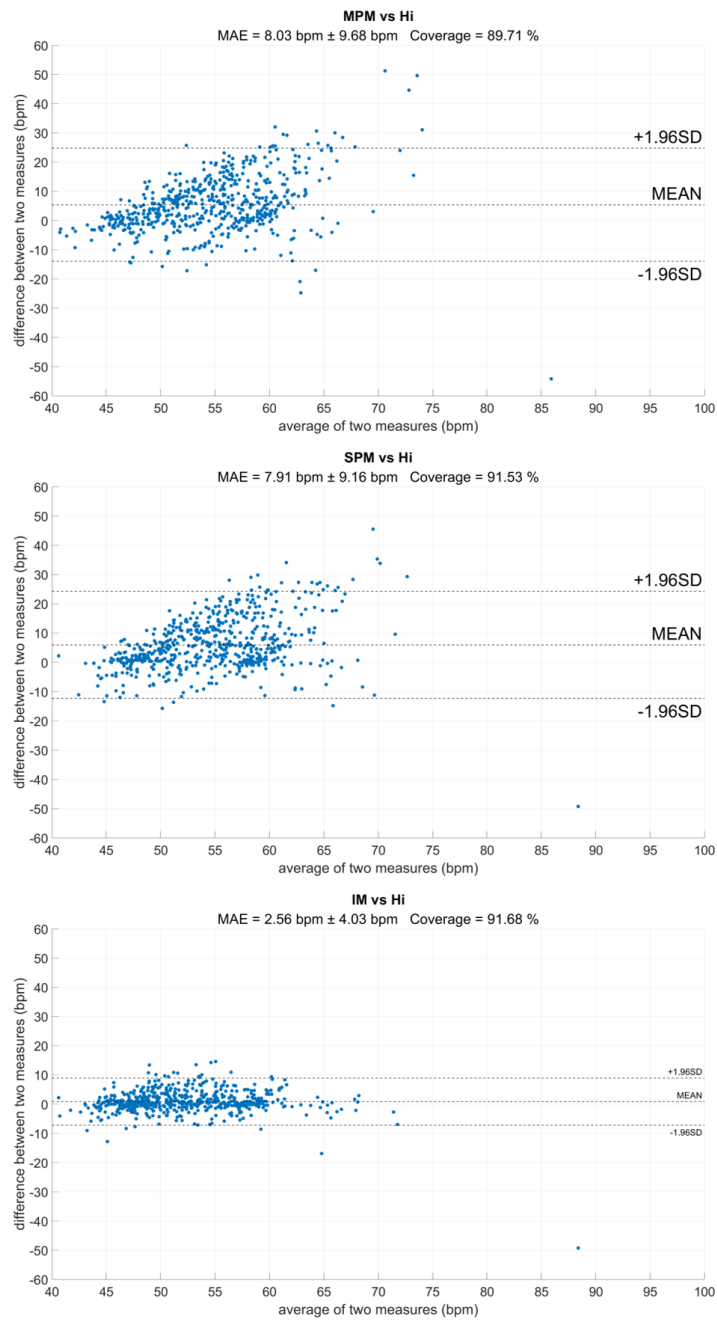


Figure 3.24: Bland Altman - Plot of the covered acquisition of Subject 7: HR provided every 30 s by each designed model (MPM, SPM and IM) vs Hi.

3.3 Discussion

Under the hypothesis that a unique sensor would not be able to continuously acquire, regardless the subject's positions, the ballistocardiogram during sleep, a network consisting of multiple sensors has been implemented. The results obtained in Chapter 3 actually show that the use of a multi-sensor network allows to capture the BCG signal with a greater coverage than the ballistocardiogram acquired by each individual sensor. By observing the results obtained for Subject 1, it can be noted that if the system had been based exclusively on the S2 sensor, the system would have achieved a coverage of 60.02 % and 69.59 % for heart rate calculated every 10 s and 30 s respectively. In addition, for Subjects 4, 5 and 7, the data were not provided by all four sensors, probably because, during sleep, the communication was lost due to an involuntary disconnection between a sensor and the microcontroller. Nevertheless, on average, in the two described scenarios (HR computed every 10 s and 30 s) a coverage greater than 75 % and 82 % for each individual sensor can be obtained. This result could be associated with the value of the mean cross-correlation coefficient chosen in Chapter 2, useful for the detection of heartbeats on the BCG trace. The value chosen is 0.4 and therefore it allowed the detection of beats in a not-rigorous way. This apparent disadvantage was overcome precisely by the network consisting of the four sensors. On the other hand, the use of the developed prediction models allows to obtain an average a coverage greater than 90 %, calculating the heart rate both every 10 s and 30 s. This result highlights the main advantage that can be obtained from the proposed multi-sensor network. Considering the mean absolute error, even in this case it is found that the best results are obtained by combining the information coming from each individual sensor. On average, the MPM model provides a MAE of 4.56 bpm (HR computed every 10 s) and 4.26 bpm (HR computed every 30 s), while the SPM provides an MAE of 4.25 bpm (HR computed every 10 s) and 3.86 bpm (HR computed every 30 s). By examining exclusively this parameter obtained from the proposed models, it is deduced that the results fully comply with the error limit of 5 bpm proposed by the Association for the Advancement of Medical Instrumentation (ANSI/AAMI EC13:2002) [43]. However, considering the standard deviation of the error it is possible to realize that the AAMI standard is no longer met. The reasons why this happens could be related to the implemented models. For example, for the Multi-Parameter Model a problem might be related to the scores that are assigned to the different statistical descriptors. Once these are established, the algorithm will choose the best signal based on these values. However, the results obtained from the Ideal Model built a posteriori show that, by exploiting the maximum potentiality of the multi-sensor network designed, it is possible to obtain an average MAE of $2.31 \text{ bpm} \pm 4.40 \text{ bpm}$ and a MAE of $1.80 \text{ bpm} \pm 3.22 \text{ bpm}$, for the calculation of the heart rate every 10 s and 30 s, respectively. Therefore, if the proposed models were optimized, the standard AAMI would be almost met, when the heart rate is provided every 10 s, and fully complied, when the heart rate is provided every 30 s.

Chapter 4

Conclusions and future works

This study presents a bed-based BCG system constituted of four inertial sensors for the non-invasive and non-intrusive cardiac monitoring during sleep.

The steps leading up to the design of the prototype system involved both hardware and software development. Initially, a literature review was carried out to evaluate which inertial sensors, among those produced by the company STMicroelectronics, would be the most suitable for this type of work. Therefore, a network consisting of four IIS2ICLX inclinometers has been implemented. Each pair of sensors was soldered on two stripboards. These were interfaced to the STM32L4 microcontroller of the STWIN via 4-wire SPI. Subsequently, a firmware capable of managing the sampling and data storage on the micro SD card was developed. After that, an analysis to identify the most suitable sensors positions on the mattress for the acquisition of the BCG signal was carried out. This analysis focused on the morphology assessment of the acquired signals, for each region tested. The areas of the mattress that have offered the possibility of recording a BCG with a high SNR are those closest to the corners of the mattress itself. In addition, this choice has allowed to minimize the encumbrance of the system on the mattress. Finally, a time-based algorithm capable of calculating the heart rate has been implemented, while the information from the four sensors was managed through the development of two prediction models: the *Multi-Parameter Model* and the *Single-Parameter Model*. The results obtained from these two models were compared with an *Ideal Model* built a posteriori in order to evaluate the performance of the proposed system.

4.1 Conclusions

This project demonstrated the usefulness of using an inertial multi-sensor network for heart rate detection using ballistocardiographic signals. This solution offers several advantages, such as non-invasiveness and non-intrusiveness. Regarding the former, the proposed system does not come into direct contact with the subject. Regarding the latter, the non-intrusiveness of the system could result in greater acceptability by the patient who needs to use this solution for long-term monitoring. Moreover, it is worth mentioning the low costs of this system and the minimal maintenance it requires (for example the battery recharging) which are of no less importance. Ultimately, concerning the heart rate computation, it could be noted that, although the system is able to provide a high coverage, the implemented models should be optimized in order to select the sensor that acquires the signal with the highest SNR.

However, some aspects related to each developed field that could be investigated are reported below:

- **Hardware design:**
 - design of a PCB (Printed Circuit Board) for the connection of the four sensors;
 - making the system wireless, for example by connecting a STWIN to each pair of sensors and synchronizing these via Bluetooth.
- **Firmware design:**
 - embedding of the proposed algorithm for the heart rate computation.
- **Signal capture:**
 - engaging more subjects to achieve a larger dataset;
 - video recording the sleep session in order to provide a visual feedback, useful for evaluating the performance of the system.
- **Data processing:**
 - optimization of the proposed MPM and SPM models;
 - improving the detection of the motion artifacts;
 - computing other vital parameters (such as Heart Rate Variability (HRV), BR (Breathing Rate), etc.) in order to detect sleep stages.

Bibliography

- [1] *Mortality-and-Global-Health-Estimates @ Www.Who.Int*. URL: <https://www.who.int/data/gho/data/themes/mortality-and-global-health-estimates>.
- [2] Sanjay Sood et al. "What is telemedicine? A collection of 104 peer-reviewed perspectives and theoretical underpinnings". In: *Telemedicine and e-Health* 13.5 (2007), pp. 573–590. ISSN: 15305627. DOI: 10.1089/tmj.2006.0073.
- [3] WHO Group Consultation on Health Telematics. *A health telematics policy in support of WHO's Health-for-all strategy for global health development : report of the WHO Group Consultation on Health Telematics, 11-16 December, Geneva, 1997*. en. Geneva PP - Geneva. URL: <https://apps.who.int/iris/handle/10665/63857>.
- [4] Seewon Ryu. "Telemedicine: Opportunities and Developments in Member States: Report on the Second Global Survey on eHealth 2009 (Global Observatory for eHealth Series, Volume 2)". In: *Healthcare Informatics Research* 18.2 (2012), p. 153. ISSN: 2093-3681. DOI: 10.4258/hir.2012.18.2.153.
- [5] Babar Rao and Adriana Lombardi. "Telemedicine: current status in developed and developing countries." eng. In: *Journal of drugs in dermatology : JDD* 8.4 (2009), pp. 371–375. ISSN: 1545-9616 (Print).
- [6] Enrico Coiera. "Essentials of Telemedicine and Telecare". In: *Bmj* 324.7345 (2002), p. 1104. ISSN: 14685833. DOI: 10.1136/bmj.324.7345.1104.
- [7] Knut Sevre. *Handbook of cardiac anatomy, physiology, and devices*. Vol. 15. 1. 2006, p. 59. ISBN: 1588294439. DOI: 10.1080/08037050500369058.
- [8] *What-Is-Cardiovascular-Disease @ Www.Heart.Org*. URL: <https://www.heart.org/en/health-topics/consumer-healthcare/what-is-cardiovascular-disease>.
- [9] Mohamed Adel Serhani et al. "ECG monitoring systems: Review, architecture, processes, and key challenges". In: *Sensors (Switzerland)* 20.6 (2020). ISSN: 14248220. DOI: 10.3390/s20061796.

- [10] L. Su, S. Borov, and B. Zrenner. “12-lead Holter electrocardiography: Review of the literature and clinical application update”. In: *Herzschrittmachertherapie und Elektrophysiologie* 24.2 (2013), pp. 92–96. ISSN: 09387412. DOI: 10.1007/s00399-013-0268-4.
- [11] *Electrocardiography @ en.wikipedia.org*. URL: <https://en.wikipedia.org/wiki/Electrocardiography>.
- [12] J W Gordon. “Certain Molar Movements of the Human Body produced by the Circulation of the Blood”. eng. In: *Journal of anatomy and physiology* 11.Pt 3 (Apr. 1877), pp. 533–536. URL: <https://pubmed.ncbi.nlm.nih.gov/17231163%20https://www.ncbi.nlm.nih.gov/pmc/articles/PMC1309740/>.
- [13] Yandell Henderson. “The Mass-Movements of the Circulation as Shown by a Recoil Curve”. In: *American Journal of Physiology-Legacy Content* 14.3 (1905), pp. 287–298. ISSN: 0002-9513. DOI: 10.1152/ajplegacy.1905.14.3.287. URL: <https://doi.org/10.1152/ajplegacy.1905.14.3.287>.
- [14] Isaac Starr et al. “Studies on the Estimation of Cardiac Output in Man, and of Abnormalities in Cardiac Function, from the Heart’s Recoil and the Blood’s Impacts; the Ballistocardiogram”. In: *American Journal of Physiology-Legacy Content* 127.1 (1939), pp. 1–28. ISSN: 0002-9513. DOI: 10.1152/ajplegacy.1939.127.1.1. URL: <https://doi.org/10.1152/ajplegacy.1939.127.1.1>.
- [15] Laurent Giovannardi et al. “Ballistocardiography - A method worth revisiting”. In: *Proceedings of the Annual International Conference of the IEEE Engineering in Medicine and Biology Society, EMBS* (2011), pp. 4279–4282. ISSN: 1557170X. DOI: 10.1109/IEMBS.2011.6091062.
- [16] Chang Sei Kim et al. “Ballistocardiogram: Mechanism and Potential for Unobtrusive Cardiovascular Health Monitoring”. In: *Scientific Reports* 6 (2016), pp. 1–6. ISSN: 20452322. DOI: 10.1038/srep31297. URL: <http://dx.doi.org/10.1038/srep31297>.
- [17] W. R. Scarborough et al. “Proposals for Ballistocardiographic Nomenclature and Conventions: Revised and Extended”. In: *Circulation* 14.3 (1956), pp. 435–450. DOI: 10.1161/01.CIR.14.3.435. URL: <https://doi.org/10.1161/01.CIR.14.3.435>.
- [18] Ibrahim Sadek. “Ballistocardiogram signal processing: A literature review”. In: *arXiv* (2018), pp. 1–23. ISSN: 2047-2501. DOI: 10.1007/s13755-019-0071-7. arXiv: 1807.00951. URL: <https://doi.org/10.1007/s13755-019-0071-7>.
- [19] S H Hwang et al. “Unconstrained Sleep Apnea Monitoring Using Polyvinylidene Fluoride Film-Based Sensor”. In: *IEEE Transactions on Biomedical Engineering* 61.7 (2014), pp. 2125–2134. ISSN: 1558-2531 VO - 61. DOI: 10.1109/TBME.2014.2314452.

- [20] Jarmo Alametsä and Alpo Värri. “The potential of EMFi sensors in heart activity monitoring”. In: ... : *Integration ECG into the ...* (2004), pp. 2–6. URL: http://www.openecg.net/WS2%7B%5C_%7Dproceedings/Session11/S11.2%7B%5C_%7DPA.pdf.
- [21] Y Kurihara and K Watanabe. “Development of Unconstrained Heartbeat and Respiration Measurement System With Pneumatic Flow”. In: *IEEE Transactions on Biomedical Circuits and Systems* 6.6 (2012), pp. 596–604. ISSN: 1940-9990 VO - 6. DOI: 10.1109/TBCAS.2012.2189007.
- [22] Mark Brink, Christopher H Müller, and Christoph Schierz. “Contact-free measurement of heart rate, respiration rate, and body movements during sleep”. In: *Behavior Research Methods* 38.3 (2006), pp. 511–521. ISSN: 1554-3528. DOI: 10.3758/BF03192806. URL: <https://doi.org/10.3758/BF03192806>.
- [23] D Heise and M Skubic. “Monitoring pulse and respiration with a non-invasive hydraulic bed sensor”. In: *2010 Annual International Conference of the IEEE Engineering in Medicine and Biology*. 2010, pp. 2119–2123. ISBN: 1558-4615 VO -. DOI: 10.1109/IEMBS.2010.5627219.
- [24] Sven Poeggel et al. “Optical fibre pressure sensors in medical applications”. In: *Sensors (Switzerland)* 15.7 (2015), pp. 17115–17148. ISSN: 14248220. DOI: 10.3390/s150717115.
- [25] Zhihao Chen et al. “Portable fiber optic ballistocardiogram sensor for home use”. In: *Optical Fibers and Sensors for Medical Diagnostics and Treatment Applications XII* 8218 (2012), p. 82180X. ISSN: 1605-7422. DOI: 10.1117/12.909768.
- [26] Yun-Hong Noh, Soo-Young Ye, and Do-Un Jeong. “Development of the BCG feature extraction methods for unconstrained heart monitoring”. In: *5th International Conference on Computer Sciences and Convergence Information Technology*. 2010, pp. 923–928. DOI: 10.1109/ICCIT.2010.5711192.
- [27] Yating Hu et al. “Physiological Acoustic Sensing Based on Accelerometers: A Survey for Mobile Healthcare”. In: *Annals of Biomedical Engineering* 42.11 (2014), pp. 2264–2277. ISSN: 1573-9686. DOI: 10.1007/s10439-014-1111-8. URL: <https://doi.org/10.1007/s10439-014-1111-8>.
- [28] Federica Landreani et al. “Assessment of ultra-short heart variability indices derived by smartphone accelerometers for stress detection”. In: *Sensors (Switzerland)* 19.17 (2019), pp. 1–16. ISSN: 14248220. DOI: 10.3390/s19173729.
- [29] Massimo Conti et al. “Heart rate detection with accelerometric sensors under the mattress”. In: *Proceedings of the Annual International Conference of the IEEE Engineering in Medicine and Biology Society, EMBS 2020-July* (2020), pp. 4063–4066. ISSN: 1557170X. DOI: 10.1109/EMBC44109.2020.9175735.
- [30] *iis3dhhc @ www.st.com*. URL: <https://www.st.com/en/mems-and-sensors/iis3dhhc.html>.

- [31] *iis2iclx @ www.st.com*. URL: <https://www.st.com/en/mems-and-sensors/iis2iclx.html>.
- [32] Murata. “The Sca61T Inclinometer Series”. In: *Murata 8261900* (), pp. 1–17. URL: https://www.murata.com/%7B~%7D/media/webrenewal/products/sensor/gyro/selectionguide/sca61t%7B%5C_%7Dinclinometer.ashx.
- [33] Analog Devices. “Digital Output MEMS Accelerometer”. In: (2012), pp. 1–43. URL: <https://www.analog.com/media/en/technical-documentation/data-sheets/ADXL362.pdf>.
- [34] Analog Devices. “Low Noise, Low Drift, Low Power, 3-Axis MEMS Accelerometers ADXL354/ADXL355”. In: (2016), pp. 1–42. URL: https://www.analog.com/media/en/technical-documentation/data-sheets/adxl354%7B%5C_%7Dadxl355.pdf.
- [35] *steval-mki209v1k @ www.st.com*. URL: <https://www.st.com/en/evaluation-tools/steval-mki209v1k.html>.
- [36] *steval-stwinkt1 @ www.st.com*. URL: <https://www.st.com/en/evaluation-tools/steval-stwinkt1.html%7B%5C#%7Doverview>.
- [37] *Serial Peripheral Interface - Wikipedia*. URL: https://en.wikipedia.org/wiki/Serial%7B%5C_%7DPeripheral%7B%5C_%7DInterface.
- [38] R S GUBNER, M RODSTEIN, and H E UNGERLEIDER. “Ballistocardiography; an appraisal of technic, physiologic principles, and clinical value”. In: *Circulation* 7.2 (1953), pp. 268–286. ISSN: 0009-7322 (Print). DOI: 10.1161/01.cir.7.2.268.
- [39] *Digital Filter Basics*. 2007. URL: https://en.wikipedia.org/wiki/Digital%7B%5C_%7Dfilter.
- [40] *Savitzky–Golay filter - Wikipedia*. URL: https://en.wikipedia.org/wiki/Savitzky%E2%80%93Golay%7B%5C_%7Dfilter.
- [41] Xin Wen et al. “A Correlation-Based Algorithm for Beat-to-Beat Heart Rate Estimation from Ballistocardiograms”. In: *Proceedings of the Annual International Conference of the IEEE Engineering in Medicine and Biology Society, EMBS* (2019), pp. 6355–6358. ISSN: 1557170X. DOI: 10.1109/EMBC.2019.8856464.
- [42] Eduardo Pinheiro, Octavian Postolache, and Pedro Girão. “Theory and Developments in an Unobtrusive Cardiovascular System Representation: Ballistocardiography”. In: *The Open Biomedical Engineering Journal* 4.1 (2010), pp. 201–216. ISSN: 1874-1207. DOI: 10.2174/1874120701004010201.
- [43] Aami E C Wg. “American National Standard”. In: *SMPTE Journal* 95.5 (2012), pp. 601–602. ISSN: 0036-1682. DOI: 10.5594/j17740.